WT-1613

This document consists of 126 pages.

No. 111 of 195 copies, Series A

Operation

HARDTACK

April - October 1958

Project 1.8

GROUND MOTION PRODUCED BY NUCLEAR DETONATIONS (U)

Issuance Date: May 3, 1962

HEADQUARTERS FIELD COMMAND
DEFENSE ATOMIC SUPPORT AGENCY
SANDIA BASE, ALBUQUERQUE, NEW MEXICO

FORMERLY RESTRICTED DATA

Handle as Restricted Data in foreign dissemination. Section 144b, Atomic Energy Act of 1954.

This material contains information affecting the national defense of the United States within the meaning of the espionage laws Title 18, U. S. C., Secs. 793 and 794, the transmission or revelation of which in any manner to an unauthorized person is prohibited by law.

SECRET

When no longer required, this document may be destroyed in accordance with applicable security regulations.

DO NOT RETURN THIS DOCUMENT

SECRET

WT-1613

OPERATION HARDTACK — PROJECT 1.8

GROUND MOTION PRODUCED BY NUCLEAR DETONATIONS (U)

by

L. M. Swift, ~~Project Officer~~
F. M. Sauer
W. M. Wells

Stanford Research Institute
Menlo Park, California

SECRET

ABSTRACT

The objective was to measure ground motion produced by nuclear explosions at Eniwetok Proving Ground (EPG) as it varied with input pressure level, depth, and yield, and to correlate the measurements with similar data obtained at Nevada Test Site (NTS).

Measurements were obtained at three nominal pressure levels—100, 200, and 600 psi—on two surface shots: Cactus (~18 kt) and Koa (~1.3 Mt). At each station (pressure level), airblast, acceleration (at 0-, 10-, 30-, 50-, and 100-foot depths), and relative displacement (between 0 and 50, and 0 and 100 feet) were measured. In addition, preshot seismic velocity profiles were determined for use in calculating soil constants for delineating effects of the soil on the character of the ground motion.

The airblast from Shot Cactus was characterized by a short-lived precursor that caused lower-than-ideal overpressures out to at least 158 ft/kt$^{1/3}$, after which it rapidly cleaned up. Koa airblast showed higher-than-ideal overpressure between 180 and 283 ft/kt$^{1/3}$, perhaps because of the influence of the unusual geometry of the device on fireball hydrodynamics.

In general, the ground motion on Cactus and Koa outruns the airblast because of the high seismic velocity of the near-surface substratum.

Maximum vertical and horizontal accelerations at 10-foot depth on Cactus and Koa agree on a scaled basis with results of previous EPG tests and United Kingdom experiments. Maximum acceleration is independent of yield at the same scaled ground range. Attenuation of maximum vertical and horizontal acceleration with depth is compatible with that measured at NTS, and it appears to be independent of yield and overpressure.

Maximum vertical particle velocity at 10-foot depth agrees with data from EPG tests and United Kingdom experiments and is a function of scaled ground range. Horizontal velocity shows more scatter, and the average as a function of A-scaled ground range cannot be drawn with the same confidence. There is some evidence (on Koa at Δp_s ~1,000 psi) that bolsters the theory that the maximum particle velocity is equal to the overpressure divided by the impedance (ρC) of the medium.

No conclusive results were obtained on transient displacements. Maximum vertical surface displacements on Koa were from 2.5 to 2 inches downward at 2,000-, 3,144-, and 3,950-foot ground ranges, in that order, with a possible 2.5-foot upward and 15-foot outward displacement at 2,000 feet due to crater lip formation. At 840-foot ground range on Cactus, maximum downward surface displacement was approximately 1 to 1.5 inches. All other vertical and horizontal displacements were uncertain, and it is impossible to specify the attenuation of displacement with depth. Without suggesting that it be taken as a generalization, it appears that transient displacements on Cactus and Koa are a weak function of ground range (or pressure level), under conditions of outrunning ground motion and are independent of yield.

FOREWORD

This report presents the final results of one of the projects participating in the military-effect programs of Operation Hardtack. Overall information about this and the other military-effect projects can be obtained from ITR-1660, the "Technical Summary of Military Effects, Programs 1-9 (DASA)." This technical summary includes: (1) tables listing each detonation with its yield, type, environment, meteorological conditions, etc.; (2) maps showing shot locations; (3) discussions of results by programs; (4) summaries of objectives, procedures, results, etc., for all projects; and (5) a listing of project reports for the military-effect programs.

PREFACE

The planning and execution of the project were under the direction of L. M. Swift, Project Officer, with L. H. Inman serving as field party chief and W. M. Wells as assistant to the project officer. Other members of the field party included R. E. Aumiller, D. R. Knirck, V. E. Krakow, R. V. Ohler, C. M. Westbrook, and H. C. Wuner.

W. E. Perret of the Sandia Corporation acted as consultant in the planning of the project, and that organization furnished the design of the displacement gages.

The cooperation and assistance of Lt Col J. W. Kodis and Lt F. E. Shoup, of DASA Field Command, are gratefully acknowledged.

CONTENTS

FIGURES

Chapter 1

INTRODUCTION

1.1 OBJECTIVES

The objective was to measure ground motion produced by nuclear explosions at Eniwetok Proving Ground (EPG) as it varied with input pressure level, depth, and yield, and to correlate the measurements with similar data obtained at Nevada Test Site (NTS). The ultimate objective is to develop techniques for the establishment of design criteria for hard protective construction, especially for areas where some of the soil parameters are known or can be measured.

1.2 BACKGROUND

The Armed Forces are faced with the requirement of the design and construction of facilities that will remain operative in spite of exposure to nuclear bursts at close range. In general, some of these facilities may be, in effect, fully underground. In many cases, the most probable damage will be to the contents of structures rather than to the structures themselves, so that insuring that the structure survives is not adequate protection. A full analysis, then, requires the description of the input conditions followed by analysis of the response of the structure and its contents. This project is concerned primarily with the first step.

When Operation Hardtack was planned, the immediate requirements for the design of protective construction were limited to overpressure levels of 100 to 200 psi, and the original experiment plan for this project was limited to those levels. However, it was expected that requirements would arise for the design of harder construction within the next 2 years. The scheduling of the nuclear tests did not permit a later experiment; therefore, it was decided that the studies of this project should be extended to higher levels—at least to 600 psi.

Studies of ground motion due to underground explosions have been conducted in considerable detail (Reference 1) but are not directly applicable to surface or above-ground detonations. A few measurements were made of underground accelerations due to aboveground detonations during Operations Tumbler/Snapper (Reference 2) and Upshot/Knothole (Reference 3), but these were largely at relatively low pressure levels. Earth stress and strain were also measured at a few stations during Upshot/Knothole (Reference 4).

During Operation Plumbbob (References 5 and 6), extensive measurements were made of earth acceleration, stress, and strain as they varied with depth and ground range (overpressure level) from a 37-kt nuclear explosion at a burst height of 700 feet at NTS. The measurements provide a reasonable basis for prediction of subsurface effects for that set of conditions. Seismic and soil analysis measurements were also made as a part of this program, and efforts were made to develop a more generalized prediction scheme. Project 1.8 was designed to provide data obtained under different soil conditions and from larger yield explosions to permit extension and confirmation of these analyses.

During Operation Plumbbob, ground motion measurements involved over 120 gage channels on a single shot. This permitted investigation of effects over a wide range of

input overpressure level and measurement depths. At the time this project was planned, it was not considered necessary or desirable to repeat these extensive measurements, because study of the differences observed at a relatively small number of points should permit the extrapolation of Plumbbob data to Hardtack conditions.

1.3 THEORY

The theory of earth motion caused by nuclear detonations is far from complete. Without detracting from the magnitude of the airblast problem, detailed analysis of the ground motion problem is a more formidable undertaking as illustrated by a brief qualitative description of events that occur underground during a surface detonation.

Ground motion from nuclear detonations may be induced by two distinct processes: (1) airblast loading and (2) direct conversion of hydrodynamic energy into mechanical energy of ground motion during the detonation. Airblast loading induces ground motion by imposing tractions, i.e., normal pressure and tangential shear, at the ground surface over a fairly large area and for a comparatively long time. The second process induces initially more violent motion over a much shorter distance (of the order of the crater depth) and acts for a very short time, roughly comparable to the time to breakaway of the shock wave from the fireball for an airburst. The induced motion of the second process, although larger initially than that of the first process, probably attenuates faster with distance because of spherical spreading.

For near surface airbursts, for surface bursts, or for underground detonations that rent the surface both processes contribute to the generation of ground motion in varying degree. In addition, the differing geometrical attenuation of each generation process means that the relative amount of energy arriving at the observation point will differ markedly depending on the location of the observation point in relation to the detonation and the refraction of energy by the geological formation. For example, ground motion at a point near the ground surface at a distance from the detonation may be predominantly airblast induced, while the motion at the same slant range but below the surface may be predominantly directly induced motion. At short ground ranges, the motion at the surface as well as that at depth may be predominantly directly induced, especially if considerable refraction is present, whereas at long ground ranges the motion will be entirely airblast induced, either by local airblast or by refracted and reflected airblast-induced energy.

Close to the detonation (following the hydrodynamic action of the fireball) there are large plastic deformations and fracture of the medium. Any theory taking these factors into account must necessarily be very complex, and there is little hope of obtaining practical solutions. Even a simplified problem of predicting motion such as in a semi-infinite elastic medium is far from easy and has not yet been solved in a more than an approximate manner.

Because the airblast wave is axially symmetric about a vertical axis through ground zero, the ground motion problem is basically three-dimensional. However, if the ground is considered homogeneous or if nonhomogeneities can be specified by their variation in the vertical direction only, then the entire problem is axially symmetric. Three further restrictions make the problem tractable. (1) The depth of the point of observation must be small compared with its radial position (Reference 7). With this premise the blast wave may be considered to be planar and the earth motion problem one of plane strain. (2) The velocity and magnitude of the pressure pulse are invarient with time (or distance). (3) The problem is quasi-steady, i.e., to an observer moving at the velocity of the blast wave, stress and displacement are functions of distance but not of time. This third assumption implies that a great amount of time has transpired since the zero time and all time-dependent aspects have died away.

The quasi-steady state homogeneous elastic plane strain problem has been solved for a moving concentrated line (Dirac delta function) load (References 8 and 9) for stresses (Reference 10) and displacements (Reference 11) induced by a Friedlander type of pressure pulse and for an exponentially decaying pressure pulse (Reference 12) The Friedlander relation is

$$\frac{\Delta p}{\Delta p_s} = (1 - t/t_+)e^{-t/t_+}$$

Where: Δp_s = the shock overpressure

Δp = overpressure

t = time

t_+ = positive phase duration

Quasi-steady state solutions have also been used as input function for the calculation of response spectra (Reference 13). Response spectrum is defined as the maximum response of a linear, single-degree-of-freedom, spring mass system (reed gage) relative to the motion of the ground.

The quasi-steady plane strain problem for a layered fluid, i.e., a medium which cannot support shear waves, has been studied for the moving concentrated line load (Reference 14). The assumption of a concentrated load is not restrictive, since solutions for arbitrary time dependence of the loading pulse may be accomplished by Duhamel superposition (Reference 15).

These solutions show that a differing phenomenological behavior may be expected when the airblast wave velocity is larger than the compressional wave velocity of the medium and when the compressional wave velocity is the larger. There are in fact three theoretical cases:

$C_s < C_l < U$, superseismic case

$C_s < U \leq C_l$, transseismic case

$U \leq C_s < C_l$, subseismic case

Where: C_s = the shear wave velocity

C_l = compressional (longitudinal) wave velocity

U = airblast velocity

In the transseismic and subseismic cases (Figure 1.1), the ground motion will outrun the blast wave, i.e., arrive earlier at a surface station than the airblast wave, in a manner similar to the effect of refraction. The initial motion, however, will be upward and inward as opposed to refraction outrunning in which the initial motion will be upward and outward (Reference 11).

Because of outrunning of the compressional wave in the transseismic and subseismic situations, the quasi-steady state hypothesis requires the ground motion to be initiated infinitely far from the point of observation. As a consequence, the vertical (or both the vertical and horizontal) velocity becomes infinite as the airblast wave passes over the observation point and the displacements contain an arbitrary constant and therefore are ambiguous as time approaches infinity.

Another characteristic of the quasi-steady hypothesis is that the displacements do not return to zero after passage of the airblast wave, i.e., there is no rebound from the maximum transient displacement. These difficulties are avoided in Reference 16 in which

a solution is presented of the plane strain homogeneous elastic problem for step function normal (pressure) and tangential (shear) loadings moving at constant velocity outward from the origin. This solution is obtained by dynamic similarity techniques in the form of complex potential functions, which require numerical evaluation before specific results can be presented. This particular technique cannot be used for the stratified medium problem. The analysis shows that the quasi-steady hypothesis leads to neglect of compressional, von Schmidt, and shear regions, which follow the compressional and shear mach waves in the superseismic case (Figure 1.2). Because the trailing regions produce unloading, as $t \to \infty$, the static solution is obtained, e.g., zero stress and displacement for an airblast wave of finite duration.

Ground motion wavefront diagrams for transseismic and subseismic airblast are shown in Figure 1.1. In the quasi-steady approximation of the transseismic stage, the von Schmidt and compression waves converge at $r \to \infty$, and the shear wave lags behind at $r \to \infty$. In the subseismic stage the shear, von Schmidt, and compression wave converge at $r \to \infty$. This behavior leads to the heuristic argument that the quasi-steady solutions for these two cases do not represent the real behavior of blast-induced ground motion to sufficient approximation to be of significant value.

Both the quasi-steady and the similarity solution result in surface displacements that tend toward infinity as the airblast wave velocity approaches the Rayleigh wave velocity, i.e., the Rayleigh wave singularity. This behavior is the result of the constant blast wave velocity assumption and can be removed as the airblast wave velocity is allowed to vary with distance, as it must for a true blast wave (Reference 7).

Nonelastic solutions have been confined to one-dimensional or spherically symmetric wave propagation. These solutions are of value as approximations in the high-pressure region where large permanent displacements may be expected or at lower pressures only if the blast wave is highly superseismic. Progress is also being made on the axially symmetric elastic problem (References 12, 17, and 18). However, these programs are not sufficiently developed to add significant new material.

These solutions, although approximate, add insight into the fundamental nature of the phenomenon. However, caution should be exercised in taking any of these results too literally, especially where the actual conditions depart significantly from those assumed in the theoretical analysis.

Elastic theories lead to infinite peak accelerations for shock-type overpressure waveforms in the superseismic region and do not permit very large attenuation of particle velocity and stress with depth, except that which results from changes in acoustic impedance. In addition, the airblast-induced motion may become coupled with the earth-transmitted motion because of refracted energy originating from points closer to ground zero, especially at depth. This may be particularly true for the horizontal (radial) motions and is exaggerated when the seismic velocity of the medium is large compared with the velocity of the blast wave. These complications cause decided variations from simplified theory, and the contribution of each is not completely established.

In spite of the complications, certain guides to the prediction of the phenomena are presented by the simplified theory:

1.3.1 Stress. In the simplified case of the step function load, the ultimate vertical stress at any depth is equal to the input pressure and is independent of soil characteristics. In the real case, the finite velocity and duration of the blast wave cause an attenuation of peak stress with depth. This attenuation is obviously a function of duration and should be less with longer durations, but the nature and magnitude of this function are not evident from presently available data. The peaked form of the input also permits reflections from layers of different acoustic impedance to affect the shape and magnitude of the stress wave.

1.3.2 Particle Velocity. In the absence of reflected energy, the instantaneous particle velocity should be a function of stress and the elastic constants of the soil and should therefore resemble the input pressure waveform in the superseismic region. Upward-traveling reflections, however, contribute to velocity in the opposite direction from that of the primary wave so that a reflection that increases the instantaneous stress decreases the instantaneous velocity, and the resemblance is lost. When the reflecting horizon is pronounced and shallow, such as the water table at Eniwetok Atoll, this effect is very marked.

1.3.3 Strain and Relative Displacement. Under the elastic assumption, strain is obviously proportional to stress. In the real earth, hysteresis is so often great that little resemblance is observed, except for a rough correlation between peak values. The elastic modulus, as calculated by the ratio of peaks, is generally somewhat lower than that calculated from seismic velocity.

Relative displacement between two (depth) points is always the integrated strain over that range. It serves as a measure of gross strain predicted for a buried structure and as a check on displacements calculated from double integration of acceleration.

1.3.4 Acceleration. Under any elastic assumption, the initial acceleration produced at any depth by a superseismic shock wave input is infinite. In the real case, the observed peak acceleration is very large at shallow depths but finite, and its measurement is sometimes limited by the response of the measuring system. At depths, the attenuation of peak acceleration is always steeper than that of peak velocity or stress, as a result of the increase of rise time of those functions with depth. If the input pressure has a finite rise time, peak accelerations are reduced, especially at shallow depths.

The details of the curve of acceleration versus time are modified markedly by reflected energy, but the peak value is seldom affected because of its early occurrence.

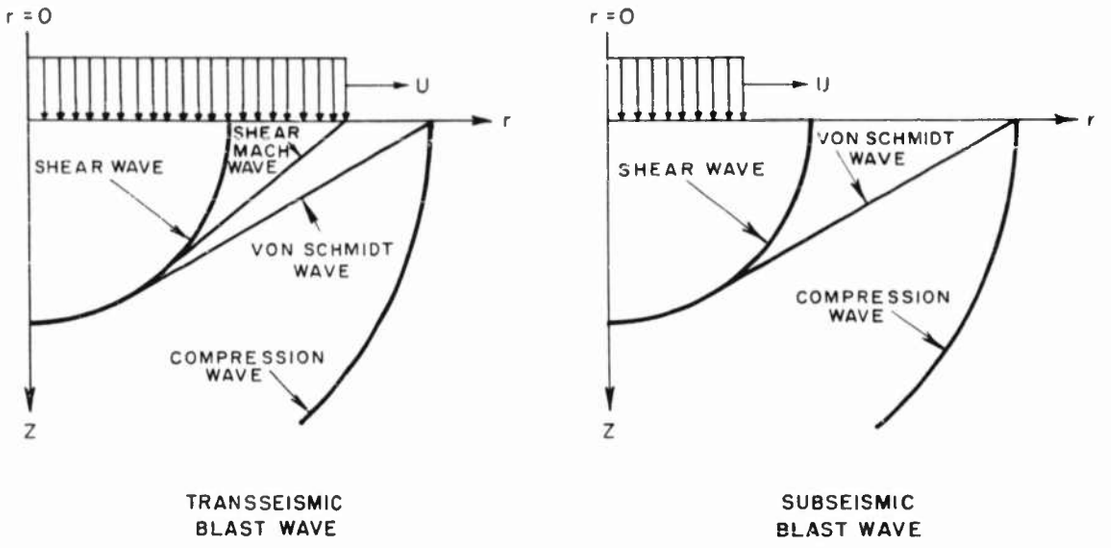

Figure 1.1 Wavefront diagrams for transseismic and subseismic blast waves.

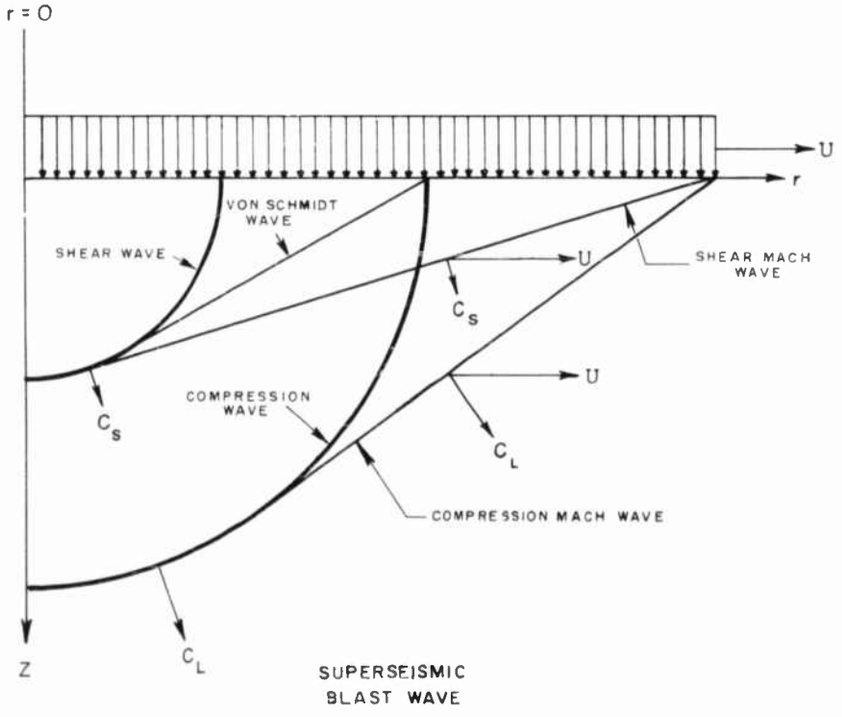

Figure 1.2 Wavefront diagram for superseismic blast wave.

Chapter 2

EXPERIMENT DESIGN AND INSTRUMENTATION

The experimental layout of this project was designed to provide measurements to extend presently available data to (1) a widely different soil type and (2) a much larger yield, with the resultant longer duration of the positive phase of overpressure. To separate these variations, it was necessary to participate in two shots—one in the kiloton range and one in the megaton range. It was also necessary that the shots be adjacent to sufficient land masses to provide gage stations at suitable distances. The choice was quickly narrowed to Shots Cactus and Koa, surface shots of 15-kt and 2-Mt predicted yield, respectively, located on islands Yvonne and Gene. (Other DOD projects were faced with the same requirements, and the choice of shots was made jointly.) Although the zero height of burst of these shots was representative of most probable applications, it represented a variable with respect to the previously studied conditions at NTS. This variation was accepted as necessary and was not expected to make a serious difference in analysis.

2.1 STATION LOCATIONS

To stay within the cost limits imposed, it was necessary to limit the stations to three on each shot, in the belief that relatively complete measurements at a few ranges are more valuable than partial data at many ranges. Predicted peak overpressures of 100, 200, and 600 psi were selected as being most useful, the first two representing levels where considerable data was obtained on Shot Priscilla during Operation Plumbbob at NTS, and the last added to extend the data to much higher pressures (Section 1.2).

The precise locations of the gage stations (Figures 2.1 and 2.2; Table 3.1) were selected by Programs 1 and 3, coordinating the several projects involved.

2.2 PARAMETERS MEASURED

The ultimate objective of the project made desirable the description of all possible free-field effects, including soil stress and strain as well as motion. Past experience, however, indicated that stress measurements have been of somewhat doubtful validity under the best of circumstances and required placement techniques that are impossible in the soil conditions at Eniwetok Atoll. Most of the useful data available has come from measurements of acceleration, from which velocity and displacement can be derived. Measurements of relative displacement, or strain over a long baseline, have been found useful and feasible (Reference 6). Therefore, the parameters measured were limited to acceleration, displacement, and air overpressure point.

Twelve gage channels were available for each gage station. They were distributed as follows: (1) airblast, one channel; (2) relative displacement between depths of 0 and 50 feet and 0 and 100 feet, two channels; and (3) vertical acceleration at depths of 0, 10, 30, 50, and 100 feet and horizontal acceleration at the same depths except zero, nine channels.

In addition, backup channels were available as a part of the proof-testing of the miniaturized magnetic recording equipment (Appendix).

Two sets of this equipment were installed for Shot Koa, one at Station 12 and one at Station 13A, 250 feet behind Station 13 (Figure 2.2). Each of these sets provided five recording channels. At Station 12, these channels were used to measure surface level overpressure, vertical and horizontal acceleration in the free field at 2-foot depth, and vertical and horizontal acceleration of the inner (shock mounted) canister. At Station 13A, three channels were devoted to measurement of vertical acceleration of the floors of Stations 322.02 and 322.04, as a service to Project 3.2 (Reference 19). The other two channels were used to measure vertical acceleration in the free field at 2-foot depth and vertical acceleration of the inner canister. The acceleration measurements were designed primarily to evaluate the effectiveness of the shock mounting, which had been designed for protection of the instrumentation at pressure levels up to 200 psi, but the free-field data was expected to be applicable also to the primary objective of the project.

Aside from the basic measurements during each shot, seismic measurements were made before the shots to describe the seismic velocity profile of the ground, for use in the calculation of soil constants for delineating the effects of various soils on the phenomena.

2.3 INSTRUMENTATION

2.3.1 Central Station. All central station channels of instrumentation were essentially identical to those used on a number of previous projects, including Plumbbob 1.4 (Reference 5). Wianeko 3-kc oscillators supplied carrier power to the transducers themselves and to modified Wianeko demodulators. The demodulated signal was applied to William Miller Co. oscillograph recorders. Provisions were included for applying automatically a synthetic calibrating signal to each channel immediately prior to zero time, for purposes of comparison of the final deflection on the record with the deflection produced by the same signal read at the time of calibration. A highly accurate timing signal of 1,000 and 100 cps was also applied simultaneously from a single source having an accuracy of better than 10 parts per million. This provided means for time correlation of records to a high degree of accuracy.

Banks of storage batteries were the prime power supply for all instruments during the shots. Suitable converters were used to produce 115-volt ac for components requiring this power source. An individual converter was used for each rectifier power supply, thus minimizing the probability of gross loss of data due to converter failure.

Instruments were powered at suitable times before zero time by Edgerton, Germeshausen, and Grier (EG&G) relay circuits, with lock-in relays controlled by a time-delay to continue operation for approximately 1 minute after zero time, even though the EG&G relays dropped out sooner. Utmost attention was paid to circuitry and procedures to insure maximum reliability of operation. Dual relay contacts or dual relays were used wherever feasible. A multipen sequence recorder was connected to provide a record of time and sequence of operation of various elements so that any failure that might occur could be traced to its source on a posttest study.

To protect central station equipment from damage from the induction signal at zero time, multicontact relays were wired to short the incoming signal leads to ground at -5 seconds and to remove this ground immediately after zero time. This system had been used on many previous operations with complete success. Without it, considerable damage to equipment and loss of data were experienced during Shot 4 of Operation Tumbler.

On each shot, 36 central station gage channels were installed. On Shot Cactus, 12 of these were connected to dual-recording systems, consisting of one galvanometer on each of two recorders. These dual channels were assigned to the most important channels to minimize loss due to any single recorded failure. On four of these 12 channels, one of the galvanometers used had a natural frequency of 200 cps, and the remainder had a natural

frequency of 300 cps. The channels incorporating one 200-cps galvanometer were assigned to the displacement gages, since there the uncertainty of the predicted peak was greatest and the expected signal was of the type that would not be degraded by the response of the lower frequency galvanometer. Since there was an appreciable difference in the sensitivity of the galvanometers thus used on a single channel, a wider range of input signal could be accommodated without loss of data.

On Shot Koa, a third recorder was used, and all 36 gage channels were connected to dual-recording systems. Six of these were of dual sensitivity type and were also assigned to displacement gages.

2.3.2 Recording Shelters. On Shot Cactus, the recording shelter was old Greenhouse Station 57, at a ground range of about 2,400 feet (Figure 2.1). This ground range corresponded to a predicted peak pressure of about 10 psi. This range involved no serious problems in protection of equipment from shock, and only a moderate earth cover was required to limit the total radiation dose to less than 10 r inside the shelter.

On Shot Koa, the situation was more severe. A pressure level of 30 to 40 psi was predicted for the extreme eastern end of island Irene. No shelter was available at this point, and cost consideration dictated the use of an available shelter, Ivy Station 600, at a ground range of 4,700 feet, at a predicted pressure level of 60 to 70 psi (Figure 2.2). Fortunately, this structure (Station 14) was very massive, with 3-foot concrete walls and heavy earth cover. Nevertheless, the expected shock was higher than that previously experienced on a central station, and additional protection was considered necessary in the form of shock mounting of parts or the equipment.

Shock mounting of the equipment itself was considered but was rejected as not feasible, particularly since it was felt that incomplete shock mounting is often worse than none. As an alternative, all instruments including recording oscillographs were mounted so that they were tightly wedged between the top and bottom of the shelter, without depending on mounting bolts or the like to keep them in place. All cable runs were lashed down to the racks or instruments. In short, every effort was made to see that the instrumental components moved with the massive structure.

On both central stations, earth cover of 5-foot minimum depth was placed, extending so that the earthfill section in the direction of ground zero was 30 feet or more. This was applied primarily for radiation shielding but was expected to reduce the effects of airblast. Film badges were placed in each shelter, in cooperation with Project 1.9, to check the total radiation dose, which was expected to be well under 10 r total.

2.3.3 Cables and Trenches. All gage cables were vinyl-jacketed, polyethylene-insulated, 3-conductor shielded cables manufactured to specifications by Sequoia Wire of Redwood City, California. The cable and all splices were designed to be completely immersionproof and highly resistant to abrasion and cutting by coral. The cables were laid in the trenches with ample slack, and, at the gage stations, the terminal portion of the cable was spirally wrapped around a length of elastic cord to provide resilience and protection from breakage by earth movement.

All cable runs were laid in trenches 2 or more feet deep, the depth being largely limited by the ability to keep an open trench in the formation encountered, or by the water table. All cable splices were protected by Scotchcast splicing moulds, which were made by pouring an epoxy resin plastic around the splice. When freshly mixed, the plastic is quite fluid, but it hardens to the consistence of hard rubber.

2.3.4 Gages and Gage Mounts. Standard Wiancko variable-reluctance accelerometers were used (Reference 1). They were enclosed in protective canisters carrying a horizontal

and a vertical accelerometer and designed to be oriented at depths with special placement tools (Figures 2.3 and 2.4).

Both standard Wianeko and Ultradyne balanced-reluctance pressure gages (Reference 20) were mounted in baffles set flush with the earth's surface to measure surface level side-on pressure.

The displacement gages (Figures 2.5 and 2.6) were a modification of those used by Teapot Project 1.5. The redesign was primarily that of providing complete sealing against water and a simplification of mounting. The actuating wire was surrounded for its full length by a continuous metal bellows, and the lower end was sealed (Figure 2.7).

2.3.5 Gage Placement. At each station, two separate 100-foot holes were used for placement of the gages. One hole, used for the displacement gages, was capped with a wellhead assembly set in a slab of concrete. This assembly served to mount the two gages proper, as well as the zero-level vertical accelerometer. The other ends of the displacement gage wires were attached to anchors sand-packed in place at 100- and 50-foot depths. The electrical connecting cables were run in from beneath the concrete slab so that they were fully protected. The entire assembly was covered with a pressure-resistant dome to protect the gages from water and blast. This dome was surrounded and covered with sand to avoid thermal radiation and dynamic pressure effects.

The other hole, used for the accelerometers, had no wellhead assembly. Each accelerometer was individually sand-packed in place and the hole backfilled between canisters to present a minimum of discontinuity in the medium.

In the actual placement of the canisters and strain gage anchors, special loading poles were used for location and orientation. Ten- and 20-foot lengths of square aluminum tubing were fitted with couplings so that they could be assembled into one rigid length as they were lowered into the hole. The bottom section was arranged to fit over a square shank projecting from the top of the canister or anchor and to lock in place by a pin, which expanded small balls into sockets in the interior of the pole. This pin could be pulled by a wire extending up the inside of the pole. There were thus no projections from the outside of the loading poles. After placement and orientation of the canister, and after it was covered with several feet of sand, the wire could be pulled to allow the poles to be removed without disturbing the canister.

2.3.6 Gage Coding. For identification of channels and recorded traces with their proper gages, a systematic coding was adopted. A station number was assigned to each gage station: 1, 2, and 3, for Shot Cactus; 11, 12, and 13, for Shot Koa, in order of their ground range. These numbers were used as the first part of the gage code. The second part of the gage code was a letter indicating the type of measurement. In this project, V was used for vertical acceleration, H for horizontal (radial) acceleration, B for air pressure, S for displacement, and SV for vertical strain. A third part of the code indicated the depth of the gage (or anchor) below the surface in feet. The zero was omitted for surface measurements.

Typical gage code numbers were then 3V50 for Station 3, vertical acceleration at 50 feet; 1B for airblast at the surface, etc.

2.3.7 Instrument Response. The complex pattern of the ground accelerations makes a precise statement of error due to frequency response intractable; however, for simple inputs such as a half sine wave, for damping between 0.5 and 0.6 critical, transient pulses are reproduced fairly well for pulse frequencies of $\frac{1}{6}$ the gage frequency. When the pulse frequency becomes equal to or greater than $\frac{1}{2}$ the gage frequency, considerable error in

gage response along with phase distortion may be expected. For the half sine pulse, the errors are approximately 20 percent. If the damping is only 0.4 critical, overshoots of 50 to 100 percent occur.

In general, the frequency response of accelerometers used in weapon-effect experiments has increased markedly since Operation Greenhouse. The gages and their associated recording system used on Project 1.8 of Operation Hardtack were basically flat down to steady-state conditions, due to their design as a carrier-demodulator system. No corrections were therefore required for low-frequency response. The high-frequency response was limited either by the characteristics of the galvanometers or by the dynamic characteristics of the transducers.

The (nominal) 300-cps galvanometers had a natural frequency of 315 to 340 cps and were damped to have an overshoot of approximately $7\frac{1}{2}$ percent. This corresponded to a damping factor of about 0.65 critical and provided a rise time of about 1.3 msec. The nominal 200-cps galvanometers had a correspondingly longer rise time of about 1.8 msec.

The accelerometers varied widely in sensitivity and maximum range and consequently in undamped natural frequency. In general, those near the surface and at the higher pressure levels were low-sensitivity, high-range instruments with a high natural frequency, and the channel response was limited by the galvanometers. Those used at greater depths were more sensitive instruments with lower natural frequencies and were probably the limiting component of high-frequency response. Forturnately, at these depths, the input function had lost many of the higher frequencies in transmission.

Since the frequency response of the air pressure gages was very high—over 1,000 cps—the galvanometers were the limiting factor here.

The frequency response of the displacement gages is difficult to describe, since the rise time is a function of a signal magnitude and is different for positive and negative displacements. Previous experience with similar gages, however, indicates that the records obtained from a nuclear detonation have rates of change greatly lower than the minimum capability of the gage, where this capability is measured by abruptly releasing tension on the measuring wire. It is therefore believed that no correction for frequency response is required.

2.3.8 Calibration. Each gage was calibrated in the field after it had been connected to its associated cable and recording equipment and immediately prior to its final installation. Accelerometers were calibrated by the use of a spin table, which provided accelerations up to 200 g. Where accelerations greater than 200 g were anticipated, gages were calibrated up to this figure in the field, and this calibration was extrapolated on the basis of linearity checks made previously in the laboratory and by the manufacturer. Displacement gages were calibrated by the introduction of directly measured displacements.

In the calibration procedure, several deflections ranging from zero to well above the expected peak (where possible) were applied to each gage in sequence. Each galvanometer deflection was noted and recorded. In addition, the deflection caused by a synthesized calibrating signal injected into the gage was recorded. From the first deflections, a calibration curve of deflection versus input was constructed; the calibrating signal served to correct for any changes in sensitivity of the system between calibration and the final test, since an identical signal was injected in the final record about 10 seconds before zero time.

2.4 SEISMIC MEASUREMENTS

To assist the final interpretation of data from this project, seismic propagation velocities and their variation with depth, particularly in the first 100 feet, were measured

during the preparation phase of operations prior to the shots.

The holes drilled for gage placement were to be used for seismic measurements of vertical propagation velocity, but unfortunately an open hole could not be maintained in these formations, and it was necessary that casing be inserted immediately after drilling. This made it impossible to measure vertical velocities in the usual fashion. As an alternative, geophones were planted at two depths in one hole of each of the two arrays, at the same time that the other gages were planted. The hole used was at Station 3 on Cactus (Yvonne, Figure 2.1) and at Station 12 on Koa (Irene, Figure 2.2). After the hole was backfilled, measurements were made of the travel time to each of these depths from small shots at the surface. In addition, refraction profiles were shot with close geophone spacing, extending a few hundred feet. These measurements provided a measure of both vertical and horizontal propagation velocities in the shallow formations.

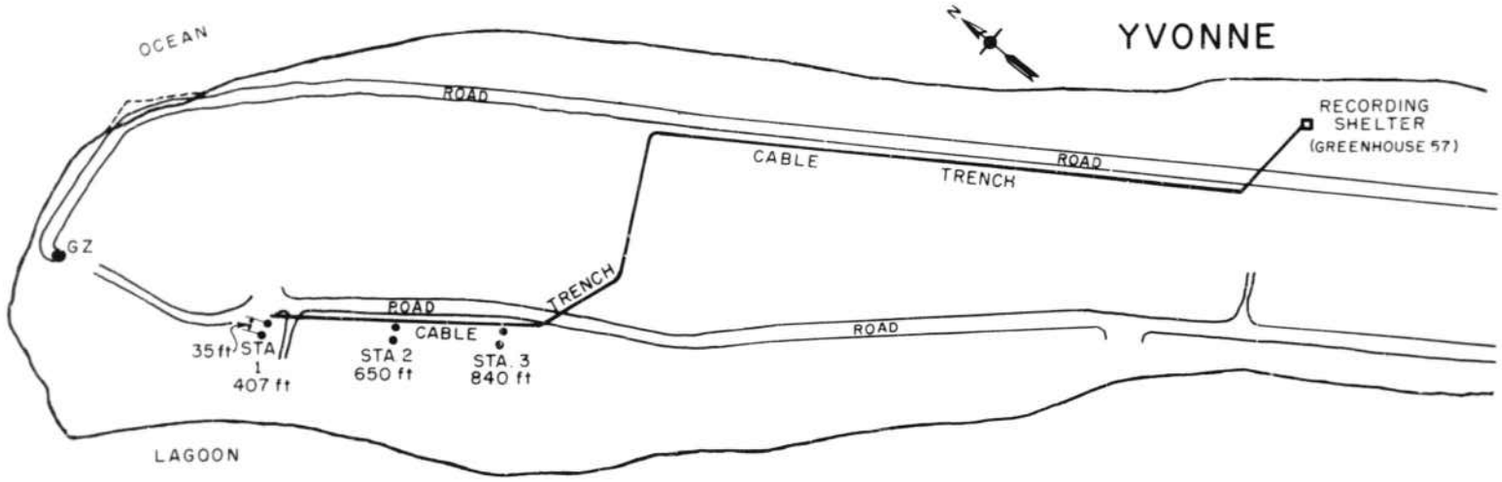

Figure 2.1 Station layout, Shot Cactus.

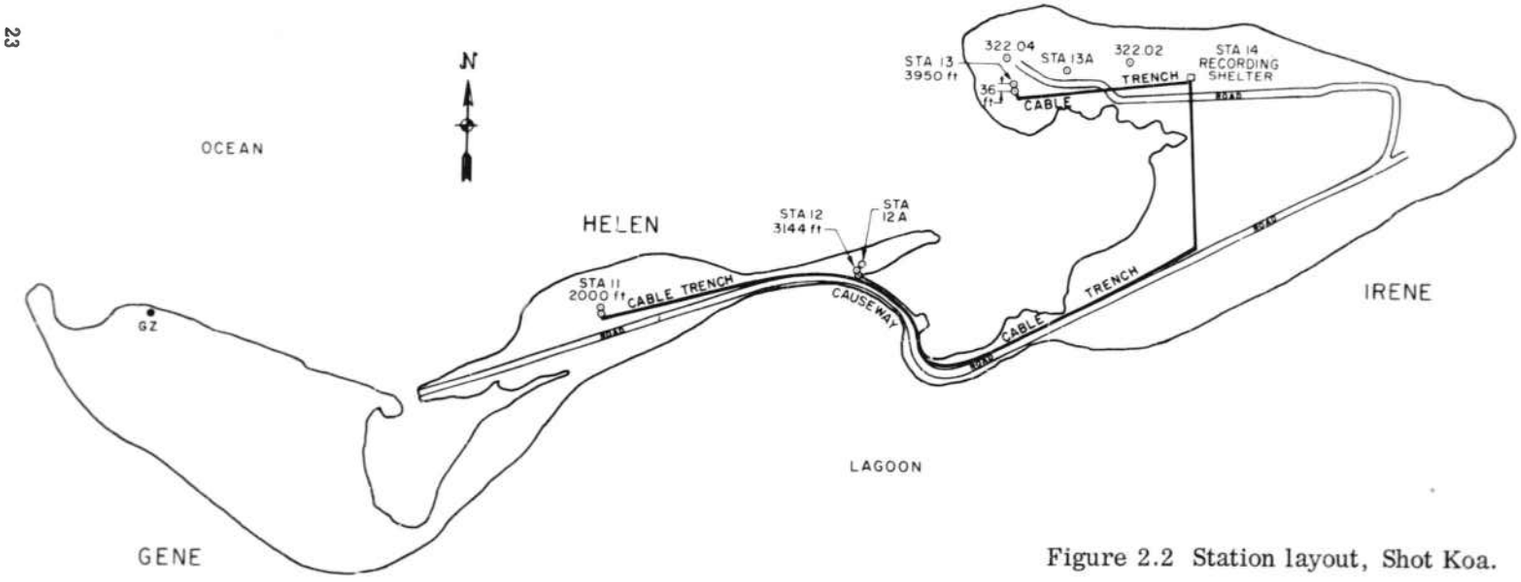

Figure 2.2 Station layout, Shot Koa.

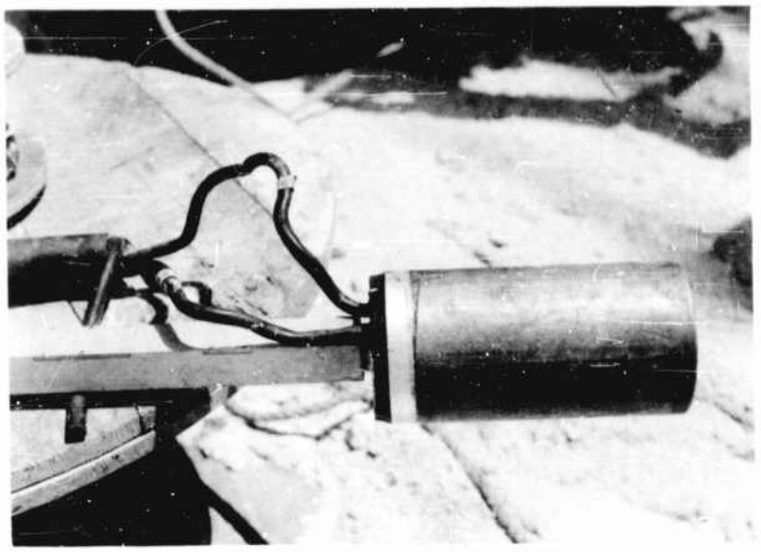

Figure 2.3 Accelerometer canister.

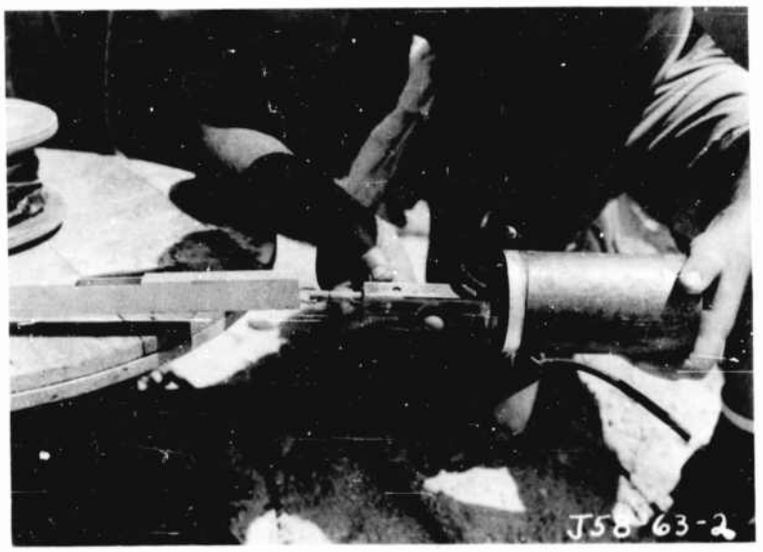

Figure 2.4 Attaching canister to positioning pole.

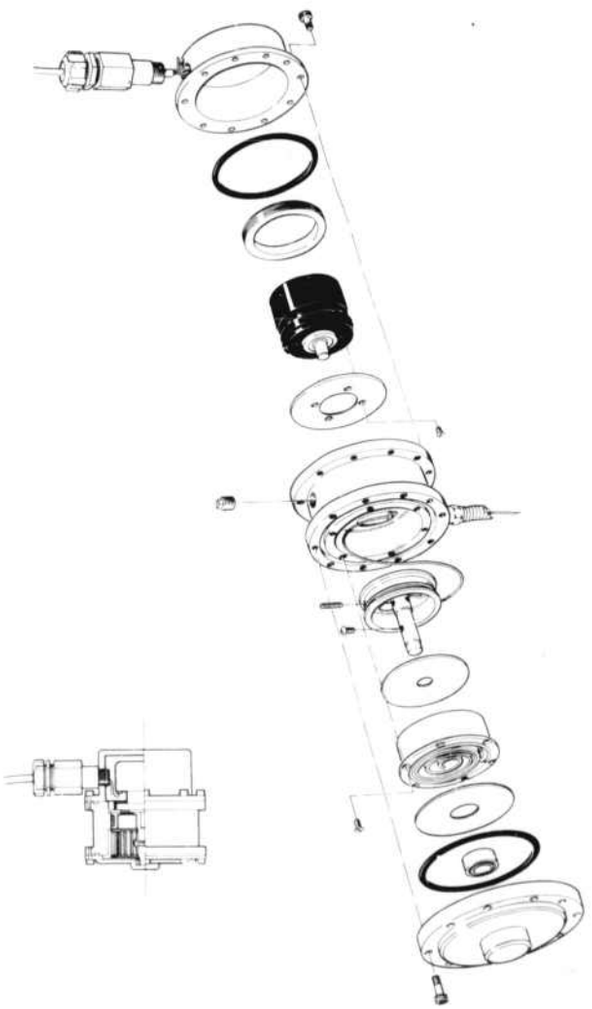

Figure 2.5 Sandia displacement gage, exploded view.

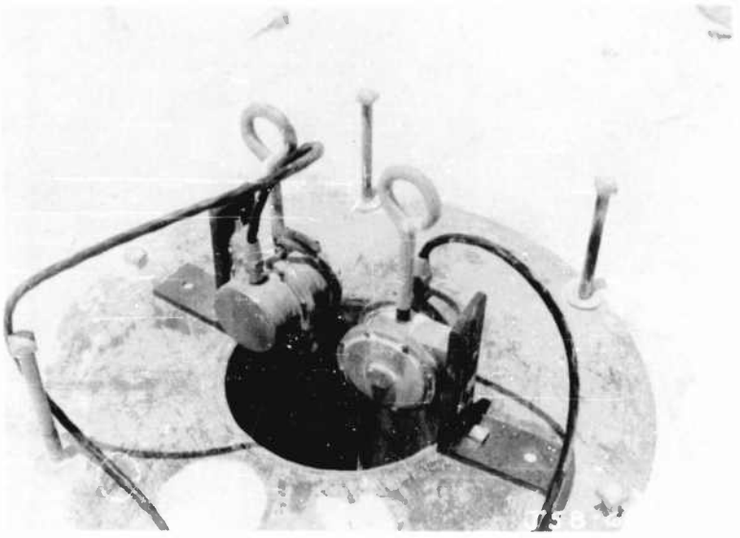

Figure 2.6 Sandia displacement gage, installed.

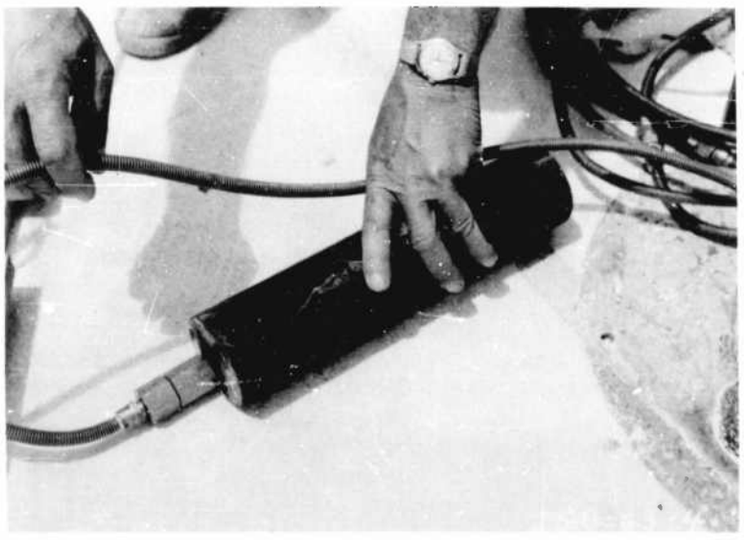

Figure 2.7 Displacement gage fixed anchor.

Chapter 3

PREDICTIONS

In planning an experiment of this type, it is necessary to predict the peak values of the functions to be measured with an accuracy sufficient to allow the sensitivity of each channel to be set closely enough so that satisfactory deflections will be obtained without overranging the recording equipment. For best results these sensitivities should be within a factor of 2 of the true value, but a factor of 3 is acceptable. A greater range is acceptable on channels where dual-sensitivity galvanometers are used. Early predictions are also important in the selection of gage ratings to insure that gages are not overranged, thereby introducing nonlinearities. Therefore, the predictions presented in this chapter are those upon which the experiment was based and reflect a best estimate of expected effects prior to the field tests.

Predictions for this purpose are somewhat different from those that formed the ultimate objective of this project. First, for range setting, only peak predictions were required; waveform and duration were of secondary importance, except as they affected the peak values of other functions. Second, the predictions of interest were those of the functions measured, not of derived functions that may be of greater interest and importance in the results. For example, peak acceleration may be of little interest to the structural designer —his interest is in the spectrum and in the waveform of the particle velocity. However, since the project was measuring acceleration to derive velocity, peak acceleration had to be predicted. The prediction methods described here were necessarily employed some 3 months before the shots and do not include some of the refinements developed since that time in the analysis of Plumbbob data (Reference 5).

3.1 AIRBLAST

Subsurface phenomena are assumed to be primarily a result of the overpressure appearing at the surface in the immediate vicinity of the station. Predictions of maximum air pressure versus ground range were used in the selection of station locations and in range setting of blast gages. It was necessary to make assumptions of probable yield for this purpose. From the best information available in January 1958, probable yields of 15 kt and 2 Mt were selected by the Program Director for Shots Cactus and Koa, respectively. Pressure-distance curves were constructed for these yields on the basis of the 1.6 W theory. This theory assumes from past experience that the pressure-distance curve from a surface burst of a given yield W is the same as that from a free-air burst of 1.6 W. Curves were drawn and distributed to the projects involved, and they formed the basis for the station locations selected. The limited land surface available on Shot Koa required some compromises in these locations, but similar locations were chosen for Shot Cactus to provide as much similarity as possible.

Other features of the airblast phenomena are of importance, since they affect the predictions of acceleration and displacement. The rise time of the blast wave is important. Examination of available data indicated that, if a precursor were to be formed on either of these shots, it would not markedly affect the rise time. Furthermore, since the majority

of the travel paths on Koa were over water, the probability of precursor formation at the gage stations was low. Subsurface predictions were therefore based on shock wave arrivals on both shots.

The duration of the blast wave is one of the variables whose effect forms a part of the objective. Since the scale ratio between Koa and Cactus was expected to be approximately 5:1, the time scale of events could be expected to differ by that ratio. At the pressure levels of interest, the pressure time curve does not resemble the simple exponential decay expected at low pressure levels. The early decay is much more rapid, that is, the exponent changes with time. For this reason, the positive-phase duration, defined as the time from first arrival to first crossover, is not the factor of chief interest. A better empirical description appears to be the time during which the pressure is greater than half the maximum pressure: this is denoted as t_s.

Data from Shot Priscilla of Operation Plumbbob and Shots Lacrosse and Blackfoot of Operation Redwing show considerable scatter, but, within the limits of 100 to 600 psi, they fit reasonably well the equation

$$t_s = 0.4\ \Delta p^{-0.7}\ W^{1/3}, \tag{3.1}$$

where Δp is the peak overpressure.

Blast wave arrival times may be of importance in underground effects. These can be derived from free-air data and the 1.6W theory.

The predicted parameters of the input airblast loading at each station are shown in Table 3.1.

3.2 SEISMIC VELOCITY AND OTHER SOIL PARAMETERS

As for seismic velocity, gage range settings were based on data available several months before the operation. More-up-to-date seismic velocity data was available only a short time before the first shot (Cactus), too late to allow gage settings to be changed.

Soil characteristics are of interest in this project only in the interpretation of measured differences between the phenomena at NTS and EPG. However, estimates of the nature of the medium are useful in the modification of available data to apply to EPG.

No reliable data has been found on the seismic velocity near the surface at EPG. Long-range refraction studies (Reference 21) have established that the deep layers have a seismic velocity of about 7,000 ft/sec, but the depth at which this velocity is reached is probably several hundred feet or more.

Drill hole logs show that the first few hundred feet are composed largely of saturated sands, with some boulders and thin layers of coral rock or submerged beach rock. Reference 22 assumes that the near-surface materials are a sand-water mixture—40 percent sand by volume—with a density of 1.7, or 106 lb/ft^3. Since sand has a much higher modulus than water, the modulus of this mixture would be about 5×10^5, and the seismic velocity would be about 4,000 ft/sec. The seismic velocity averaged over the first 50 feet at Frenchman Flat at NTS is about 2,060 ft/sec (Reference 5).

Above the water table, which varies with the tide, EPG soil is largely dry or unsaturated sand, with a very low modulus and a seismic velocity probably below 1,000 ft/sec. This layer varied from only 2 to 5 feet in thickness at the points of interest. Efforts were made to locate the surface gages as near the water table as possible without immersing them.

3.3 ACCELERATION

Peak acceleration caused by airblast is a complicated function of pressure, rise time,

and soil characteristics. Since these functions are not yet fully defined, acceleration predictions for this project were derived from empirical extrapolations of NTS data and from the few measurements previously made at EPG.

In one line of approach, acceleration measurements from Operations Plumbbob, Upshot/Knothole, and Tumbler/Snapper were tabulated in terms of $A/\Delta p_m$, the ratio of peak acceleration to maximum pressure, using only the data taken from nonprecursor input waveforms. There was observed no convincing variations of $A/\Delta p_m$ with pressure, but a very noticeable variation with depth. When the values were plotted as $A/\Delta p_m$ versus depth, the "best fit" straight line drawn through the points represented the equation.

$$A = 1.5\ \Delta p_m y^{-0.83}, \tag{3.2}$$

where y = depth in feet. In this study, there was observed no evident change of $A/\Delta p_m$ with Δp_m.

With data from Shot Lacrosse, Reference 23 derives the relation

$$A = 0.144\ \Delta p_m^{1.2}\ , \tag{3.3}$$

for accelerations measured at a depth of 2.5 feet, and from Shot Mike of Operation Ivy obtains

$$A = 0.042\ \Delta p_m \tag{3.4}$$

for accelerations measured at a depth of 17 feet.

If the variation of acceleration with depth is assumed to be proportional to y^n, then Equation 3.3 and 3.4 may be compared, considering their respective depths, to obtain

$$A = 0.26\ \Delta p_m^{1.2}\ y^{-0.66} \tag{3.5}$$

In Figure 3.1, the solid lines represent predictions of peak acceleration at depths of 1 to 100 feet from Equation 3.2, whereas the dotted lines are similar predictions from Equation 3.5. The differences between the two are evident, but the maximum ratio between the two is only slightly over 2:1 at 1-foot depth, and much less at other depths.

The differences between the two soils explain qualitatively the differences observed. Since the modulus of EPG soil is higher, smaller peak accelerations might be expected at shallow depths. NTS soil is probably more dissipative; therefore, the slope of peak acceleration with depth should be greater for that site.

On the other hand, the $y^{-0.66}$ in Equation 3.5 is based on only two depth points—2.5 and 17 feet—and those points are taken from shots of widely different yields. The pronounced change in characteristics to be expected at the water table might cause the slope to be much greater at depths of 1 to 5 feet, bringing the 1-foot points nearer to those of Equation 3.2.

A slight compromise between the two equations was used for range setting, following Equation 3.5 at depths from 10 to 100 feet but raising the 1-foot points slightly. The points are plotted in Figure 3.1 and are tabulated in Tables 3.2 and 3.3.

3.4 RELATIVE DISPLACEMENT

The relative displacement, or integrated strain, due to airblast loading, between the surface and depths of the order of 100 feet is a function of pressure, duration, and soil characteristics. The primary soil characteristic of importance is probably the effective dynamic modulus of compression, but this is almost certainly not the same as the modulus

calculated from seismic velocity, the evidence being that the measured strain is considerably greater than that calculated from this modulus and the applied stress. This conclusion is confirmed by calculations of the data available from this type of measurement during Operation Plumbbob (Reference 6).

It is probable that the effective modulus at EPG is somewhat higher than at NTS, because of water saturation of the formation. The predictions of relative displacement shown in Tables 3.2 and 3.3 are therefore somewhat of the "crystal ball" variety, being extrapolated from data from Reference 6 and then roughly halved to allow for the difference in effective modulus. These predictions were considered sufficiently accurate for range setting.

3.5 INDIRECT ARRIVALS

Predictions discussed in previous sections are based solely on the expected effects of the air pressure in the vicinity of the gages. Energy actually arrives by other paths, particularly by refraction from points closer to ground zero, but it is generally less than the direct arrivals. At close-in ground ranges, refracted arrivals are much later than direct arrivals. As the blast wave velocity decreases, the earth-transmitted signals catch up with and outrun the blast wave and become the first arrivals. In this case, the baseline for the events of greatest interest may be somewhat confused.

The point of outrunning is dependent on the time-distance curve of the blast wave and of seismic signals at the test location. The former can be predicted accurately for a given yield by composite data from other surface shots and from the free-air data and is shown for Koa (2 Mt) in Figure 3.2 and for Cactus (15 kt) in Figure 3.3. The seismic time-distance curve can be predicted only by some assumptions of near-surface velocities. Assuming 1,000 ft/sec for the first 5 feet, 4,000 ft/sec to 200 feet, and 7,000 ft/sec thereafter, the seismic curve shown in Figure 3.1 is obtained. To determine the outrunning point, the origin of this curve is moved along the airblast curve until a minimum is found. For Koa, this minimum is found with the origin in the vicinity of 2,000-foot ground range, and the indicated outrunning point is at 3,450-foot ground range. At Station 13 (100 psi), the earth wave is predicted to arrive some 80 msec before the airblast, and at the instrument shelter, some 220 msec earlier. On Cactus, from Figure 3.2, outrunning is predicted to occur at about 910-foot ground range beyond any of the gage stations.

These predictions refer to the surface arrival times. Since at depth, the earth wave will arrive earlier and the air-induced wave later, it appears that earth arrivals will be observed at all 100-foot gages except at Stations 1 (Cactus) and 11 (Koa).

TABLE 3.1 INPUT PREDICTIONS

Shot	Station	Ground Range	Maximum Overpressure (Δp)	Arrival Time (t_a)	Positive-Phase Duration * (t_s)
		feet	psi	sec	sec
Cactus	1	407	550	0.024	0.012
Cactus	2	650	195	0.072	0.025
Cactus	3	840	102	0.134	0.039
Cactus	Shelter	2,400	10	1.010	
Koa	11	2,000	600	0.121	0.058
Koa	12	3,144	220	0.328	0.117
Koa	13	3,950	125	0.555	0.176
Koa	Shelter	4,700	73	0.820	

* Time during which the pressure is greater than half the maximum pressure.

TABLE 3.2 GAGE RANGE SETTINGS, SHOT CACTUS

Ground Range	Gage	Predicted Peak	Gage Range	Natural Frequency
feet				eps
407	1B	550 psi	1,000	1,300
	1V1	750 g	1,000	1,300
	1V10	120 g	150	490
	1V30	55 g	150	490
	1V50	42 g	60	310
	1V100 NR	25 g	50	280
	1H10	40 g	60	310
	1H30	20 g	30	220
	1H50	15 g	30	220
	1H100	10 g	30	220
	1SV50 NR	5.3 inches		
	1SV100 NR	8.5 inches		
650	2B	195 psi	300	705
	2V1	220 g	500	900
	2V10	32 g	60	310
	2V30	16 g	30	220
	2V50 NR	10.5 g	30	220
	2V100	6.6 g	10	110
	2H10	12 g	30	220
	2H30	6 g	10	110
	2H50	5 g	10	110
	2H100	3.3 g	10	110
	2SV50 NR	1.75 inches		
	2SV100 NR	2.85 inches		
840	3B	102 psi	300	705
	3Va	105 g	150	490
	3V10	16 g	30	220
	3V30	10 g	30	220
	3V50	6 g	10	110
	3V100 NR	3.6 g	5	76
	3H10	6 g	10	110
	3H30	3.3 g	5	76
	3H50 NR	2.5 g	5	76
	3H100 NR	1.7 g	5	76
	3SV50	0.9 inch		
	3SV100 NR	1.5 inch		

NR, no record.

TABLE 3.3 GAGE RANGE SETTINGS, SHOT KOA

Ground Range	Gage	Predicted Peak	Gage Range	Natural Frequency
feet				cps
2,000	11B	600 psi	1,000	1,300
	11V1	800 g	1,000	1,300
	11V10	130 g	150	490
	11V30	60 g	150	490
	11V50	45 g	150	490
	11V100	27 g	50	280
	11H10	40 g	60	310
	11H30	20 g	30	220
	11H50	15 g	30	220
	11H100	10 g	30	220
	11SV50 (Replaced)	5.3 inches		
	11SV100	8.5 inches		
3,144	12B	220 psi	300	705
	12V1	250 g	500	900
	12V10	36 g	50	280
	12V30	18 g	50	280
	12V50	12 g	30	220
	12V100	7.5 g	10	110
	12H10	12 g	30	220
	12H30	7 g	10	110
	12H50	5 g	10	110
	12H100	3.3 g	10	110
	12SV50	4.5 cm		
	12SV100	7.2 cm		
3,950	13B	125 psi	300	705
	13V1	130 g	500	900
	13V10	20 g	50	280
	13V30	10 g	30	220
	13V50	7 g	10	110
	13V100 (Replaced)	4.2 g	10	110
	13H10	6 g	10	110
	13H30	3.3 g	5	76
	13H50	2.5 g	5	76
	13H100	1.7 g	5	76
	13SV50	2.4 cm		
	13SV100	4 cm		
4,700	14V1	5 psi		
	14H1	1.5 psi	5	76

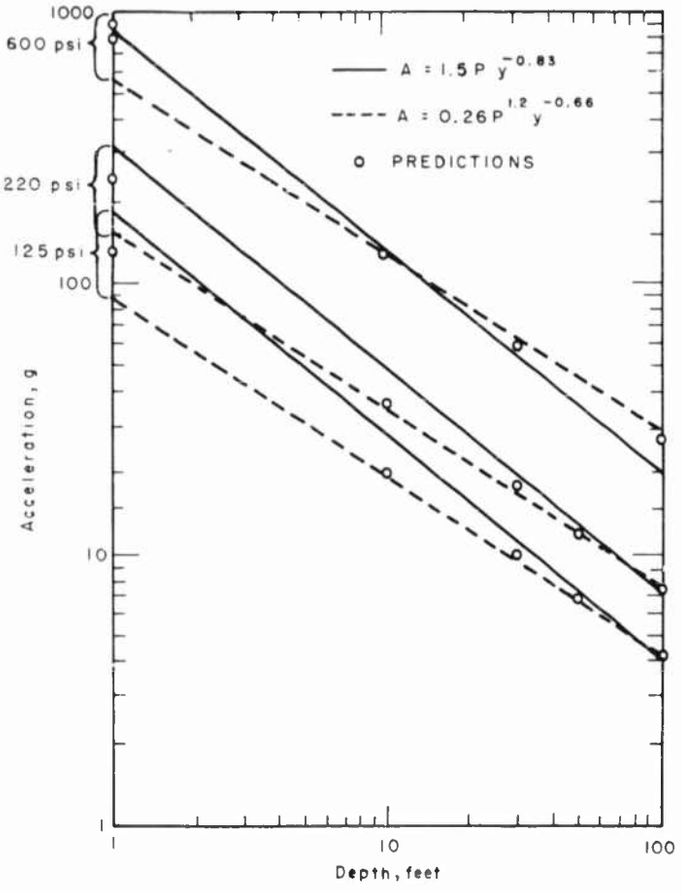

Figure 3.1 Predicted accelerations.

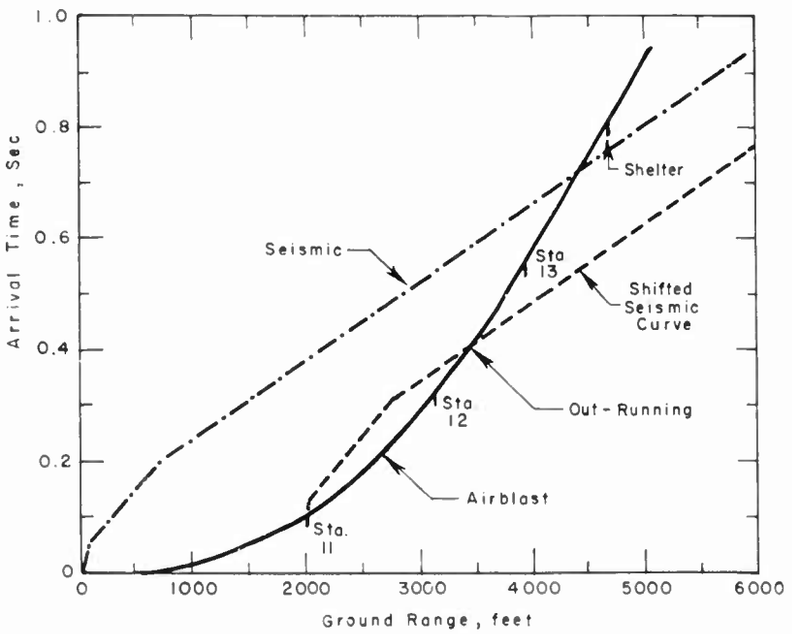

Figure 3.2 Predicted arrival times and outrunning, Shot Koa.

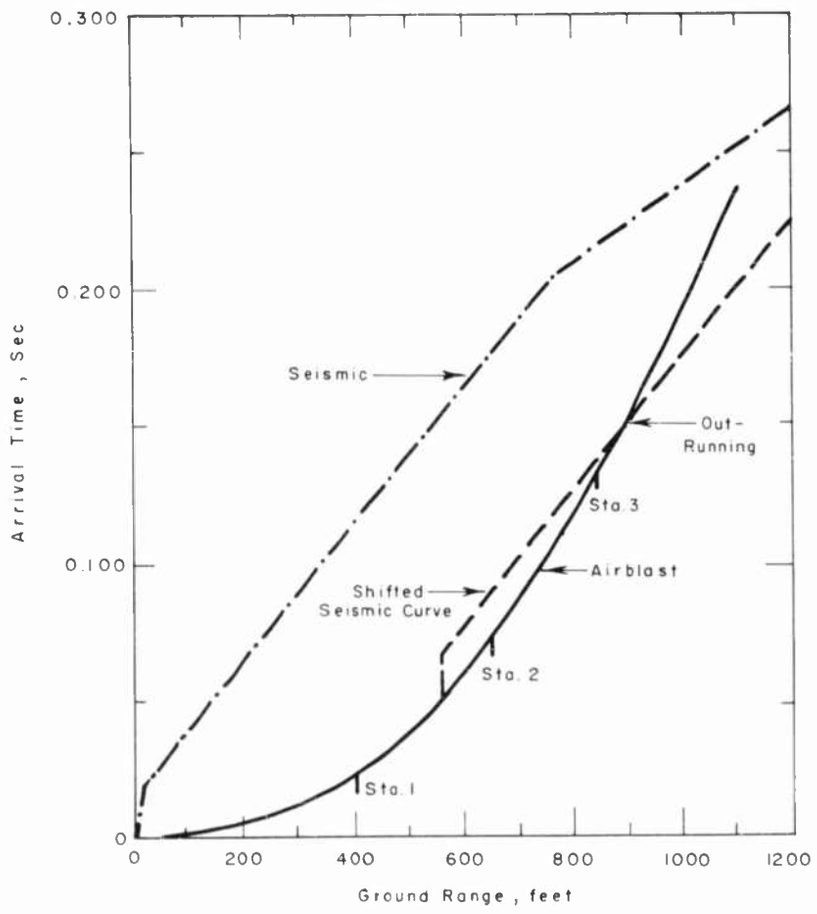

Figure 3.3 Predicted arrival times and outrunning, Shot Cactus.

Chapter 4

OPERATIONS AND RESULTS

4.1 OPERATIONS

Field operations for this project started on 13 March 1958, with the arrival of two men at EPG. The remainder of the party — seven men — arrived on 19 March. At that time, although Cactus was scheduled first, construction on Yvonne had not advanced sufficiently to start work for this shot. The party moved to the camp on Janet to start operations for Koa on Helen and Irene. Cables were laid, the central station equipment was set up, and part of the calibration was completed by 30 March. In the meantime, construction for Cactus had been expedited, and since an early firing date for that shot appeared probable, project operations were shifted to Yvonne.

By 17 April, preparations for Cactus were essentially complete, and a portion of the party moved back to Janet for continuation of operations on Koa. Installation and checkout for Cactus, including seismic measurement, were completed by 23 April. Work continued on Koa until 29 April, at which time it was necessary to evacuate the forward camps for the first scheduled firing date of Cactus. Between that time and 13 May, when Koa was shot, the party commuted from Elmer to the shot islands for field work on both shots.

No unusual problems were encountered with the preparations in general. The planting of the gages and strain gage anchors in the deep holes (Section 2.3.5) was quite time-consuming and required the full-time use of a crane and crew to pull lengths of casing at intervals as the gages were planted and the holes backfilled. For the two installations this required a total of 13 working days.

Cactus was fired on 6 May. Records were recovered on 7 May, and the central station equipment was recovered on 9 May with no unusual problems. Koa was fired on 13 May. Blocking of the door by sand and sandbags displaced from the top of the shelter, combined with high radiation levels, made early recovery impossible. On 16 May a bulldozer, provided with a shielded cab, cleared out the debris in front of the door, and the records and central station equipment were recovered on the same mission.

4.2 PERFORMANCE

4.2.1 Shot Cactus. Of the 36 gage channels installed on this shot, 26 produced records that were usable.

The remaining 10 appeared to be lost from a variety of causes. At least two of the deeply buried accelerometers had developed electrical leakage to ground after planting. These records contained noises that were obviously spurious and masked the real data. The circuits provided for protection of the central station equipment from the induction signal (Section 2.3.1) failed to operate, apparently because of failure to receive the −5 second relay timing signal. This failure was also shown by the multi-pen operational recorder installed for the purpose of tracing failures. This lack of protection caused overload of the demodulators of the Wiancko coupling units, producing noise and baseline shifts, and possibly causing the loss of some channels whose traces simply disappeared at zero time. In addition, a defective relay in one recorder caused intermittent dimming of the recording

lights, resulting in partial loss of some of the traces. Finally, only one of the relative displacement gages produced a usable record. The others suffered electrical or mechanical damage at or near zero time. A few of the traces extended beyond the boundaries of the recording paper, but estimates of peak readings could be made. It was reported that one of the wellhead covers was found sheared off its mount. This would have destroyed the two relative displacement gages it was supposed to protect. On this basis, the wellhead covers on Koa were welded to their mounts to increase the shear strength and to prevent this occurrence.

4.2.2 Shot Koa. Of the 36 gage channels installed on this shot, two failed electrically and one mechanically before the shot. One of the electrical failures (13V100) was caused by severe leakage to ground, the other (12V50) was caused by an open circuit in one side of the gage. The mechanical failure was the breakage of the actuating wire on the Displacement Gage 11SV50. An effort was made to save 12V50 by replacing the open side of the gage with a dummy at the surface, with suitable adjustment of the calibration factors. The other two were replaced by accelerometers in the instrument shelter, gage codes 14V1 and 14H1.

After the shot, it was found that six channels had failed to produce usable records. Among those which failed were 11V30, 11SV100, 12V50 (see above) and the associated 12H50, 13V1, and 13V50.

In summary, 30 usable channels were obtained, two of which were sutstitutes but of considerable value.

4.2.3 Auxiliary Equipment. The experimental magnetic-recording miniaturized equipment, located at two stations forward of the recording shelter on Koa, was not recovered at the same time as were the records and the equipment from the shelter. Later, on 19 May, a recovery party returned and recovered this equipment. (The outer canisters were left in place; they were "hot", apparently from the neutron-induced effects in the steel.) Both sets of this equipment operated as planned, and no mechanical damage was observed.

4.3 NUCLEAR DATA REDUCTION AND PRESENTATION

4.3.1 Record Reading and Processing. After each gage record was identified on the oscillograms, they were read (inches of deflection of record versus time) with an electromechanical reader, Benson-Lehner "Oscar" J. Acceleration records were read at 1-, 2-, and 5-msec intervals for Cactus and at ½-, 1-, 2-, 10-, and 20-msec intervals for Koa. Records were read to the end of the airblast positive phase or past the point of apparent signal, whichever was longer. The reader output was fed into an IBM card punch, which produced the data cards. These deflection versus time data cards, along with appropriate calibration cards, were processed by an IBM-650 electronic computer. The final reduced data came out in the form of parameter (e.g., acceleration) versus time listings corresponding to each gage record. These listings were then plotted to give data upon which this report is based.

4.3.2 Integration Procedure. The earth acceleration versus time records were succesively integrated to obtain, first, particle velocity versus time, and second, particle displacement versus time. It becomes apparent after only a few attempts at this integration process that there is a good deal of judgment involved in obtaining a meaningful result. Most integrations indicate, in varying degree, that the velocity at the end of the integration is not zero. This result can be interpreted as an acceleration record baseline shift, which is probably affected during reading of the record. If it can be assumed that there are no frequency response

problems (Chapter 2), the source of the difficulty can be traced to the character of the acceleration time waveform. The duration of the first acceleration peak is a small fraction of the total record length. Therefore, a small error, perhaps only 1 or 2 percent of the peak acceleration, will accumulate as time increases, to result in a significant error in velocity at the end of the integration.

Instrumentally, there are many possible ways the acceleration record baseline (zero signal reference) could shift. However, in this analysis the shift is considered as a reading error, a conclusion that is substantiated by the fact that the amount of correction that is necessary to achieve zero velocity at the end of the record is frequently within the least count of the reading equipment and by the fact that by keeping track of the places where the paper was shifted on the machine during reading it is possible to correlate these with the places where the baseline is shifted.

Each uncorrected velocity must be plotted and a best judgment made of the time when zero velocity is attained; thus, it is important that the acceleration-time record be read to times beyond which the signal apparently has settled down to small amplitudes.

Instead of arbitrarily making the velocity zero at the end of the overpressure, as was done on Shot Priscilla during Operation Plumbbob, zero velocity was assumed at that point on the record where there were no further oscillations of interest. The reason for this difference in procedure is that on Priscilla the blast wave was superseismic, but on Cactus and Koa the ground motion was generally outrunning, or close to it, indicating considerable refracted energy.

In summary then the integration procedure involves the following operations: (1) integration of the as-read acceleration-time record to obtain as-read velocity-time; (2) adjustment of the as-read velocity-time baseline to obtain zero velocity at an appropriate time called corrected velocity-time; (3) adjustment of the acceleration-time baseline to be consistent with the velocity-time adjustment cited in (2); and (4) integration of the adjusted velocity time record to obtain the displacement-time trace called corrected displacement-time.

The corrections as applied usually have little effect upon the as-read acceleration, more on the as-read velocity, and most upon the displacement.

The results of the Project 1.8 experiment are presented in terms of the corrected values only; maximum correction to acceleration was 7 percent with an average of 1.75 percent; corrections to velocity are shown on the figures.

4.4 NUCLEAR DATA PRESENTATION.

The measurements obtained on this project are presented as tabular listings of pertinent maximum values, times of maximum, and arrival times, along with plots of parameter versus time for each gage record. Late minor phenomena have been omitted from these plots to reduce their length. Time of arrival of the airblast first disturbance at the ground surface is noted on the traces by the symbol AB. On the gage record tracings in this report, downward motion is shown as positive and outward (away from ground zero) motion is also positive.

Some of the original records from Cactus are incomplete because of trouble with the recording lamps. Missing portions are reconstructed (dotted line) using the alternate records whenever available as guides.

4.4.1 Airblast Pressure. Ground range, maximum overpressure, arrival time, and positive-phase duration (Section 3.1) of each airblast measurement are shown in Table 4.1.

Questionable arrival times on Cactus were resolved by choosing a value on the basis of arrival times at the 1-foot accelerometer.

Tracings of the corrected airblast gage records for Cactus and Koa are given in Figures 4.1 and 4.16.

4.4.2 Acceleration. Tables 4.2 and 4.3 list the maximum values and times of evident interest taken from the vertical and horizontal acceleration records on the two shots. The complex nature of the records, compared with those obtained on airbursts at NTS, makes it difficult to follow specific peaks between records and to attribute a given deflection to a specific source, such as the local airblast effect.

Tracings of all acceleration records are presented in Figures 4.2 through 4.7 and 4.17 through 4.22. The peaks whose values are tabulated in the summary tables were indicated on these record tracings. Time of arrival of the airblast slap at the ground surface is noted on the traces by the symbol AB. It will be observed that the surface vertical accelerometers on Cactus exhibit severe ringing at about 300 cps, and these records were consequently not integrated. This was attributed to their being mounted on a heavy concrete slab, which served as a wellhead, and which may not have been supported at its center. On Koa, to avoid this ringing, these accelerometers were removed from the slab and planted alongside it.

The Cactus acceleration records (Figures 4.2 through 4.7) show that although at Station 1 it is possible to identify the main disturbance with the direct airblast slap, the same identification is rather nebulous at Stations 2 and 3. It appears that at the more remote stations, the earth-transmitted disturbances tend to mask the direct effects. The same general statements can be made concerning the Koa accelerations (Figures 4.17 through 4.22), particularly at gage depths greater than 10 feet.

Note that the acceleration-time records obtained on both shots exhibit random high-frequency, high-amplitude pulses, which arrive at late times and appear to travel upward toward the ground surface.

4.4.3 Velocity. Pertinent velocity measurements are given in Tables 4.2 and 4.3. The corrected velocity versus time plots are presented in Figures 4.8 through 4.11 and 4.23 through 4.30. The magnitude of the baseline correction necessary to obtain zero velocity at the end of the readable portion of the record is indicated on each curve; the dashed line designates the baseline of the as-read first integration.

For ease of comparison, the standard and alternate gage records are superimposed, with baseline corrections indicated on each. On the tracings, the dashed vertical line denotes a time scale damage.

4.4.4 Displacement. The corrected displacement versus time plots obtained from double integration of accelerometer records are given in Figures 4.12 through 4.14 and 4.31 through 4.36. Pertinent displacement measurements are given in Tables 4.2 and 4.3.

As in the velocity records, the standard and alternate gage records are superimposed, with baseline corrections indicated on each, and the dashed vertical line denotes a time scale change.

4.4.5 Relative Displacement. The maximum relative displacement and residual displacement of each record obtained is shown in Tables 4.2 and 4.3 and in Figures 4.15 and 4.37. The general form of these records is a rise to near maximum in 15 to 20 msec, (first major peak) followed by a long flat portion or a slight rise (second major peak) and a drop to a minimum, then a rise to a residual value. In the one record obtained from Cactus (Station 3), the minimum and residual were actually negative (representing an increased distance between the gage and the anchor).

4.5 SEISMIC DATA

4.5.1 Shot Cactus. At Station 3 (ground range, 840 feet) on Yvonne two geophones were planted at depths of 21.6 and 98.1 feet (Section 2.4). Measured travel times from a dynamite shot buried 2.5 feet from these detectors were 4 and 15 msec, respectively. Their travel times correspond to average vertical velocities of 4,800 ft/sec for the first 20 feet, and 6,950 ft/sec for the interval from 20 to 100 feet.

The results of the refraction profile also shot near this station are shown in Figure 4.38. From ground ranges of about 100 to 400 feet, the slope of the time-distance curve corresponds to an average velocity Vc_2 of 7,880 ft/sec. At shorter ranges than 100 feet, there is some scattering of data apparently due to the presence of thin layers of high- and low-velocity material, but the apparent average velocity Vc_1 is 4,950 ft/sec.

The change in slope or break in the time-distance curve corresponds to the refracted seismic wave traveling through the higher velocity material underlying the seismic profile. The depth to this high-velocity layer (time intercept, 17.0 msec) is computed to be approximately 21 feet. These results are entirely consistent with the vertical velocity measurements, since layering of the formations and the different paths of transmission of the seismic wave could readily account for the different velocities computed by the two methods. The intercept of the lower velocity slope (4,950 ft/sec) at a time of 7.5 msec indicates very shallow low-velocity layers having velocities of around 800 to 4,000 ft/sec. This probably corresponds to the dry material above the water table, 4.5 to 6 feet in depth at the point of measurement, which consists of loose sand, eroded coral, and shells.

4.5.2 Shot Koa. Two geophones were planted in the abandoned hole at Station 12 (ground range, 3,144 feet) at depths of 35 and 102 feet. When charges were fired at a depth of 2 feet, it was found that the travel time measured yielded interval velocities that were too high to be acceptable. It could only be concluded that, during the process of pulling the casing, the geophones were displaced upward from their original depths.

The results of the refraction profile shot between Stations 11 and 12 are shown in Figure 4.38. From ground ranges of about 70 feet to 400 feet, the slope of the time-distance curve corresponds to an average velocity Vk_2 of 7,690 ft/sec.

The slope of this portion of the curve was determined from the time differential Δt between the 300- and 400-foot range and projected back to the intercept. At ranges shorter than 70 feet the average velocity Vk_1 is 5,000 ft/sec.

The depth to the high-velocity layer (time intercept, 8.2 msec) is computed to be approximately 9 feet. The intercept of the low-velocity slope at a time of only 315 msec indicates that the loose unconsolidated material on Irene was shallower than that on Yvonne. Also, it consisted of layered material having velocities of from 800 to 3,900 ft/sec as is shown by the time-travel curves (Figure 4.39) of a very short refraction spread using only a blasting cap as the source of seismic energy.

No correlation of the various sand, coral, or shell layers can be made from the drillers logs supplied by Holmes and Narver. The material apparently is not consistent to any lateral extent and is not consistent in any direction more than a few feet or tens of feet.

TABLE 4.1 AIR PRESSURE, SHOTS CACTUS AND KOA

Shot	Gage	Ground Range	Arrival Time	Maximum Overpressure	Time of Maximum	Impulse	Duration*
		ft	sec	psi	sec	psi-sec	sec
Cactus	1B	407	0.016	164	0.036	7.32	0.196
	2B	650	0.057	211	0.063	8.21	0.231
	3B	840	0.116	104	0.119	5.78	0.277
Koa	11B	2,000	0.1205	978	0.1230	50.03	0.850
	11BA	2,000	0.1205	997	0.1225	47.37	0.850
	12B	3,144	0.3590	239	0.3615	25.71	1.000
	12BA	3,144	0.3590	251	0.3615	30.00	1.000
	13B	3,950	0.640	91.3	0.644	17.60	1.200
	13BA	3,950	0.640	94.7	0.644	17.78	1.200
				A-Scaled			
Cactus	1B	158	0.00635	165		2.91	0.0776
	2B	253	0.0226	212		3.27	0.0913
	3B	327	0.0461	104		2.30	0.110
Koa	11B	180	0.01104	981		4.59	0.0778
	11BA	180	0.01104	1,000		4.34	0.0778
	12B	283	0.0329	240		2.36	0.0916
	12BA	283	0.0329	252		2.75	0.0916
	13B	355	0.0586	91.4		1.62	0.110
	13BA	355	0.0586	95.0		1.63	0.110

* Not necessarily total positive phase duration; arbitrarily selected for calculation of impulse.

TABLE 4.2 CORRECTED ACCELERATION, VELOCITY, AND DISPLACEMENT, SHOT CACTUS

Gage	Ground Range	Gage Depth	Arrival Time	Acceleration								Velocity		Displacement	
				First Maxima				Second Maxima		Third Maxima		Max	Time	Max	Time
				Pos	Time	Neg	Time	Accel	Time	Accel	Time				
	ft	ft	sec	g	sec	g	sec	g	sec	g	sec	ft/sec	sec	ft/sec	sec
1V1	407	1	0.014	525	0.054	1,197	0.031	–	–	–	–	*	–	*	–
1V10A	407	10	0.022	29.4	0.040	64.0	0.028	−62.3	0.075	20.4	0.078	−8.62	0.031	−0.264	0.230
1V30A	407	30	0.023	6.41	0.075	17.8	0.071	−6.37	0.126	9.49	0.130	−5.52	0.074	−0.389	0.205
1V50	407	50	0.026	25.9	0.029	16.4	0.068	2.85	0.120	−4.05	0.124	−3.48	0.078	−0.132	0.188
1V100	NR														
1H10	407	10	0.022	42.1	0.023	17.4	0.027	−8.47	0.064	15.3	0.069	2.09	0.025	0.108	0.220
1H30	407	30	0.023	16.4	0.025	10.4	0.064	18.1	0.124	−14.3	0.128	1.60	0.029	*	–
1H50	407	50	0.026	15.9	0.028	6.30	0.039	1.36	0.116	−1.61	0.118	3.28	0.079	*	–
1H100	407	100	0.031	27.4	0.063	27.3	0.068	−2.31	0.136	–	–	5.92	0.067	0.226	0.495
2V1	650	1	0.057	124	0.059	40.4	0.065	–	–	–	–	13.5	0.081	*	–
2V10	650	10	0.057	33.3	0.109	47.2	0.072	−72.0	0.136	−15.4	0.154	−12.3	0.084	−0.418	0.204
2V30	650	30	0.056	5.74	0.073	7.12	0.098	−20.7	0.131	−12.1	0.133	1.63	0.077	−0.205	0.465
2V50	NR														
2V100	650	100	0.061	1.15	0.143	1.60	0.096	–	–	–	–	†	–	†	–
2H10	650	10	0.055	2.83	0.065	2.03	0.069	–	–	–	–	0.457	0.067	0.031	0.232
2H30	650	30	0.057	7.54	0.066	2.02	0.070	−2.97	0.100	5.59	0.107	1.44	0.103	0.317	0.475
2H50	650	50	0.057	8.73	0.066	4.35	0.070	−5.86	0.098	8.04	0.108	2.66	6.103	0.537	0.490
2H100	650	100	0.057	6.09	0.066	5.84	0.073	−7.88	0.098	9.35	0.106	2.82	0.102	0.498	0.520
3V1	840	1	0.116	162	0.120	101	0.123	–	–	–	–	*	–	*	–
3V10	840	10	0.085	24.0	0.140	52.7	0.128	−9.80	0.150	5.42	0.157	−6.69	0.132	−0.089	0.157
3V30	840	30	0.088	4.48	0.130	2.28	0.118	−2.02	0.151	3.27	0.172	1.21	0.204	−0.159	0.590
3V50	840	50	0.091	2.03	0.142	2.37	0.122	1.58	0.176	0.532	0.204	−1.45	0.135	−0.119	0.575
3V100	NR														
3H10	840	10	0.071	3.27	0.125	1.75	0.121	−3.12	0.138	2.33	0.144	1.11	0.141	0.180	0.415
3H30	840	30	0.084	4.74	0.126	4.50	0.145	−0.958	0.202	–	–	2.12	0.132	0.234	0.600
3H50	NR														
3H100	NR														

				Relative Displacement	
				inch	time (sec)
3SV50A	840	50	0.120	0.882	0.150
				0.838	0.191
1SV50					
1SV100					
2SV50		NR ‡			
2SV100					
3SV100					

* Gage not integrated. † Integration not valid. ‡ No record.

TABLE 4.3 CORRECTED ACCELERATION, VELOCITY, AND DISPLACEMENT, SHOT KOA

Gage	Gage Depth	Ground Range	Arrival Time	First Maxima				Second Maxima				Acceler		
				Pos	Time	Neg	Time	Pos	Time	Neg	Time			
	ft	ft	sec	g	sec	g	sec	g	sec	g	sec			
11V1	1	2,000	0.1225	1,114.	0.1240	289	0.1255	NRI*		16	0.32-0.33			
11V10	10	2,000	0.1250	67.3	0.1280	32.1	0.1325	5.1	0.353	6.2	0.327			
11V10A	10	2,000	0.1250	65.2	0.1280	35.4	0.1330	4.2	0.343	5.7	0.320			
11V50	50	2,000	0.1255	47.8	0.1310	22.4	0.1375	5.2	0.360	7.2	0.324	−9.2	0.415	
11V100	100	2,000	0.1240	5.23	0.1275	8.30	0.1295	0.45	0.332	0.36	0.344	NRI	–	
11V100A	100	2,000	0.1240	5.26	0.1275	9.74	0.1290	1.68	0.342	NRI	–	NRI	–	
11H10	10	2,000	0.1245	40.7	0.1280	21.1	0.1325	1.3	0.340	1.60	0.333	1.3	0.602	
11H10A	10	2,000	0.1245	40.6	0.1275	21.2	0.1325	2.3	0.344	0.96	0.332	0.82	0.602	
11H30	30	2,000	0.1260	38.1	0.1300	26.7	0.1350	1.90	0.325	5.7	0.333	2.5	0.401	
11H30A	30	2,000	0.1270	36.9	0.1310	26.4	0.1355	2.0	0.326	5.7	0.334	2.6	0.402	
11H50	50	2,000	0.1230	19.7	0.1440	12.2	0.1305	7.3	0.334	4.1	0.324	4.1	0.400	
11H100	100	2,000	0.1240	1.10	0.1310	4.72	0.1290	NRI	–	–	–	–	–	
11H100A	100	2,000	0.1235	1.04	0.1270	3.84	0.1285	NRI	–	–	–	–	–	
12V1	1	3,144	0.3175	337	0.3640	83.9	0.3670	NRI	–	6.5	0.536			
12V1A	1	3,144	0.3160	445	0.3640	101	0.3660	NRI	–	7.0	0.522			
12V10	10	3,144	0.2900	18.1	0.3670	4.7	0.3880	3.9	0.536	1.6	0.580			
12V10A	10	3,144	0.2905	17.3	0.3670	4.7	0.3870	3.4	0.536	1.6	0.582			
12V30	30	3,144	0.2850	3.94	0.3720	3.38	0.3485	1.4	0.602	2.4	0.537			
12V30A	30	3,144	0.2855	3.83	0.3715	3.15	0.3485	1.4	0.604	2.5	0.536			
12V100	100	3,144	0.2880	1.18	0.3930	0.81	0.3155	1.13	0.597	1.43	0.535			
12V100A	100	3,144	0.2910	1.12	0.3930	0.72	0.3170	1.20	0.599	1.20	0.535			
12H10A	10	3,144	0.2940	7.38	0.3700	5.52	0.3790		–		–			
12H30	30	3,144	0.2800	5.29	0.3685	2.04	0.3400	1.96	0.531	1.65	0.444			
12H30A	30	3,144	0.2800	5.37	0.3685	2.00	0.3400	2.00	0.531	1.60	0.444			
12H100	100	3,144	0.2725	1.90	0.3440	2.14	0.3235	3.00	0.527	1.04	0.503			
13V10	10	3,950	0.4080	10.03	0.6760	8.94	0.664	2.48	0.802	16.96	0.783			
13V10A	10	3,950	0.4080	9.91	0.6760	9.13	0.664	2.52	0.802	17.14	0.784			
13V30	30	3,950	0.4040	2.63	0.6600	1.25	0.624	NRI	–	6.96	0.781			
13V30A	30	3,950	0.4040	2.76	0.6600	1.41	0.624	NRI	–	7.14	0.780			
13H10	10	3,950	0.5360	2.63	0.6520	2.29	0.660	0.68	0.786	1.10	0.785			
13H30	30	3,950	0.3900	2.14	0.6520	0.91	0.728	4.22	0.782	3.32	0.789			
13H50	50	3,950	0.3920	0.97	0.6500	1.10	0.676	3.32	0.779	1.76	0.793			
13H50A	50	3,950	0.3920	0.91	0.6500	1.13	0.674	3.35	0.779	1.78	0.792			
13H100	100	3,950	0.2440	0.74	0.6500	0.93	0.668	1.85	0.771	2.08	0.800			
13H100A	100	3,950	0.2440	0.74	0.6500	0.94	0.668	1.85	0.771	2.07	0.800			
14V1A	1	4,700	0.516	1.96	1.012	1.17	0.886							
14H1A	1	4,700	0.532	2.85	0.984	1.44	1.002							

				Relative Displacement	
				in	sec
11SV50	50	2,000	NR†		
11SV100	100	2,000	NR		
12SV50A	50	3,144	0.272	2.57	0.342
12SV100A	100	3,144	0.272	2.73	0.762
13SV50A	50	3,950	0.644	−1.73	1.580
13SV100A	100	3,950	0.644	−2.19	1.480

* No record. † Not readily identifiable.

KOA

2

Acceleration								Velocity								
Second Maxima			Third Maxima		Fourth Maxima		Maximum Positive	Time	Maximum Negative	Time	Velocity Jump	Maximum Positive		mum tive	Tim
Pos	Time	Neg	Time	Accel	Time	Accel	Time									
g	sec	g	sec	g	sec	g	sec	ft/sec	sec	ft/sec	sec		ft			sec
NRI*		16	0.32-0.33	-38.2	0.408	NRI	–	45.2	0.1245	14.3	0.4145	45.2	0.22			0.6
5.1	0.353	6.2	0.327	-15.6	0.405	-14.7	0.602	5.49	0.1285	4.06	0.3330	5.49	0.04	0.138	0.22	0.3
4.2	0.343	5.7	0.320	-14.8	0.405	-13.2	0.602	5.63	0.1295	3.35	0.3330	5.63	0.04	0.139	0.15	0.4
5.2	0.360	7.2	0.324	-9.2	0.415	-9.8	0.610	6.07	0.1350	5.10	0.4940	6.02	0.23	0.296	0.93	1.3
0.45	0.332	0.36	0.344	NRI	–	NRI	–	1.04	0.2630	–	–	0.20	0.20	0.464	–	–
1.68	0.342	NRI	–	NRI	–	NRI	–	0.85	0.2580	–	–	0.20	0.14	0.462	–	–
1.3	0.340	1.60	0.333	1.3	0.602								14.5	2.320	–	–
2.3	0.344	0.96	0.332	0.82	0.602								15.4	2.22	–	–
1.90	0.325	5.7	0.333	2.5	0.401	2.0	0.600	5.02	0.1330	0.52	0.514		0.43	1.08	–	–
2.0	0.326	5.7	0.334	2.6	0.402	2.1	0.600	4.96	0.1340	0.57	0.514		0.33	1.18	–	–
7.3	0.334	4.1	0.324	4.1	0.400	3.0	0.614	2.52	0.1480	1.11	0.328		0.76	0.868	–	–
NRI	–	–	–	–	–	–	–	0.99	0.5680	0.57	0.378		0.167	0.950	0.09	0.4
NRI	–	–	–	–	–	–	–	0.78	0.5760	0.31	0.356		–		0.07	0.4
NRI	–	6.5	0.536					20.5	0.3660	1.15	0.3320	20.2	–		0.93	0.5
NRI	–	7.0	0.522					23.7	0.3650	0.99	0.3320	23.3	–		0.89	0.5
3.9	0.536	1.6	0.580					5.26	0.3850	2.76	0.888		0.66	1.22	0.34	0.6
3.4	0.536	1.6	0.582					4.61	0.3850	2.61	0.884		0.84	1.22	0.22	0.6
1.4	0.602	2.4	0.537					1.19	0.4520	1.79	0.566		0.124	0.940	0.056	0.6
1.4	0.604	2.5	0.536					0.92	0.4510	1.97	0.565		–	–	0.123	0.6
1.13	0.597	1.43	0.535					1.07	0.724	1.22	0.573		0.138	1.060	0.026	0.6
1.20	0.599	1.20	0.535					1.07	0.720	1.22	0.574		0.098	0.874	0.035	0.6
	–		–					2.98	0.494	–	–		1.30	1.38	–	–
1.96	0.531	1.65	0.444					2.86	0.636	–	–		1.78	1.42	–	–
2.00	0.531	1.60	0.444					2.84	0.559	–	–		1.99	1.46	–	–
3.00	0.527	1.04	0.503					2.30	0.898	–	–		1.42	1.47	–	–
2.48	0.802	16.96	0.783					2.46	0.782	5.24	0.668		–	–	0.40	0.5
2.52	0.802	17.14	0.784					2.56	0.782	5.51	0.668		–	–	0.44	0.5
NRI	–	6.96	0.781					3.26	0.778	1.99	0.640		0.44	1.74	0.20	0.5
NRI	–	7.14	0.780					3.05	0.778	2.01	0.640		0.29	1.18	0.20	0.5
0.68	0.786	1.10	0.785					0.663	0.656	0.38	1.02		0.08	0.832		
4.22	0.782	3.32	0.789					1.89	0.692				0.73	1.60		
3.32	0.779	1.76	0.793					1.75	0.660	0.16	1.62		0.76	2.06		
3.35	0.779	1.78	0.792					1.76	0.660	0.18	1.62		0.79	1.56		
1.85	0.771	2.08	0.800					0.97	0.778	0.44	0.514		0.27	1.18		
1.85	0.771	2.07	0.800					0.97	0.778	0.44	0.514		0.27	1.18		
								1.42	0.854	1.11	0.724		0.05	1.200	0.14	0.7
								0.91	1.53	1.98	0.992		0.42	1.23	–	

SECRET

ation				Velocity					Displacement				
Third Maxima		Fourth Maxima		Maximum Positive	Time	Maximum Negative	Time	Velocity Jump	Maximum Positive	Time	Maximum Negative	Time	
Accel	Time	Accel	Time										
g	sec	g	sec	ft/sec	sec	ft/sec	sec		ft	sec	ft	sec	
−38.2	0.408	NRI	–	45.2	0.1245	14.3	0.4145	45.2	0.22	0.303	2.50	0.612	
−15.6	0.405	−14.7	0.602	5.49	0.1285	4.06	0.3330	5.49	0.04	0.138	0.22	0.375	
−14.8	0.405	−13.2	0.602	5.63	0.1295	3.35	0.3330	5.63	0.04	0.139	0.15	0.438	
−9.2	0.415	−9.8	0.610	6.07	0.1350	5.10	0.4940	6.02	0.23	0.296	0.93	1.32	
NRI	–	NRI	–	1.04	0.2630	–	–	0.20	0.20	0.464	–	–	
NRI	–	NRI	–	0.85	0.2580	–	–	0.20	0.14	0.462	–	–	
1.3	0.602								14.5	2.320	–	–	
0.82	0.602								15.4	2.22	–	–	
2.5	0.401	2.0	0.600	5.02	0.1330	0.52	0.514		0.43	1.08	–	–	
2.6	0.402	2.1	0.600	4.96	0.1340	0.57	0.514		0.33	1.18	–	–	
4.1	0.400	3.0	0.614	2.52	0.1480	1.11	0.328		0.76	0.868	–	–	
–	–	–	–	0.99	0.5680	0.57	0.378		0.167	0.950	0.09	0.446	
–	–	–	–	0.78	0.5760	0.31	0.356		–		0.07	0.446	
				20.5	0.3660	1.15	0.3320	20.2	–		0.93	0.568	
				23.7	0.3650	0.99	0.3320	23.3	–		0.89	0.568	
				5.26	0.3850	2.76	0.888		0.66	1.22	0.34	0.616	
				4.61	0.3850	2.61	0.884		0.84	1.22	0.22	0.604	
				1.19	0.4520	1.79	0.566		0.124	0.940	0.056	0.626	
				0.92	0.4510	1.97	0.565		–	–	0.123	0.624	
				1.07	0.724	1.22	0.573		0.138	1.060	0.026	0.620	
				1.07	0.720	1.22	0.574		0.098	0.874	0.035	0.622	
				2.98	0.494	–	–		1.30	1.38	–	–	
				2.86	0.636	–	–		1.78	1.42	–	–	
				2.84	0.559	–	–		1.99	1.46	–	–	
				2.30	0.898	–	–		1.42	1.47	–	–	
				2.46	0.782	5.24	0.668		–	–	0.40	0.688	
				2.56	0.782	5.51	0.668		–	–	0.44	0.690	
				3.26	0.778	1.99	0.640		0.44	1.74	0.20	0.678	
				3.05	0.778	2.01	0.640		0.29	1.18	0.20	0.680	
				0.663	0.656	0.38	1.02		0.08	0.832			
				1.89	0.692				0.73	1.60			
				1.75	0.660	0.16	1.62		0.76	2.06			
				1.76	0.660	0.18	1.62		0.79	1.56			
				0.97	0.778	0.44	0.514		0.27	1.18			
				0.97	0.778	0.44	0.514		0.27	1.18			
				1.42	0.854	1.11	0.724		0.05	1.200	0.14	0.782	
				0.91	1.53	1.98	0.992		0.42	1.23	–		

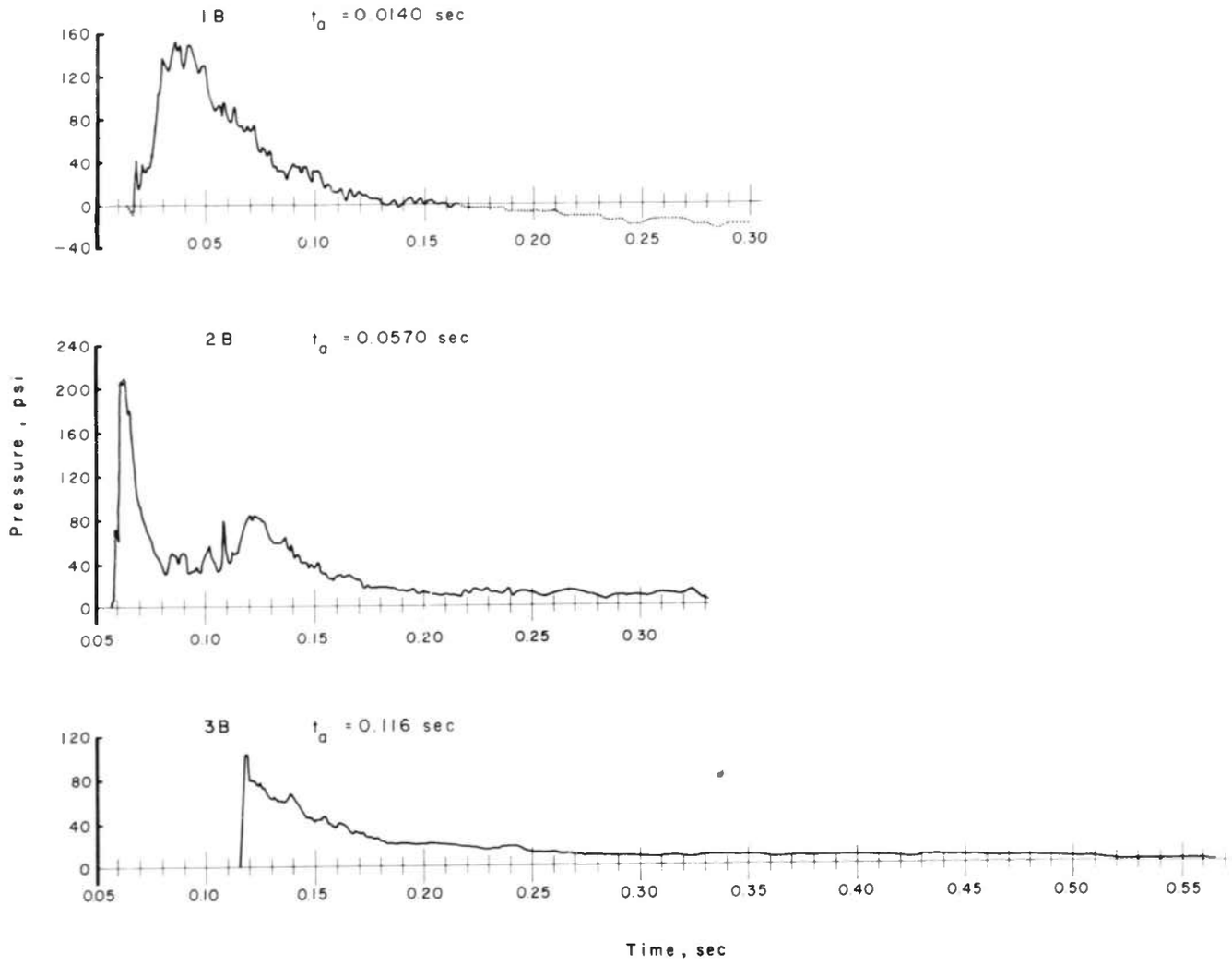

Figure 4.1 Overpressure versus time, Stations 1 through 3, Shot Cactus.

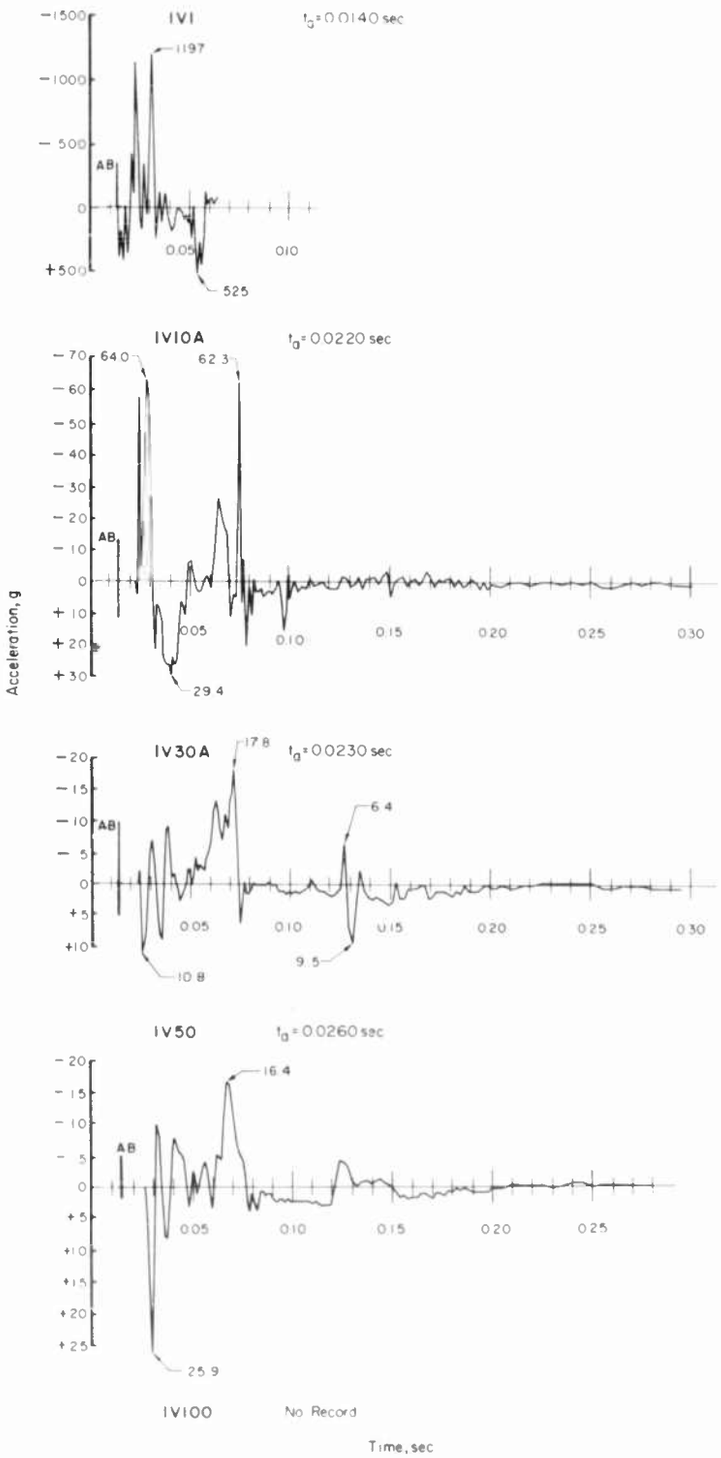

Figure 4.2 Vertical acceleration versus time, Station 1, Shot Cactus.

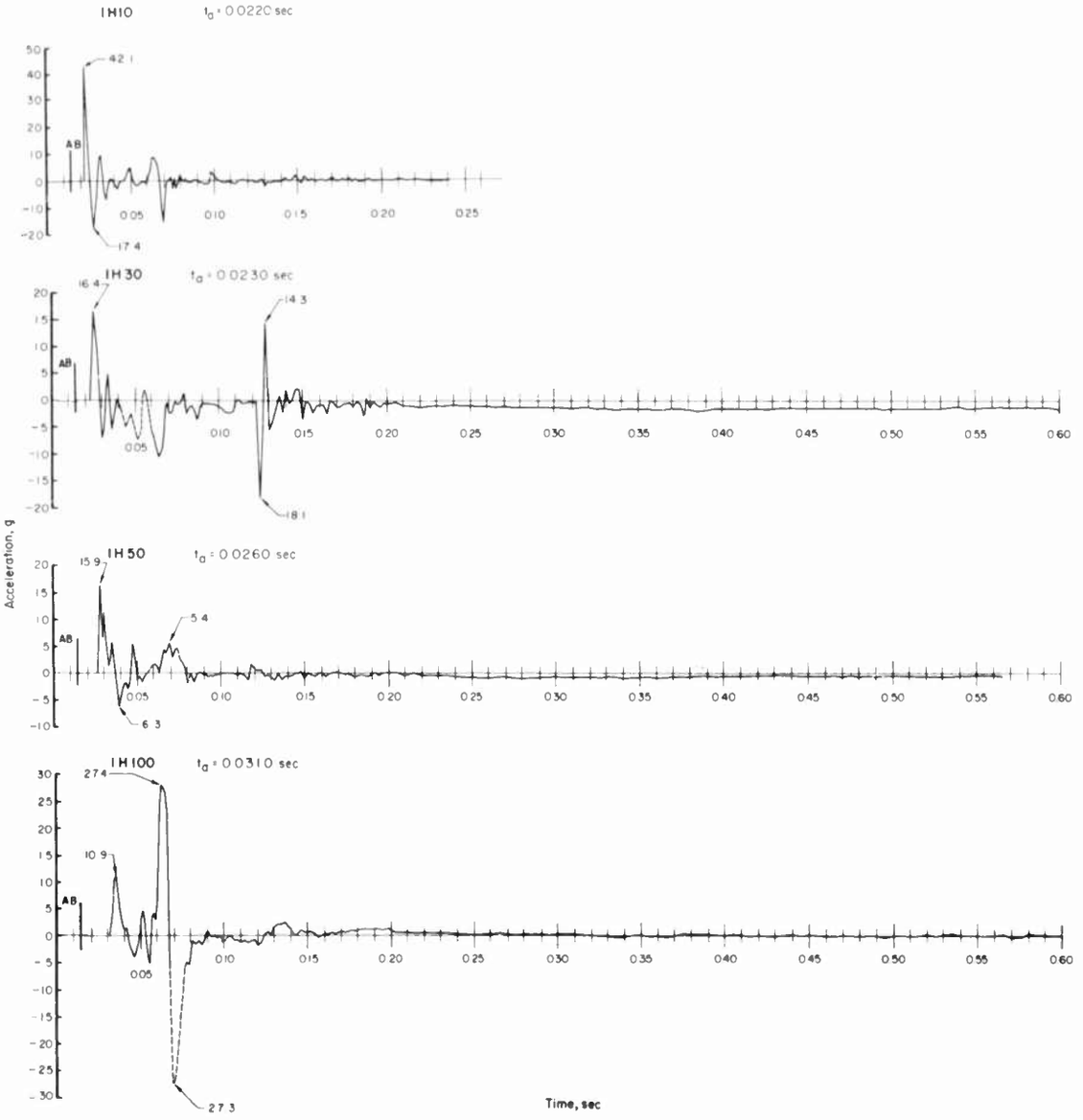

Figure 4.3 Horizontal acceleration versus time, Station 1, Shot Cactus.

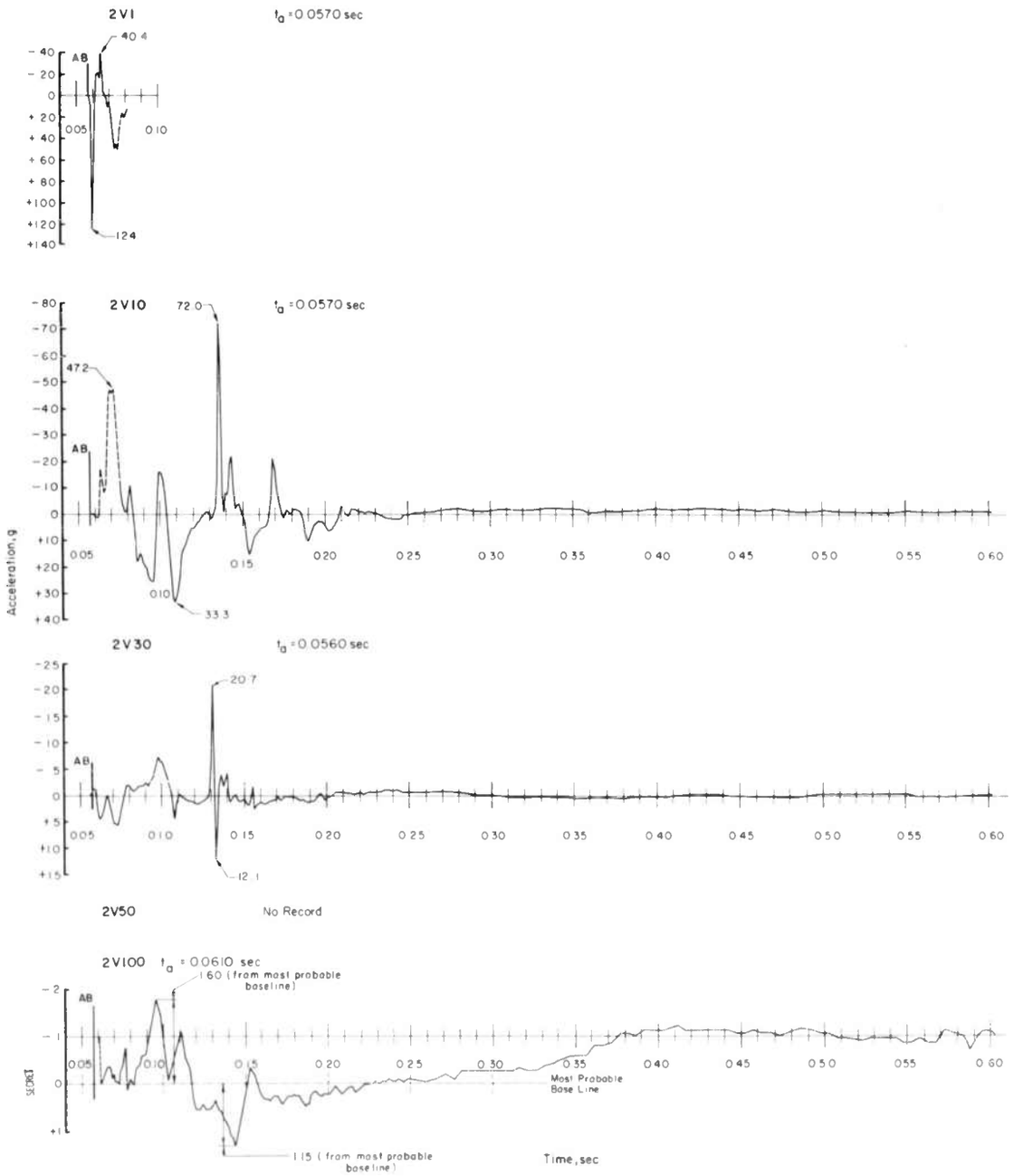

Figure 4.4 Vertical acceleration versus time, Station 2, Shot Cactus.

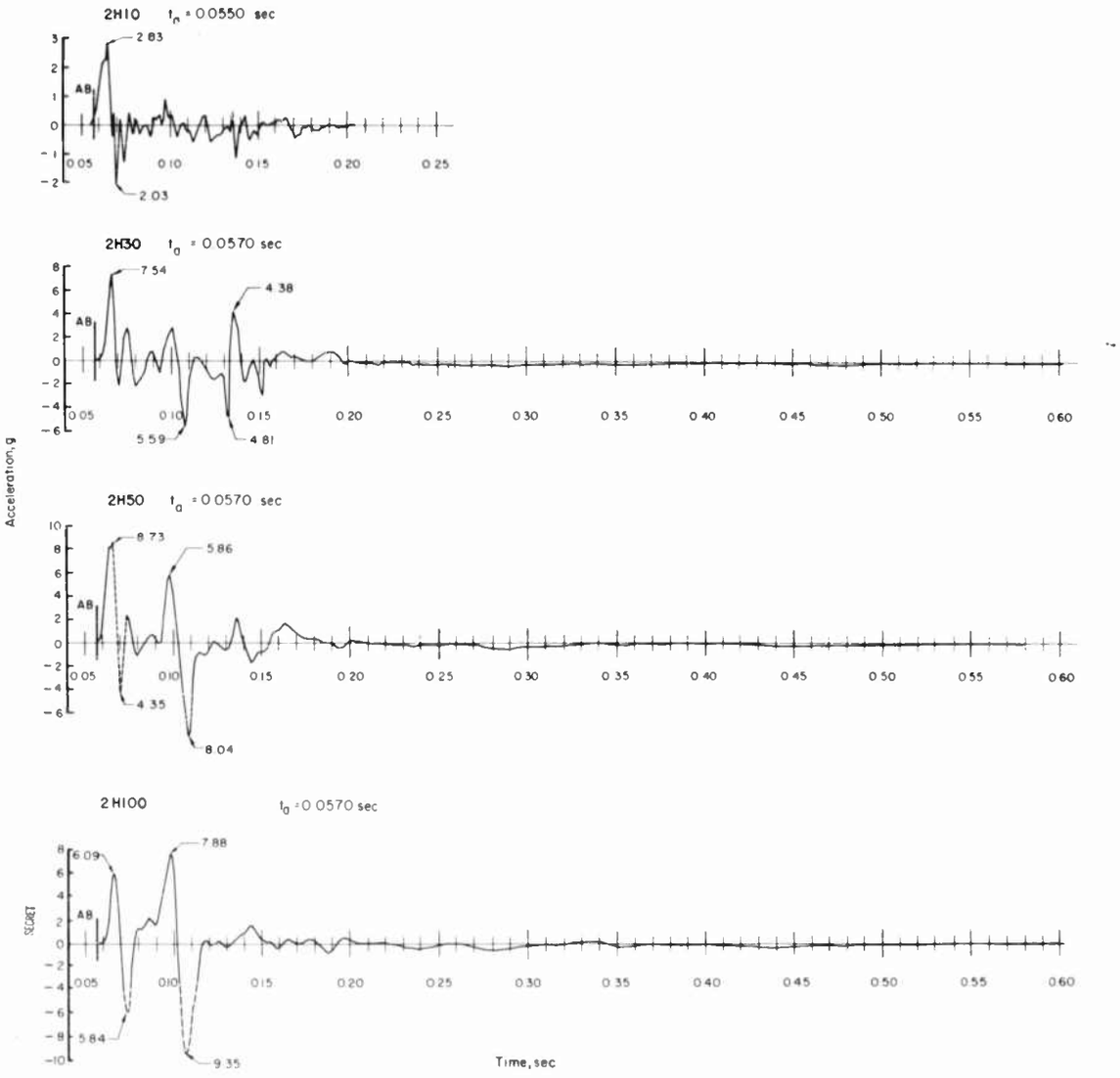

Figure 4.5 Horizontal acceleration versus time, Station 2, Shot Cactus.

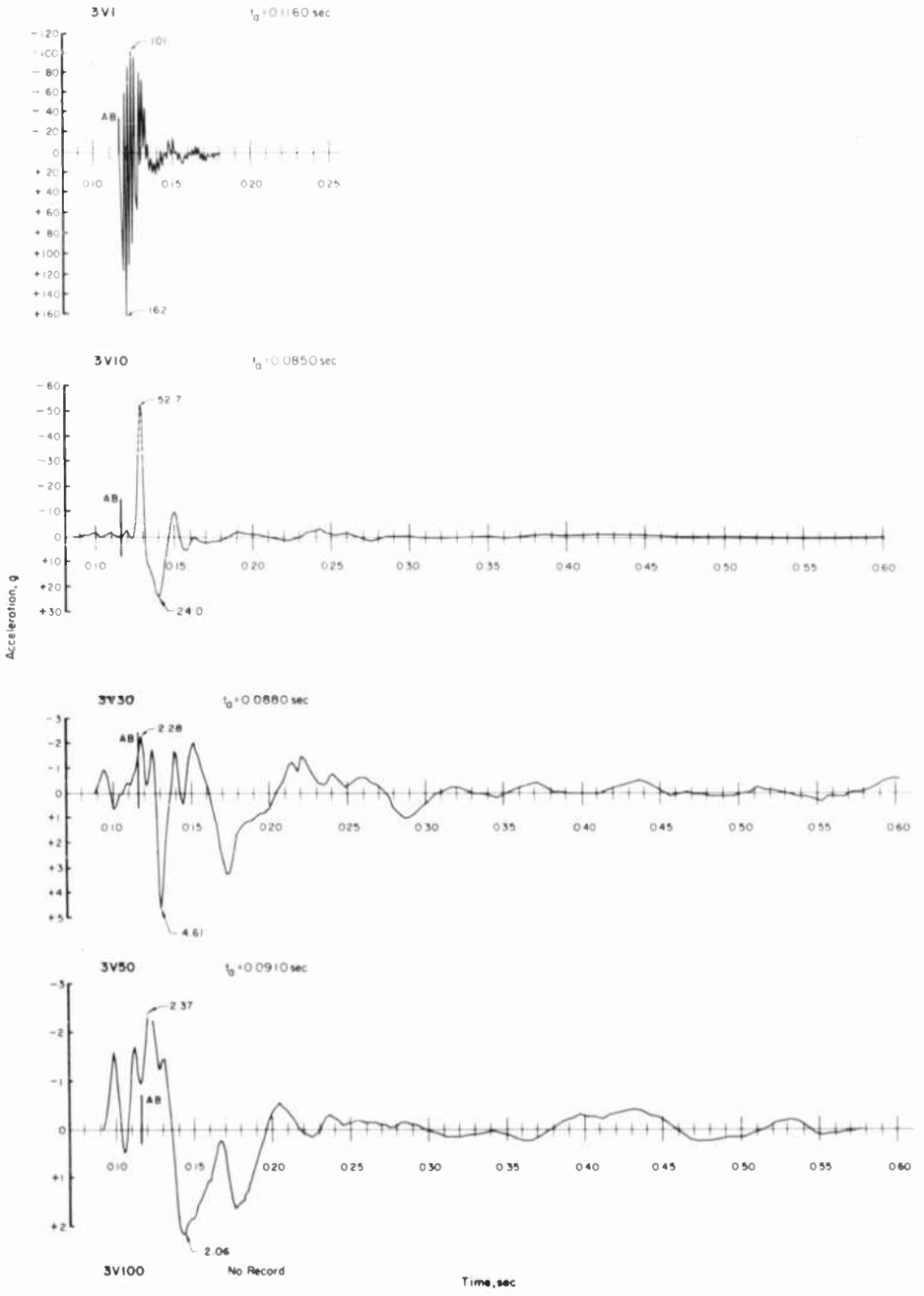

Figure 4.6 Vertical acceleration versus time, Station 3, Shot Cactus.

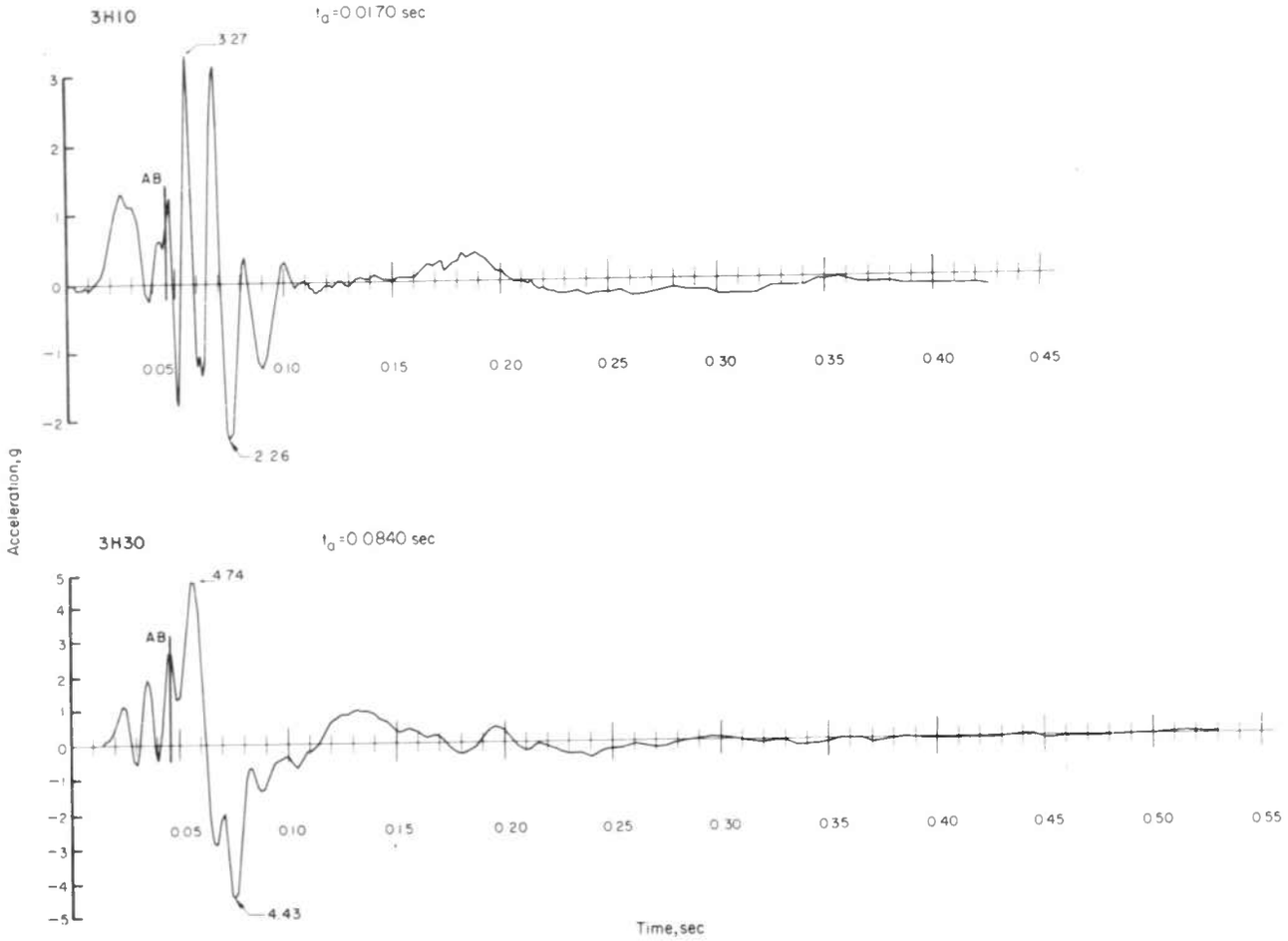

Figure 4.7 Horizontal acceleration versus time, Station 3, Shot Cactus.

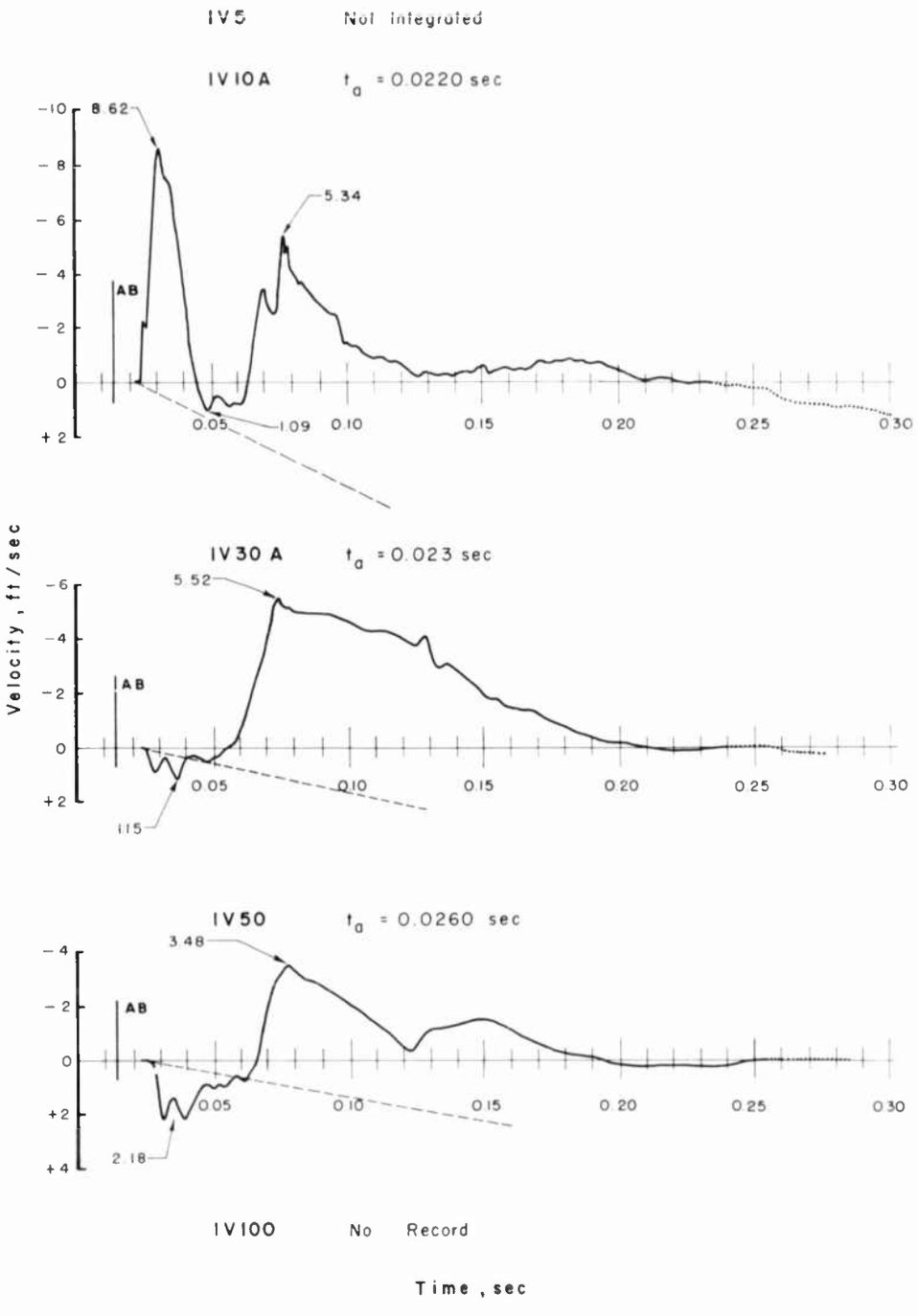

Figure 4.8 Vertical velocity versus time, Station 1, Shot Cactus.

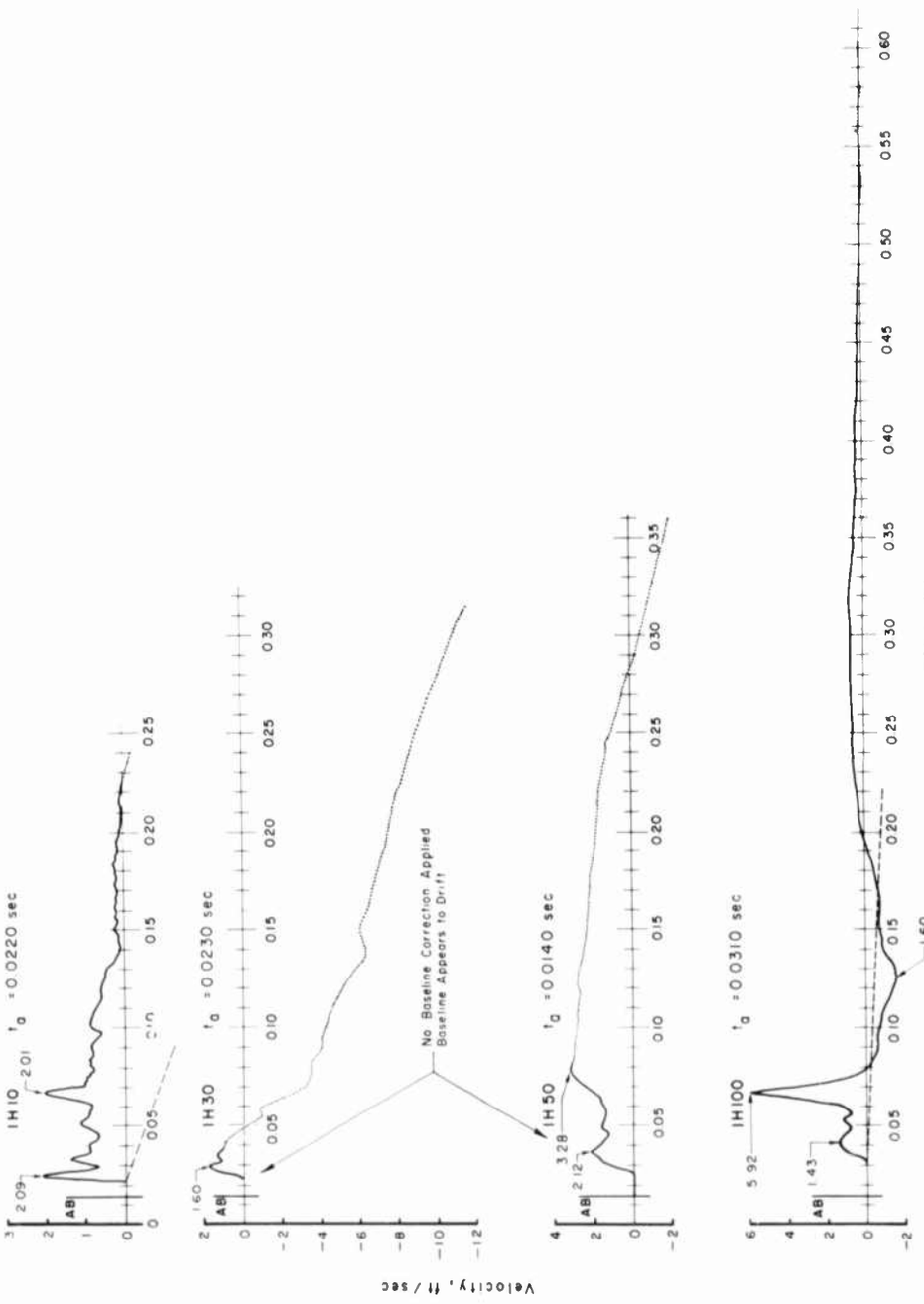

Figure 4.9 Horizontal velocity versus time, Station 1, Shot Cactus.

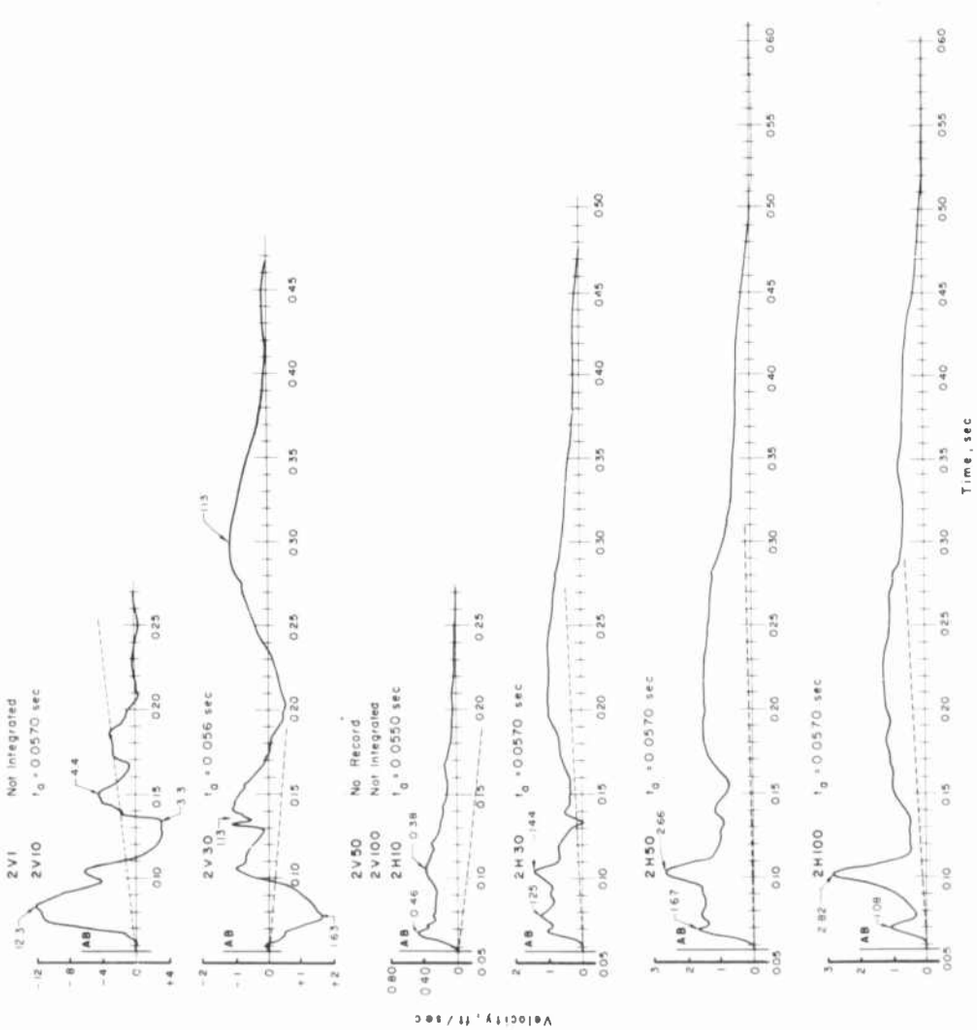

Figure 4.10 Vertical and horizontal velocity versus time, Station 2, Shot Cactus.

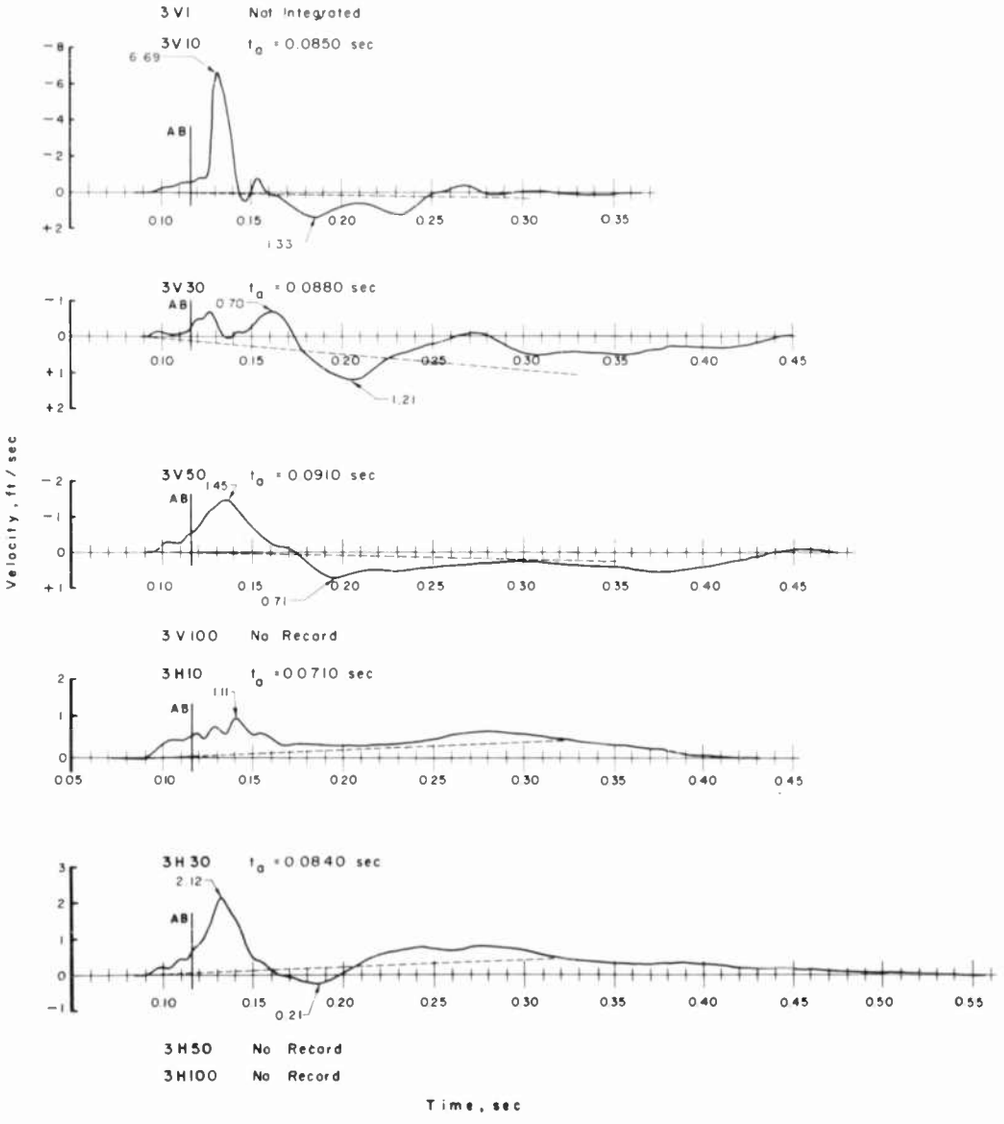

Figure 4.11 Vertical and horizontal velocity versus time, Station 3, Shot Cactus.

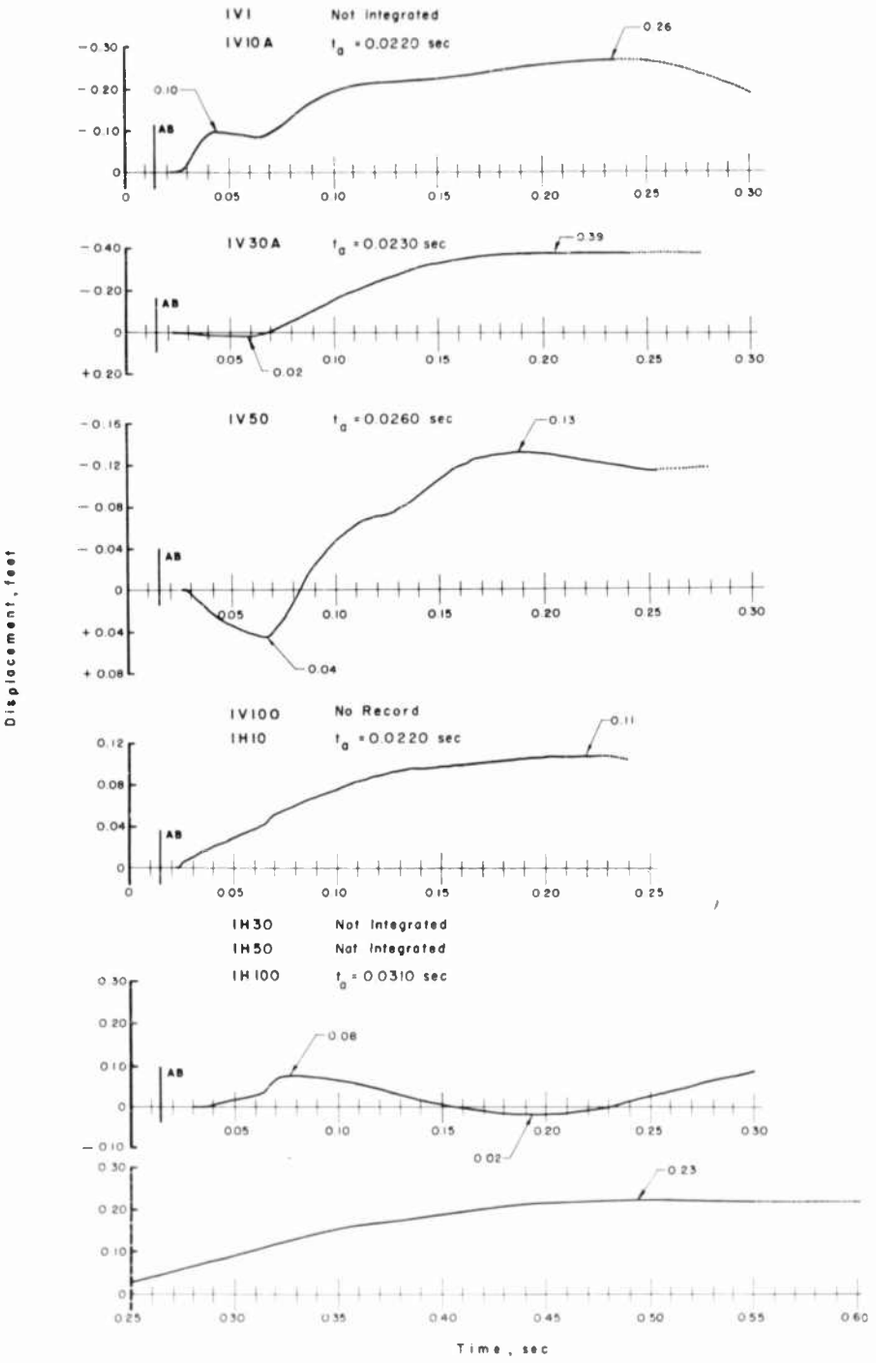

Figure 4.12 Vertical and horizontal displacement versus time, Station 1, Shot Cactus.

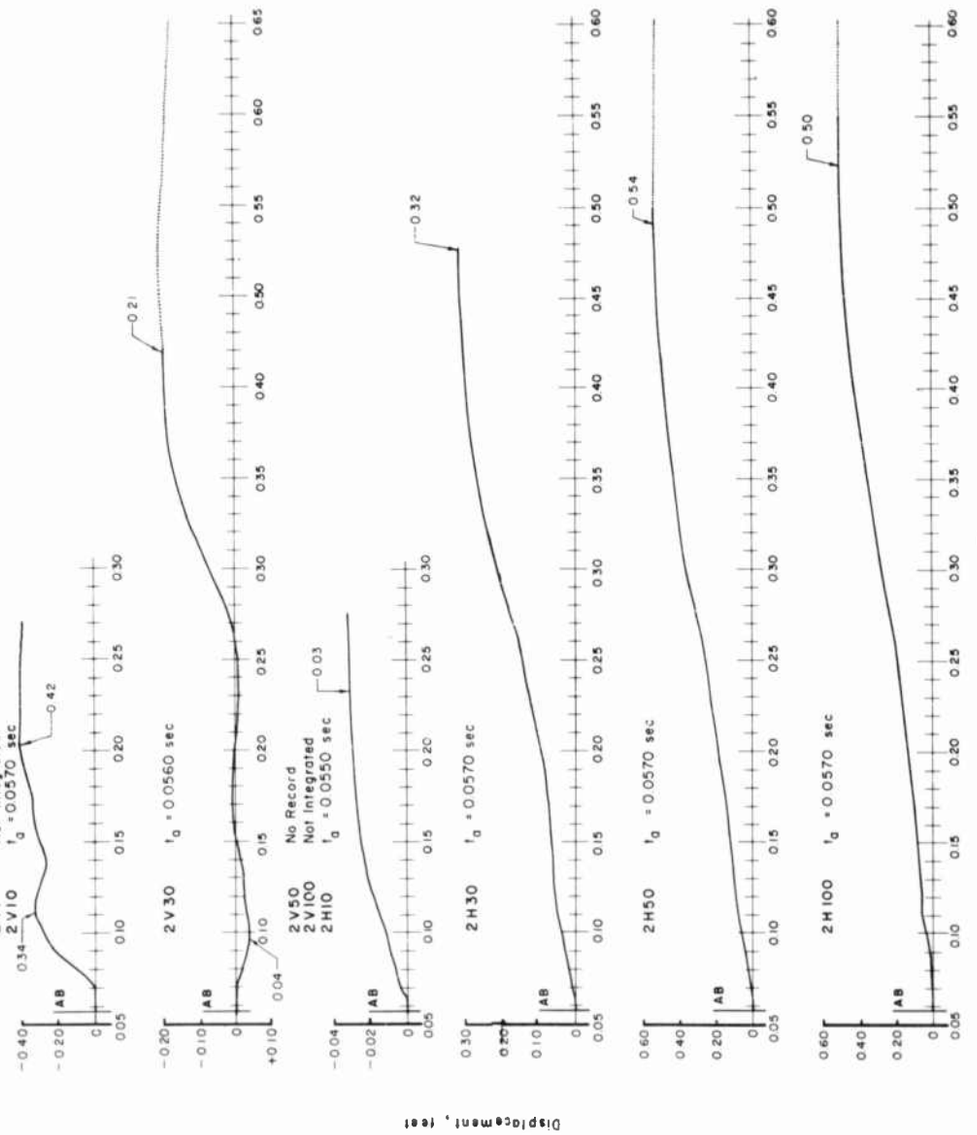

Figure 4.13 Vertical and horizontal displacement versus time, Station 2, Shot Cactus.

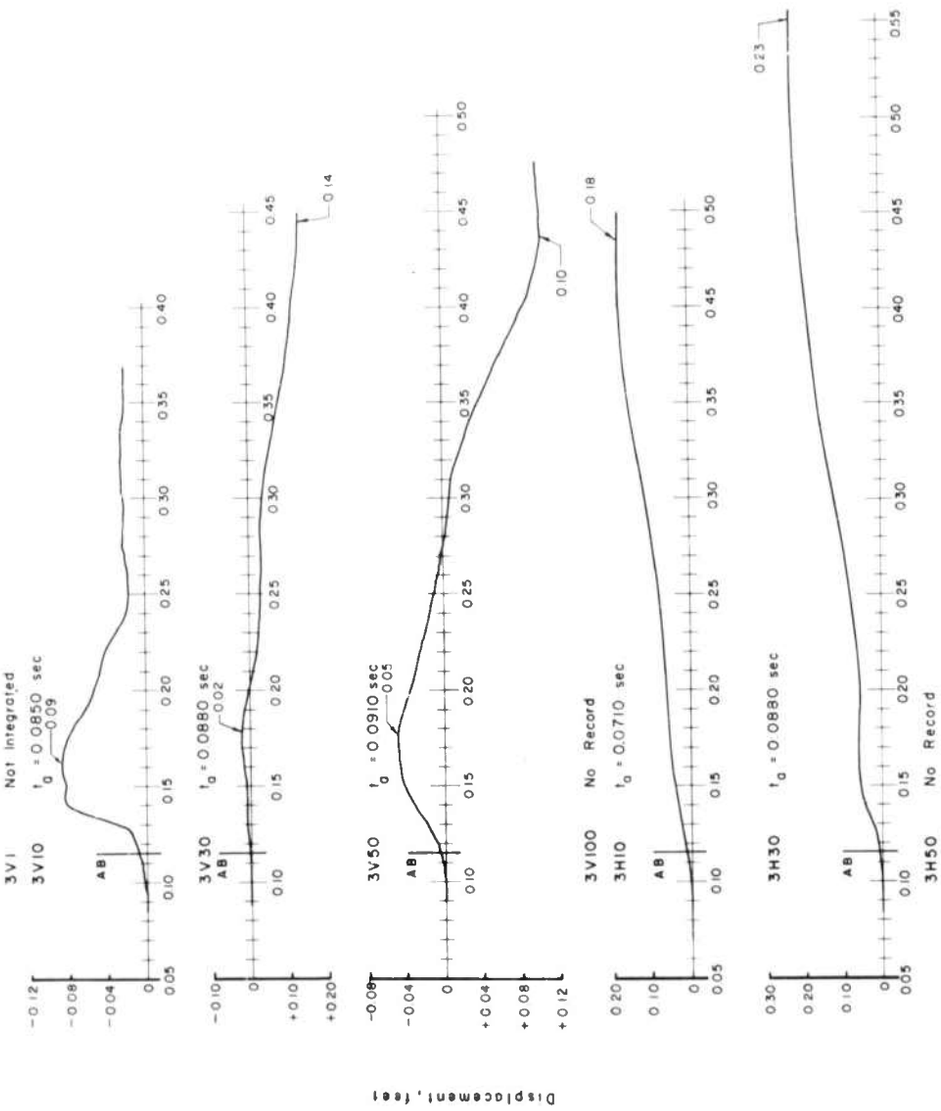

Figure 4.14 Vertical and horizontal displacement versus time, Station 3, Shot Cactus.

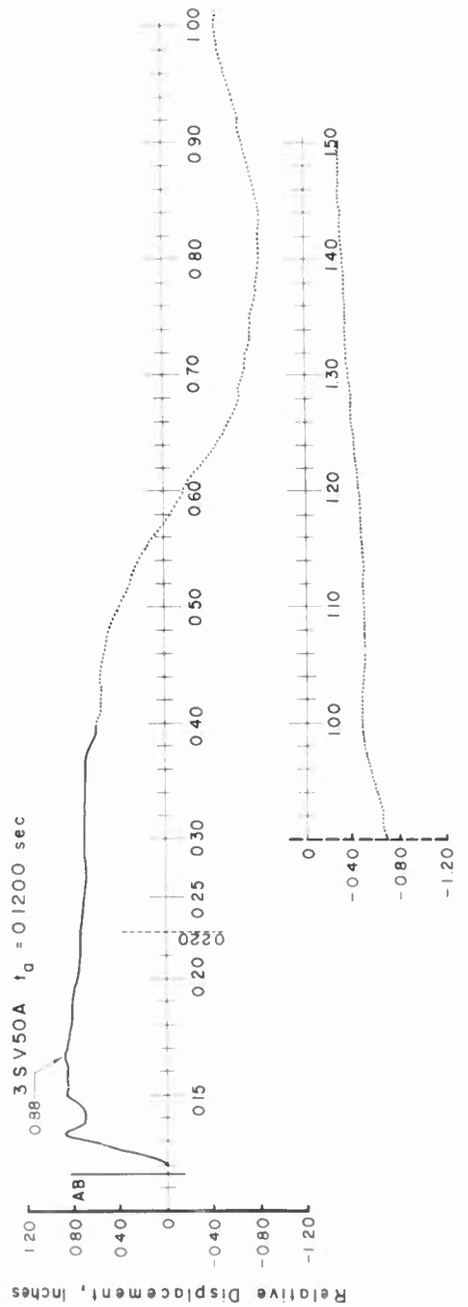

Figure 4.15 Relative displacement versus time, Station 3, Shot Cactus.

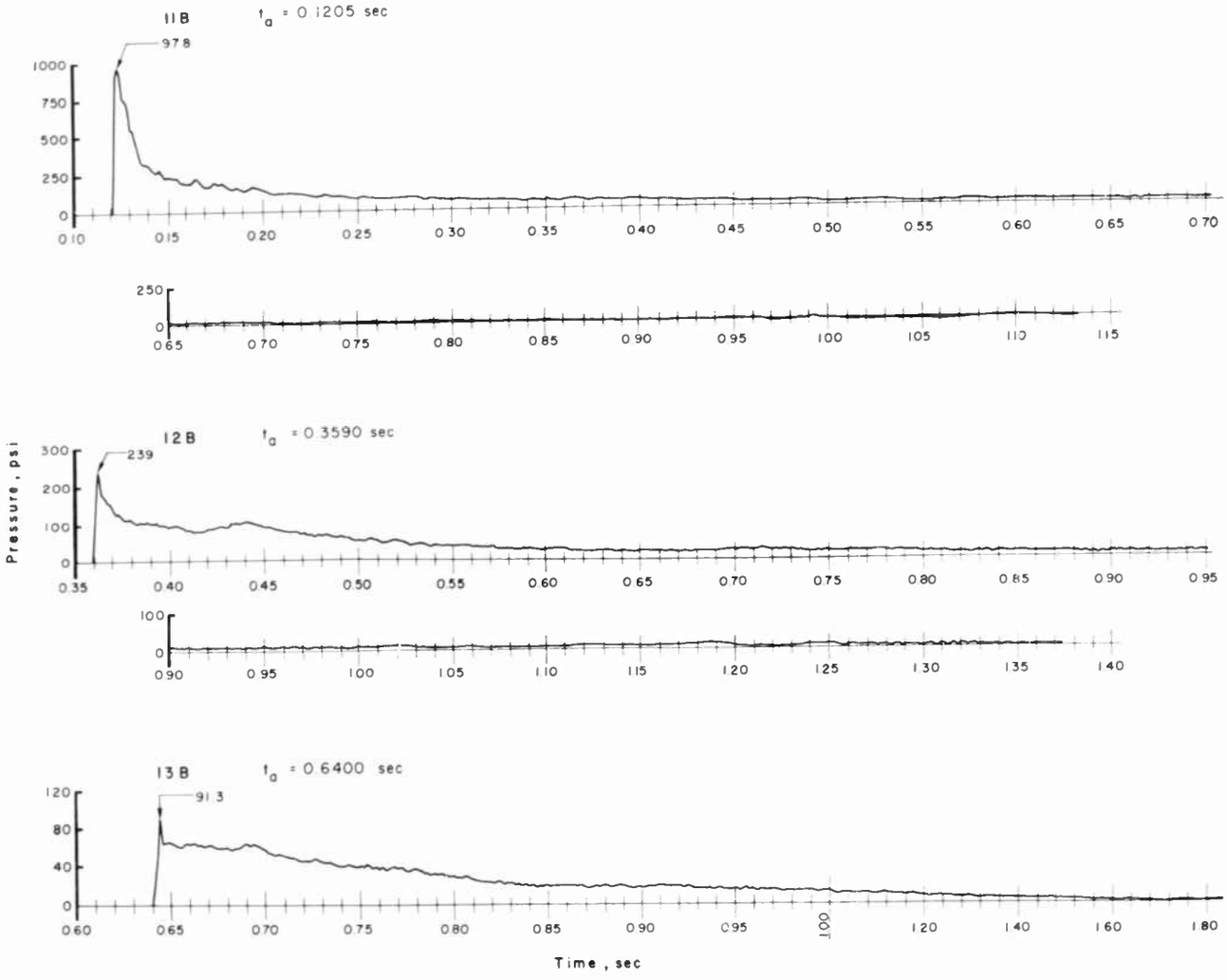

Figure 4.16 Overpressure versus time, Stations 11 through 13, Shot Koa.

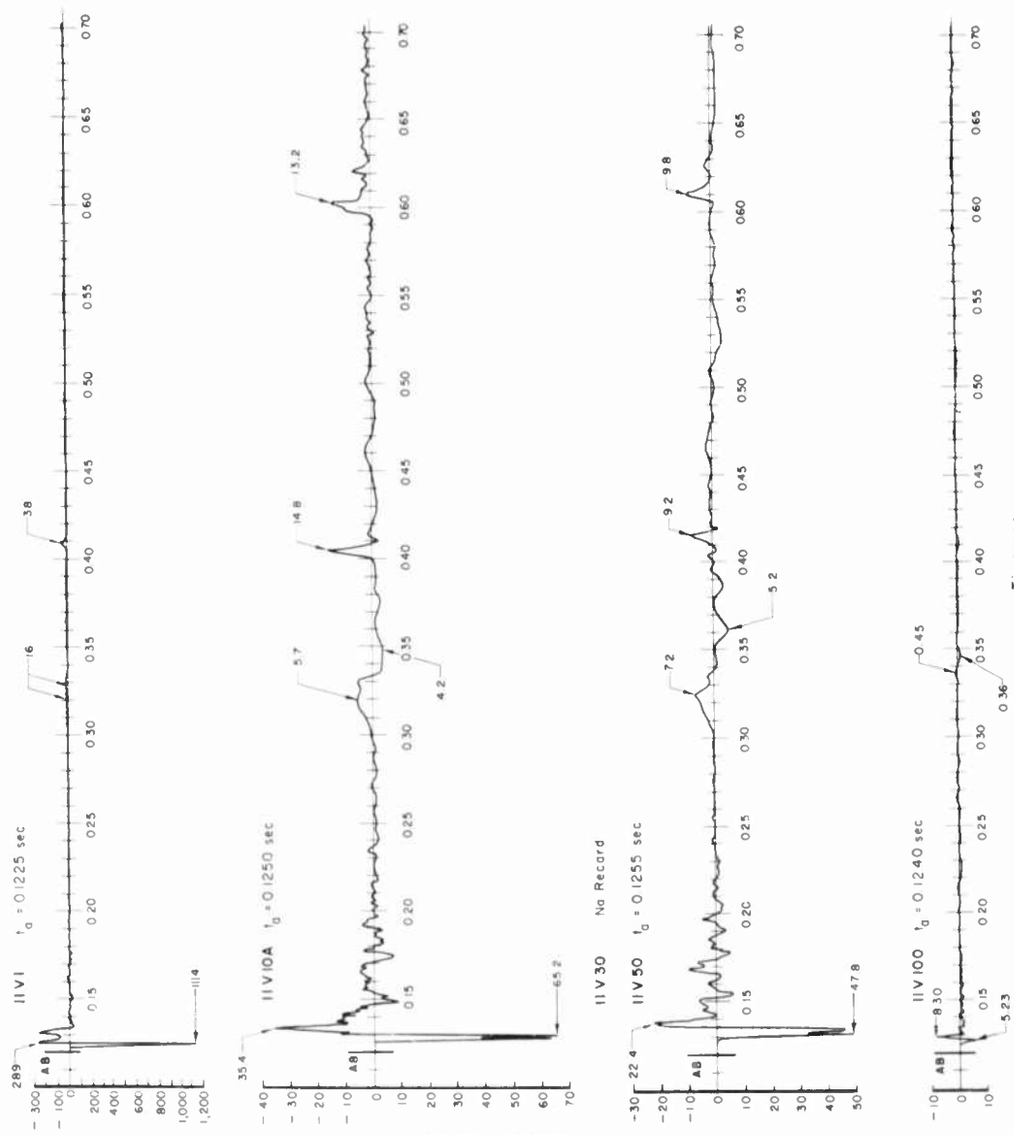

Figure 4.17 Vertical acceleration versus time, Station 11, Shot Koa.

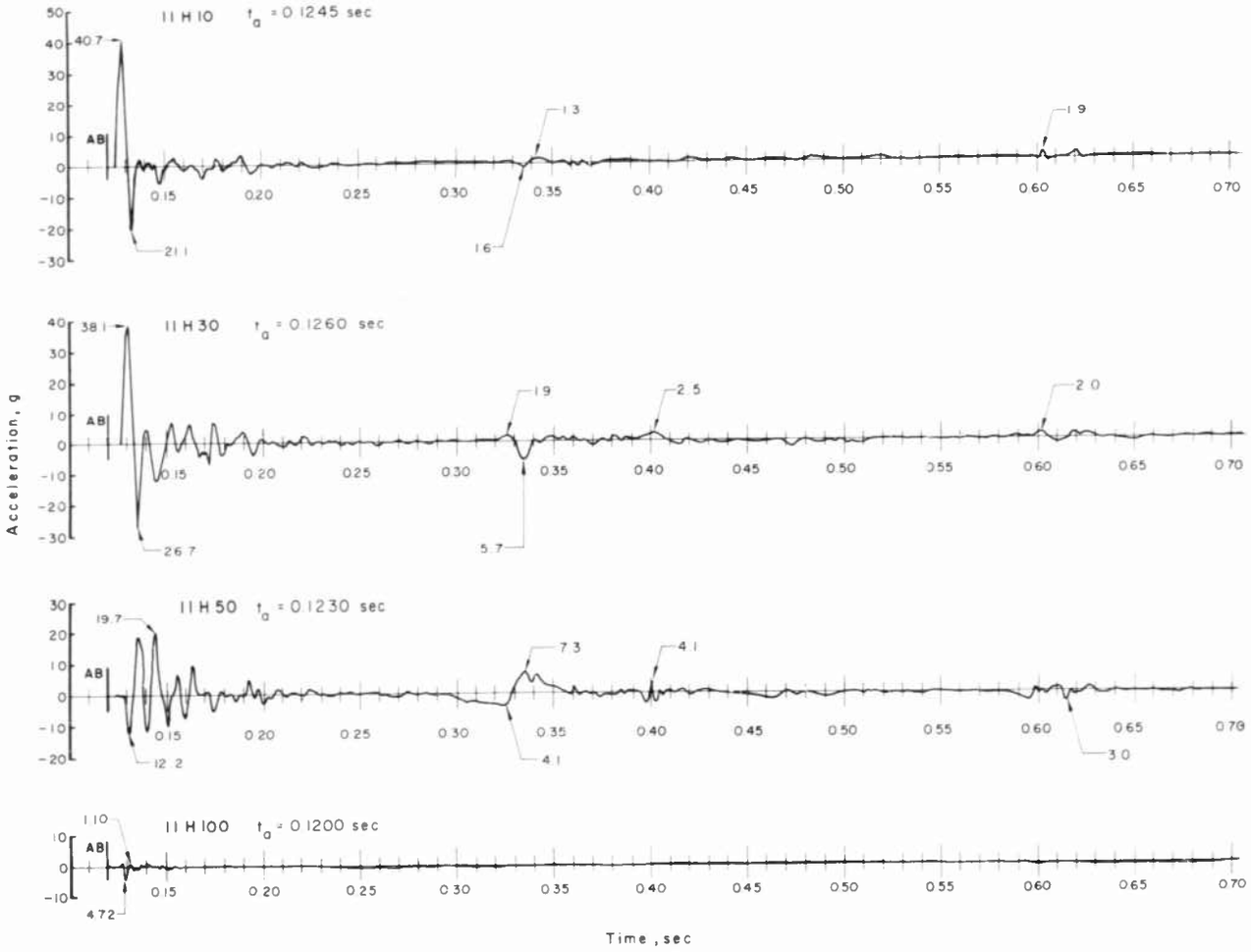

Figure 4.18 Horizontal acceleration versus time, Station 11, Shot Koa.

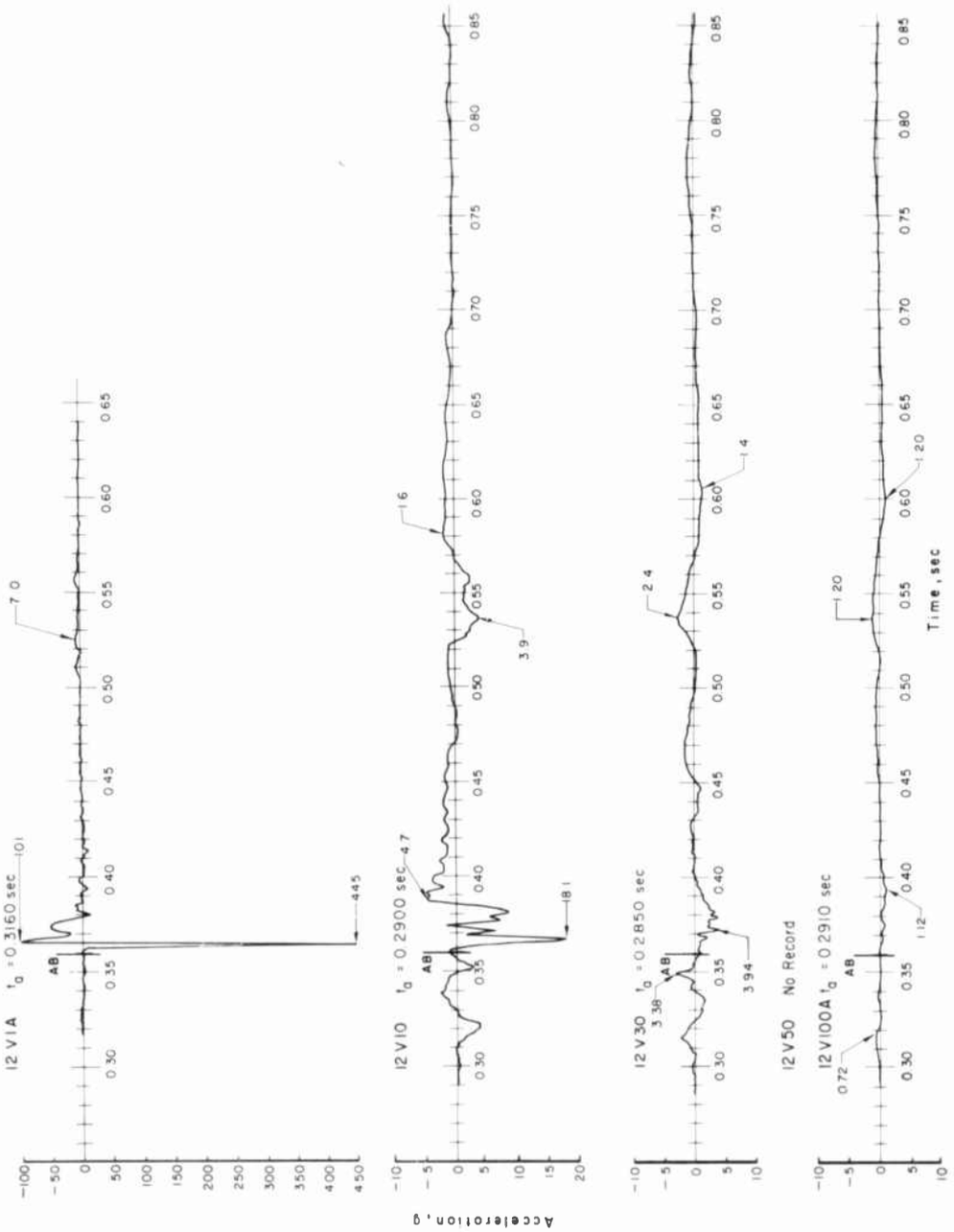

Figure 4.19 Vertical acceleration versus time, Station 12, Shot Koa.

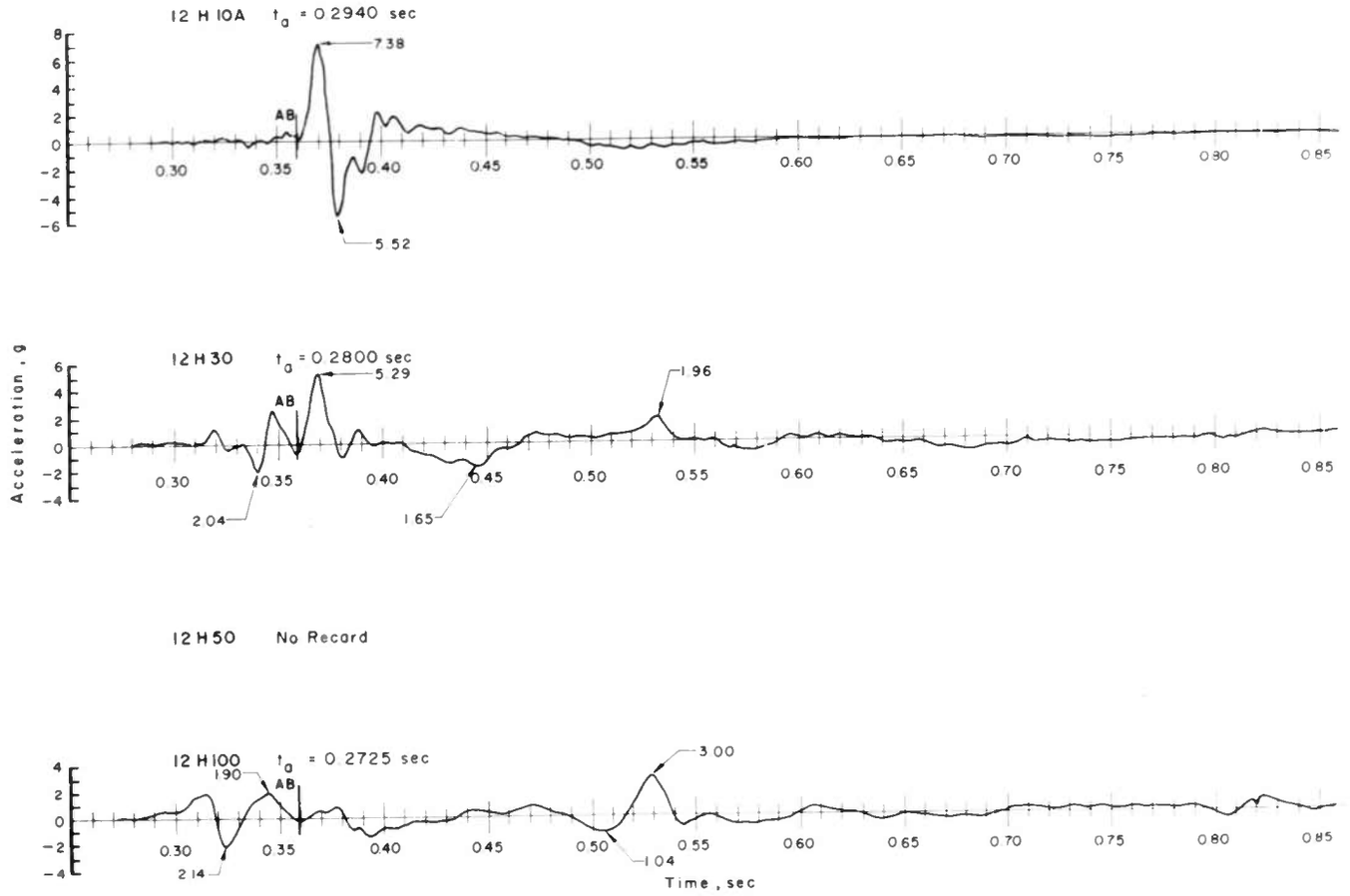

Figure 4.20 Horizontal acceleration versus time, Station 12, Shot Koa.

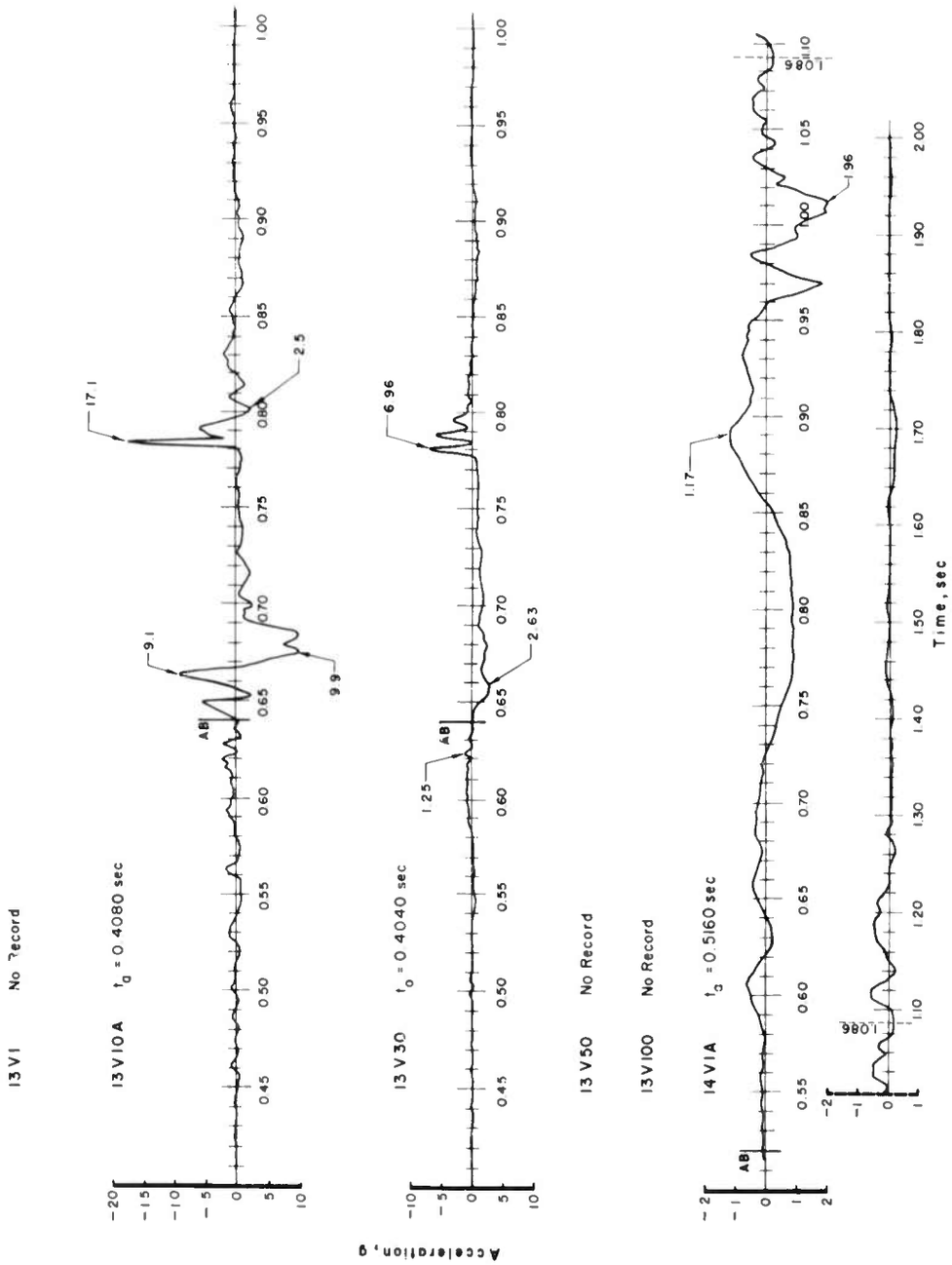

Figure 4.21 Vertical acceleration versus time, Stations 13 and 14, Shot Koa.

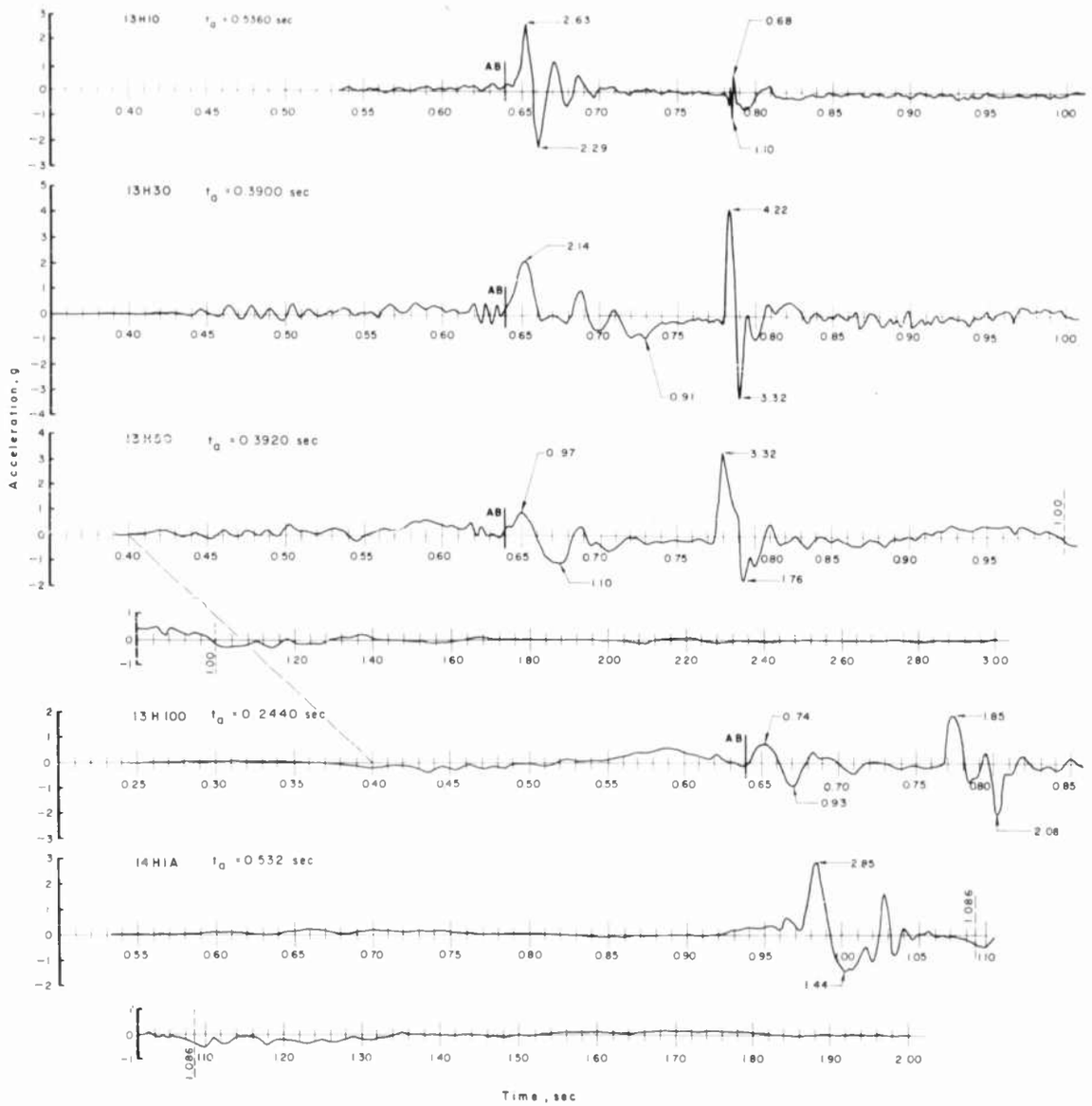

Figure 4.22 Horizontal acceleration versus time, Stations 13 and 14, Shot Koa.

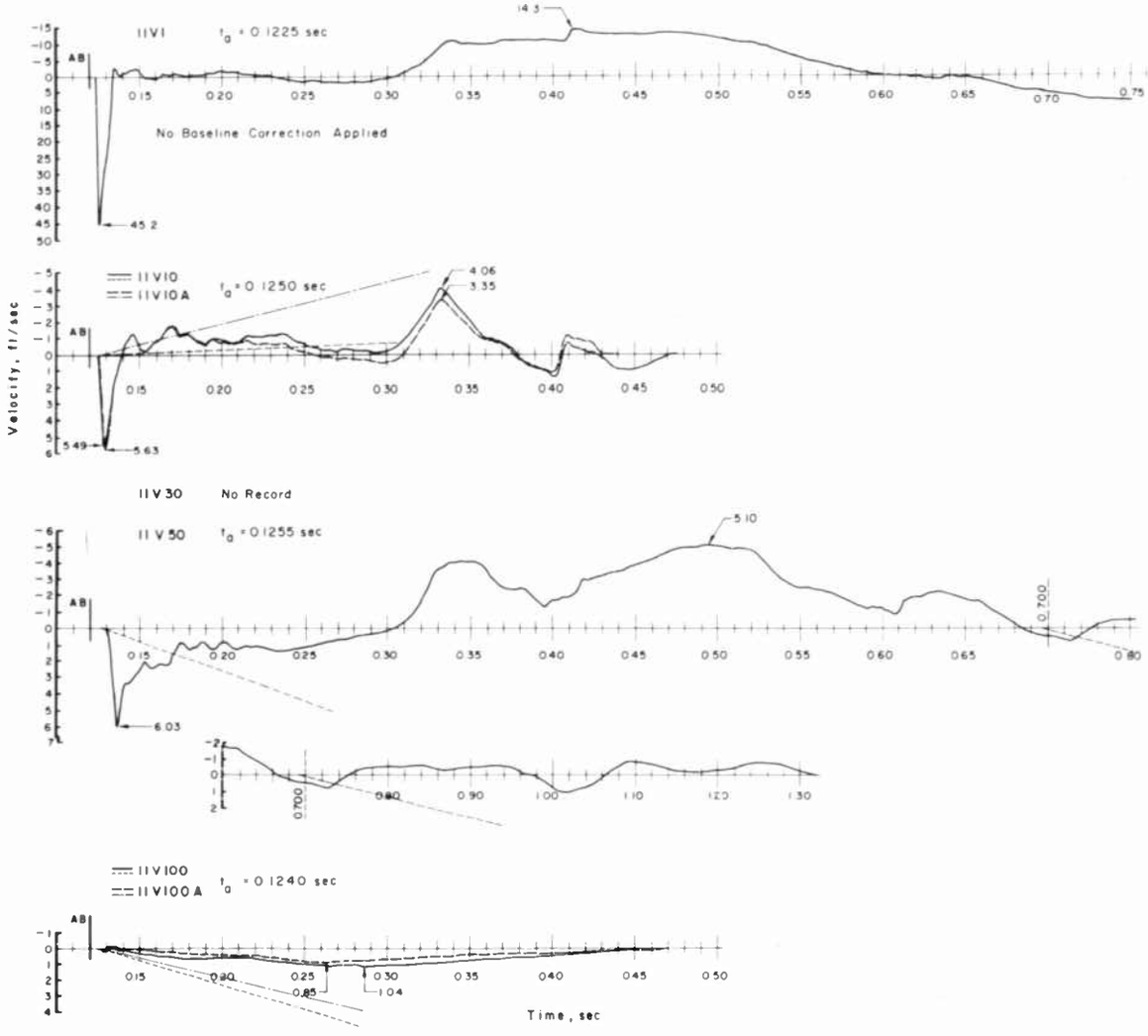

Figure 4.23 Vertical velocity versus time, Station 11, Shot Koa.

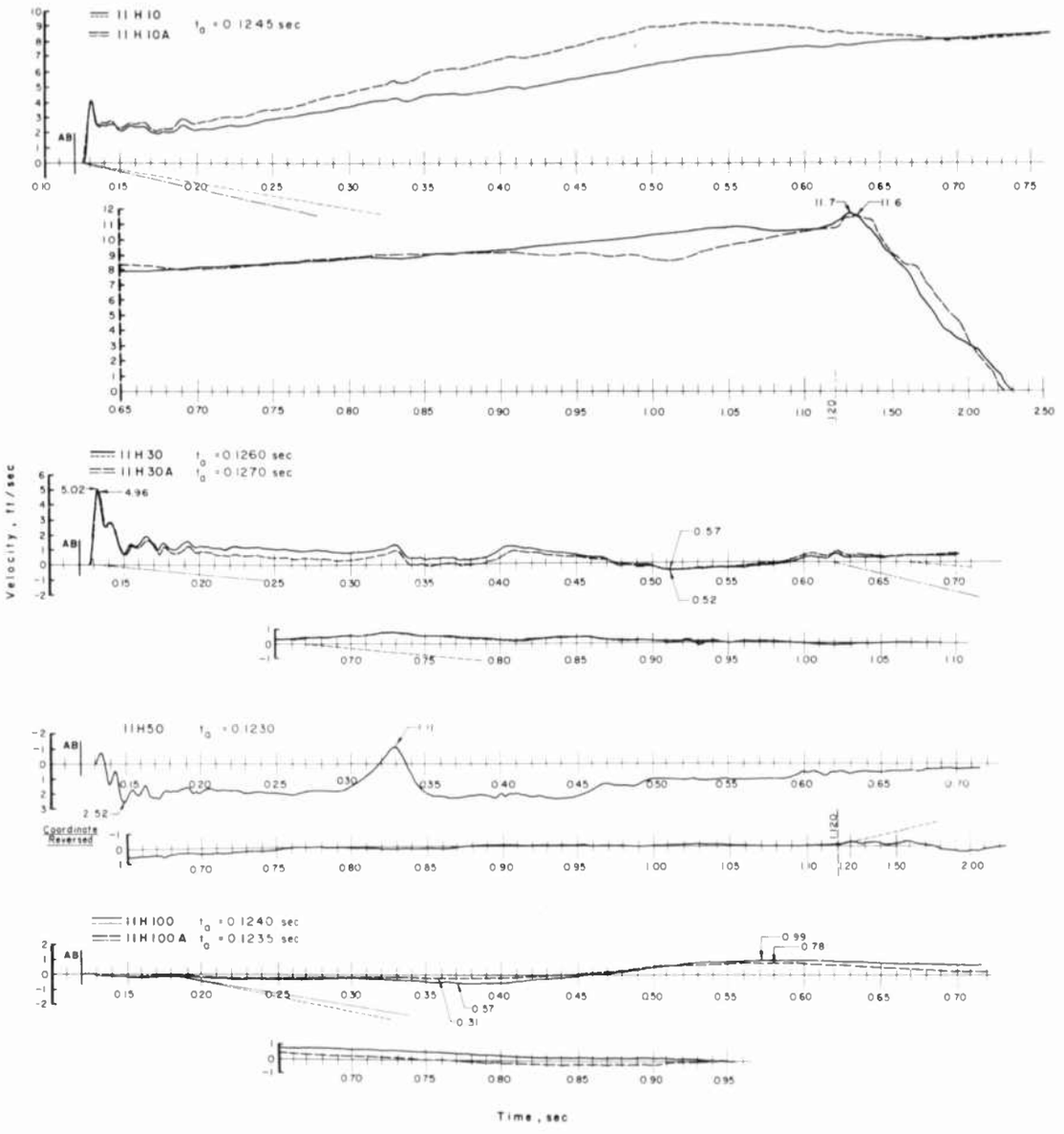

Figure 4.24 Horizontal velocity versus time, Station 11, Shot Koa.

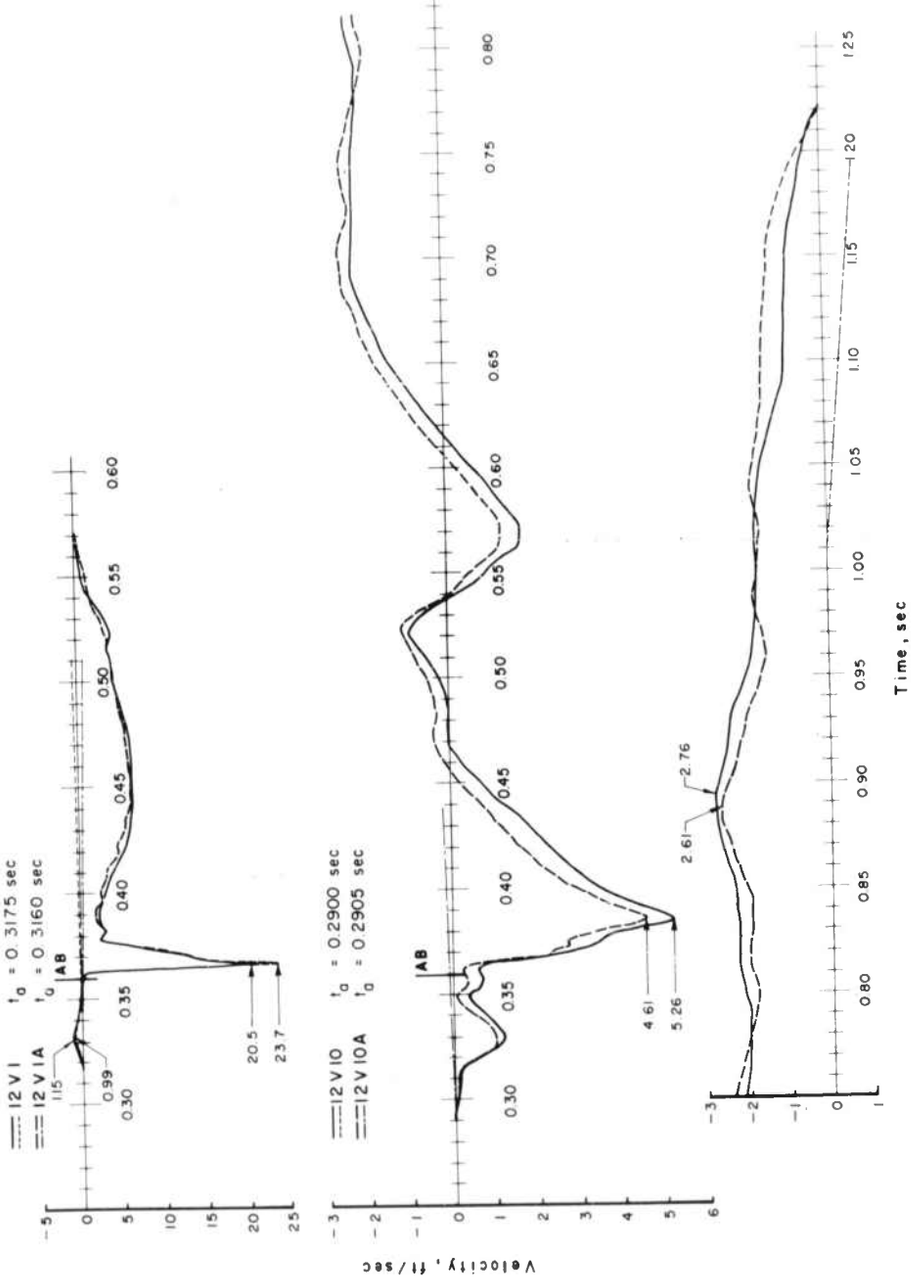

Figure 4.25 Vertical velocity versus time, 1- and 10-foot depths, Station 12, Shot Koa.

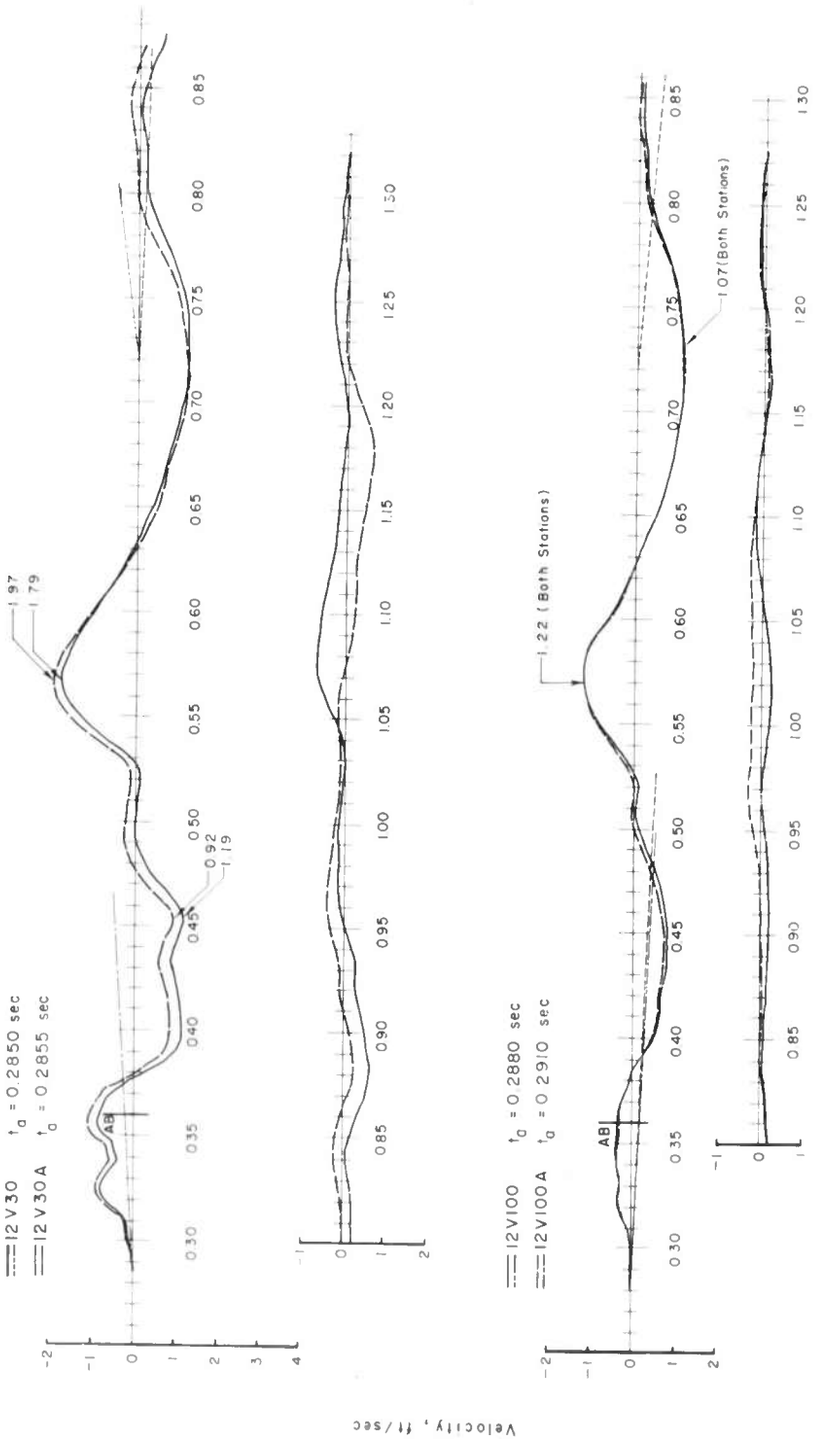

Figure 4.26 Vertical velocity versus time, 30- and 100-foot depths, Station 12, Shot Koa.

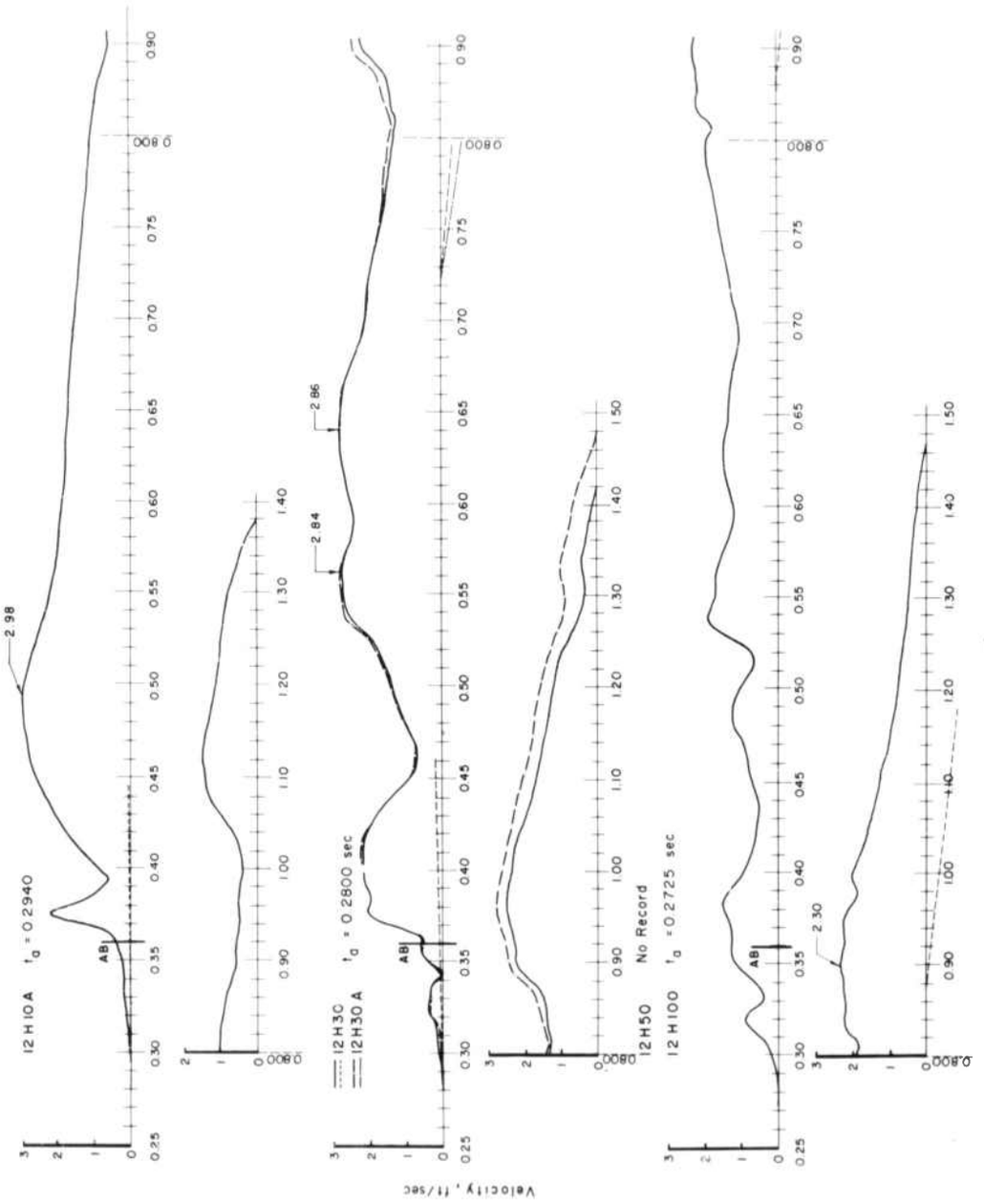

Figure 4.27 Horizontal velocity versus time, Station 12, Shot Koa.

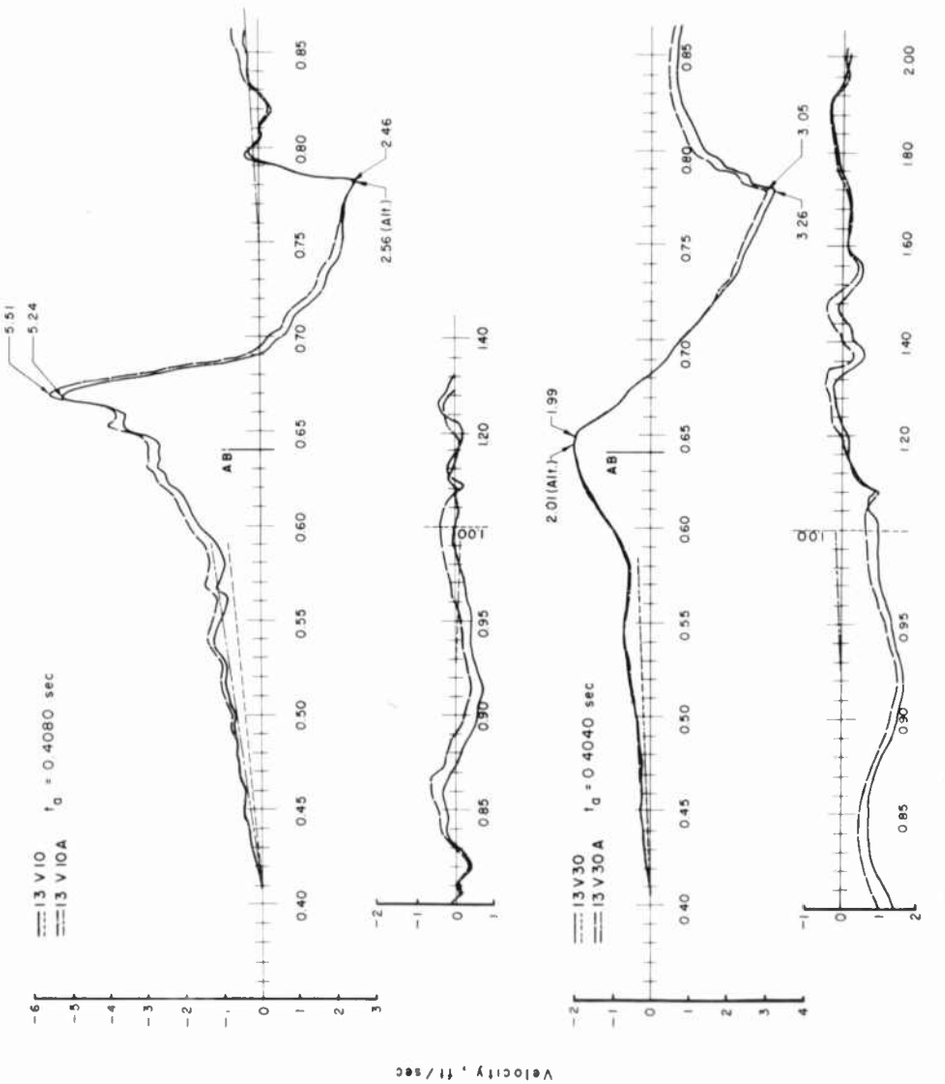

Figure 4.28 Vertical velocity versus time, Station 13, Shot Koa.

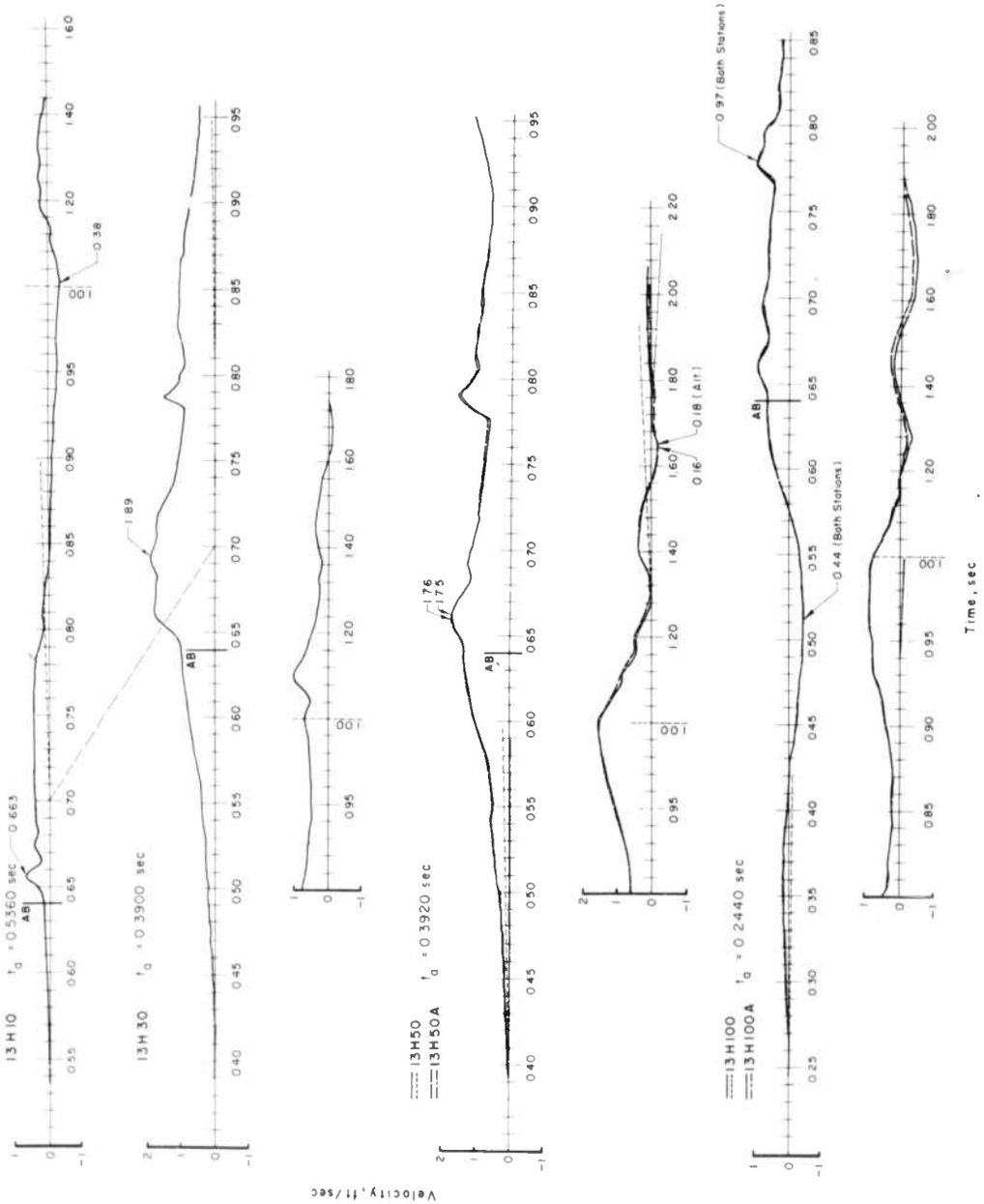

Figure 4.29 Horizontal velocity versus time, Station 13, Shot Koa.

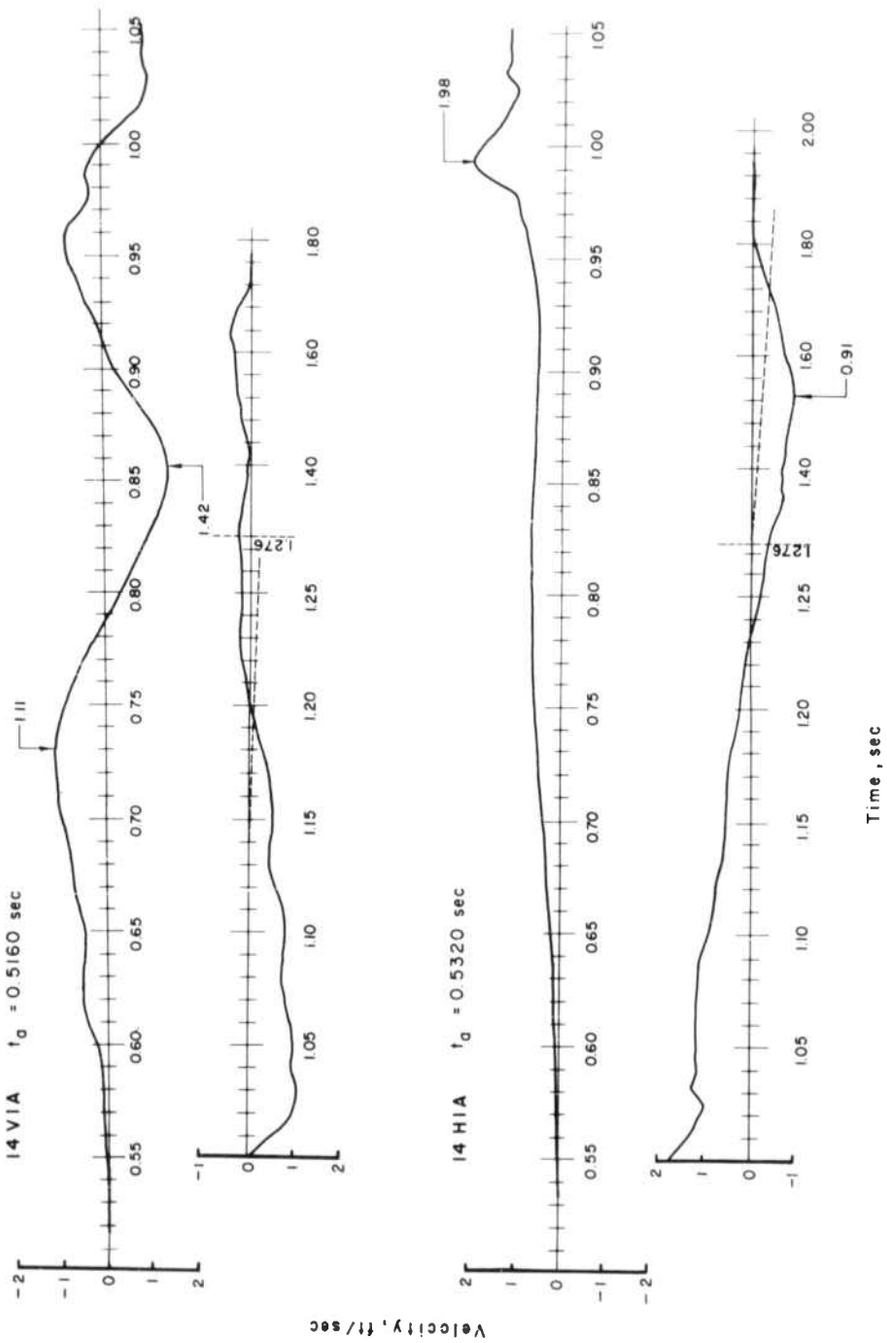

Figure 4.30 Vertical and horizontal velocity versus time, Stations 13 and 14, Shot Koa.

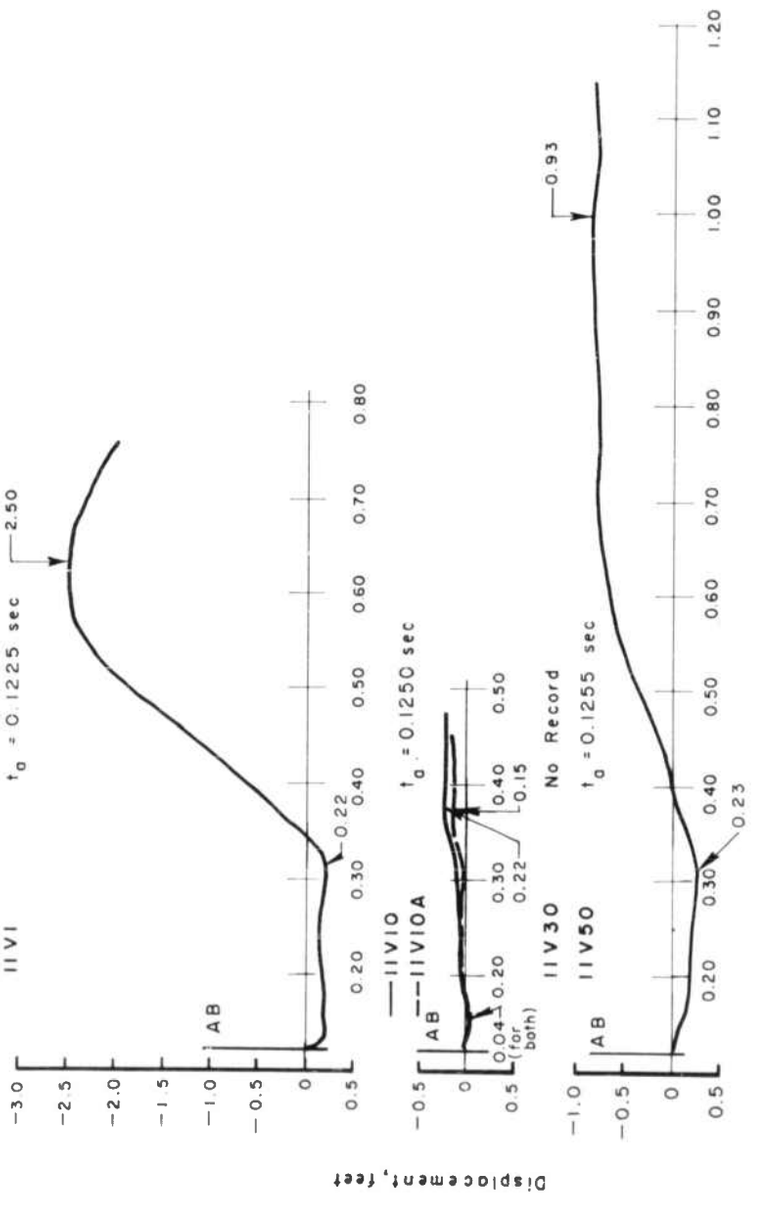

Figure 4.31 Vertical displacement versus time, Station 11, Shot Koa.

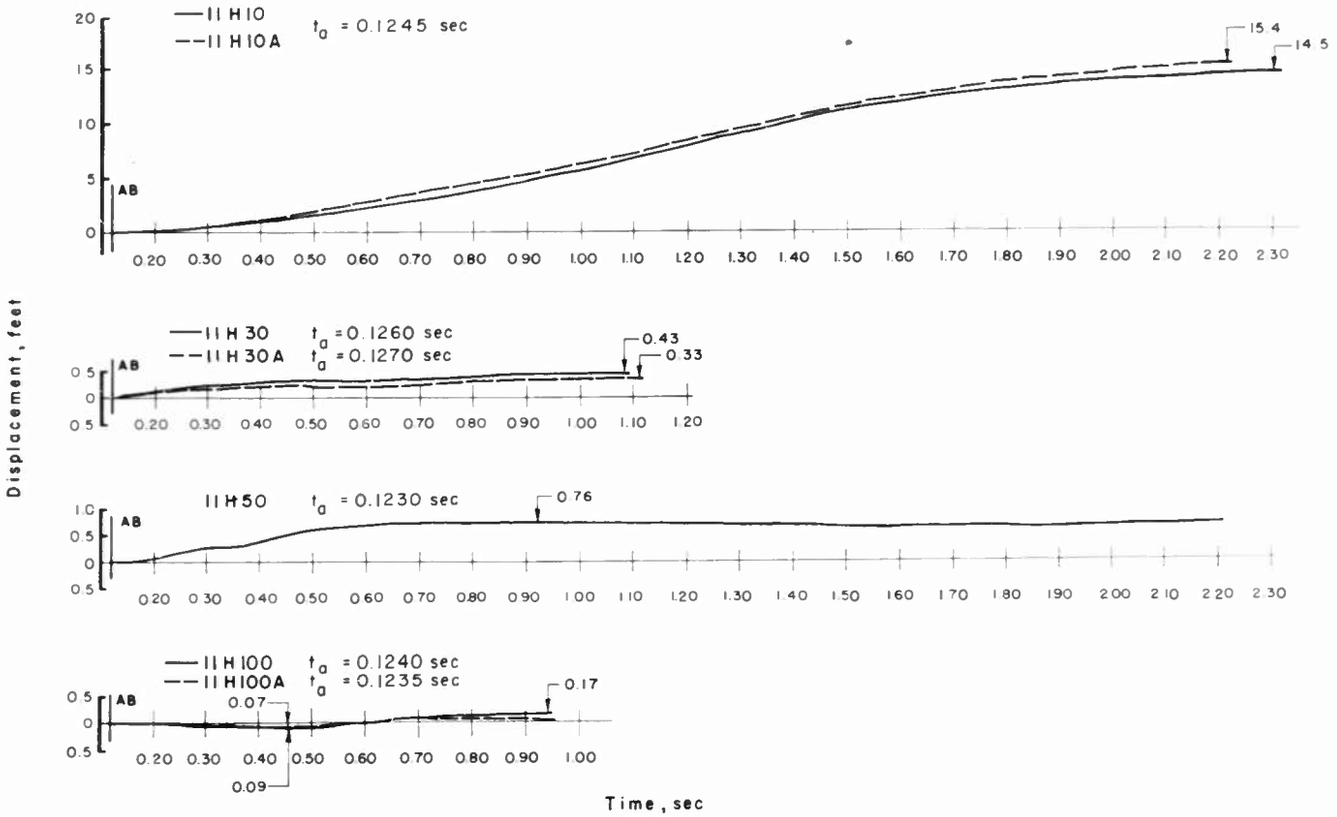

Figure 4.32 Horizontal displacement versus time, Station 11, Shot Koa.

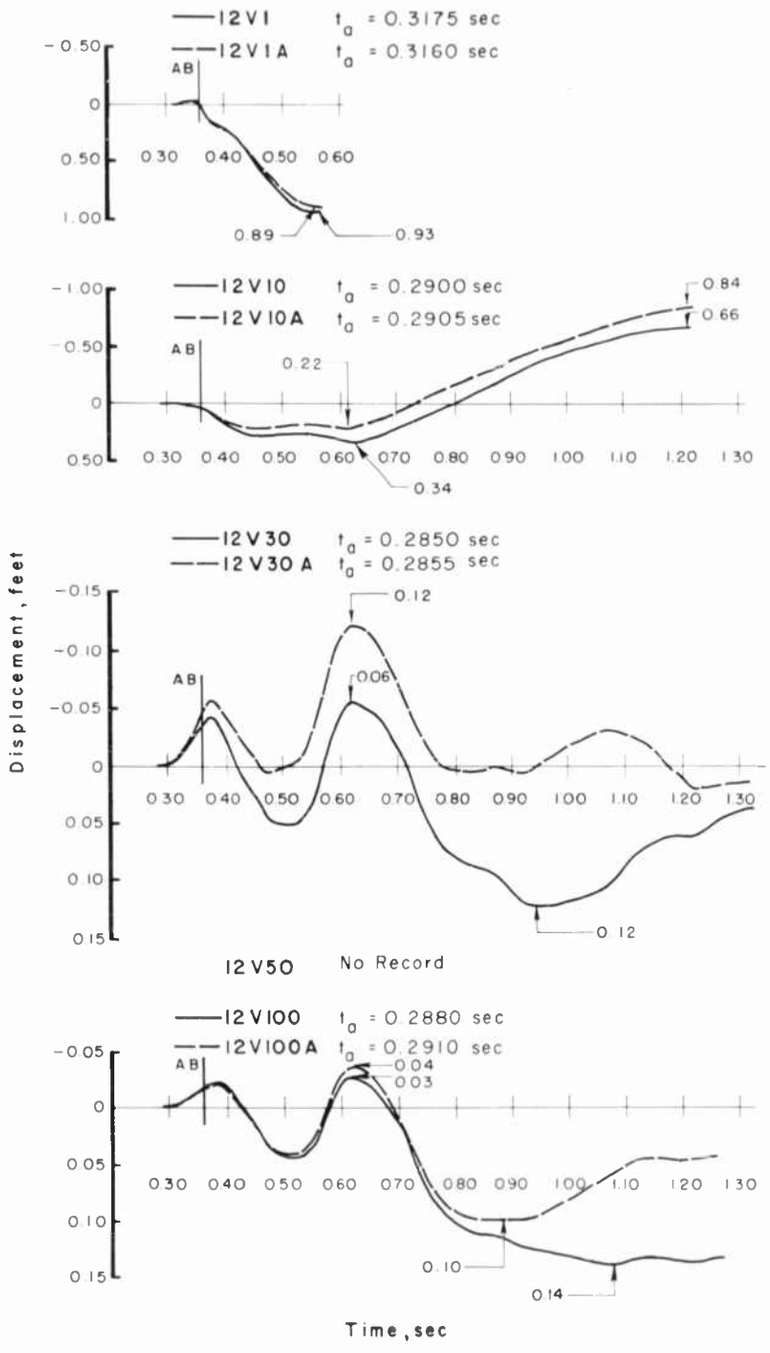

Figure 4.33 Vertical displacement versus time, Station 12, Shot Koa.

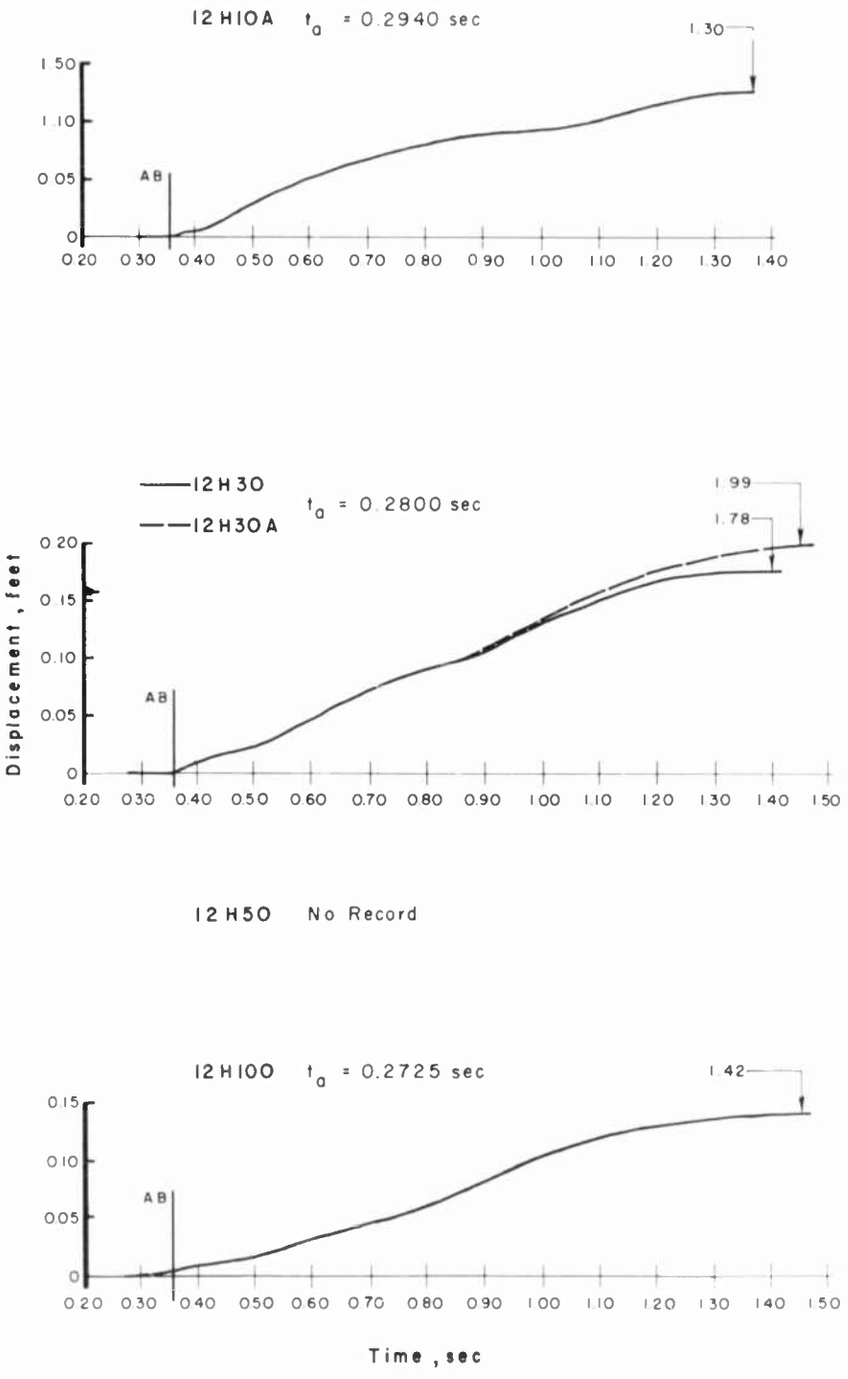

Figure 4.34 Horizontal displacement versus time, Station 12, Shot Koa.

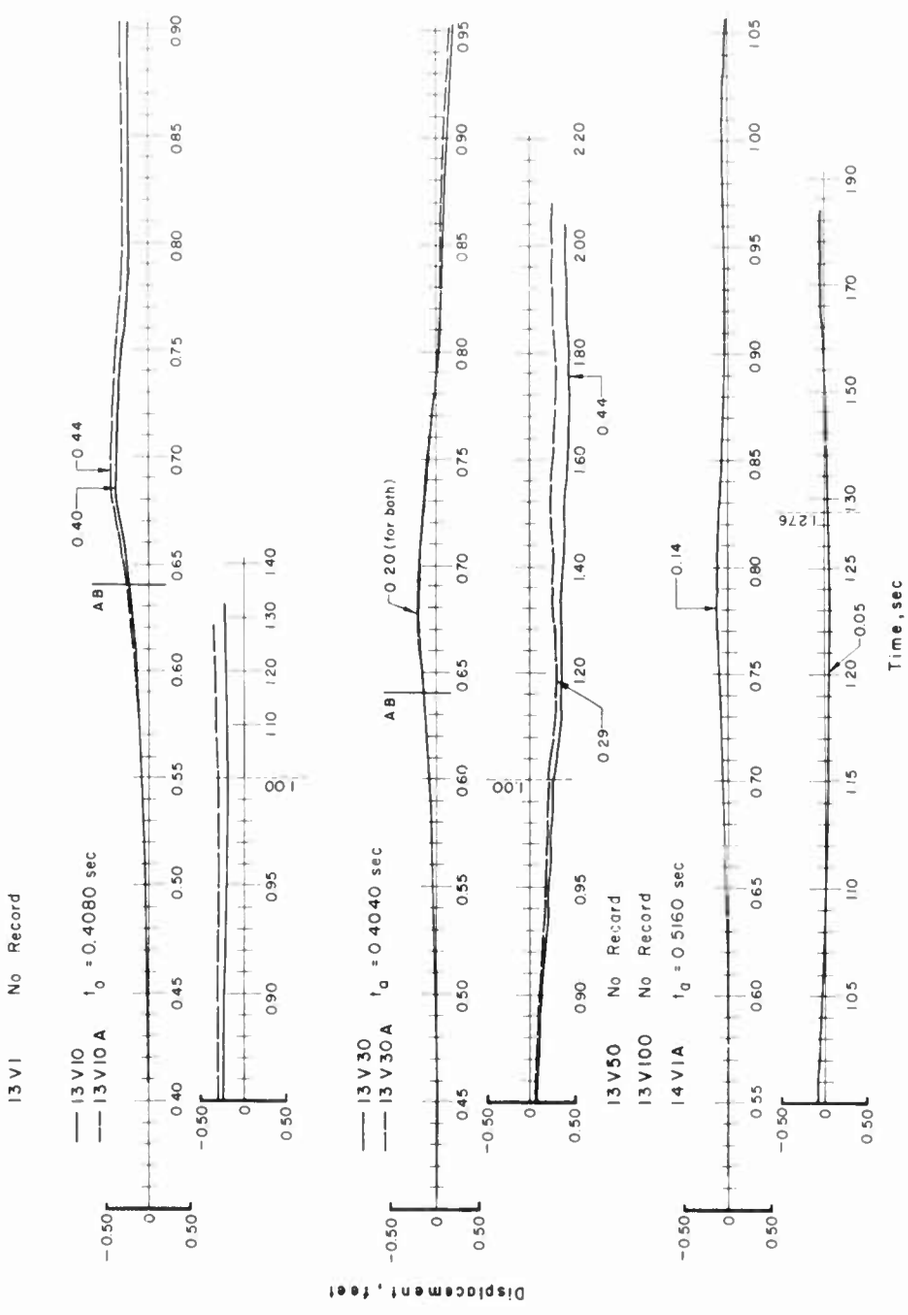

Figure 4.35 Vertical displacement versus time, Stations 13 and 14, Shot Koa.

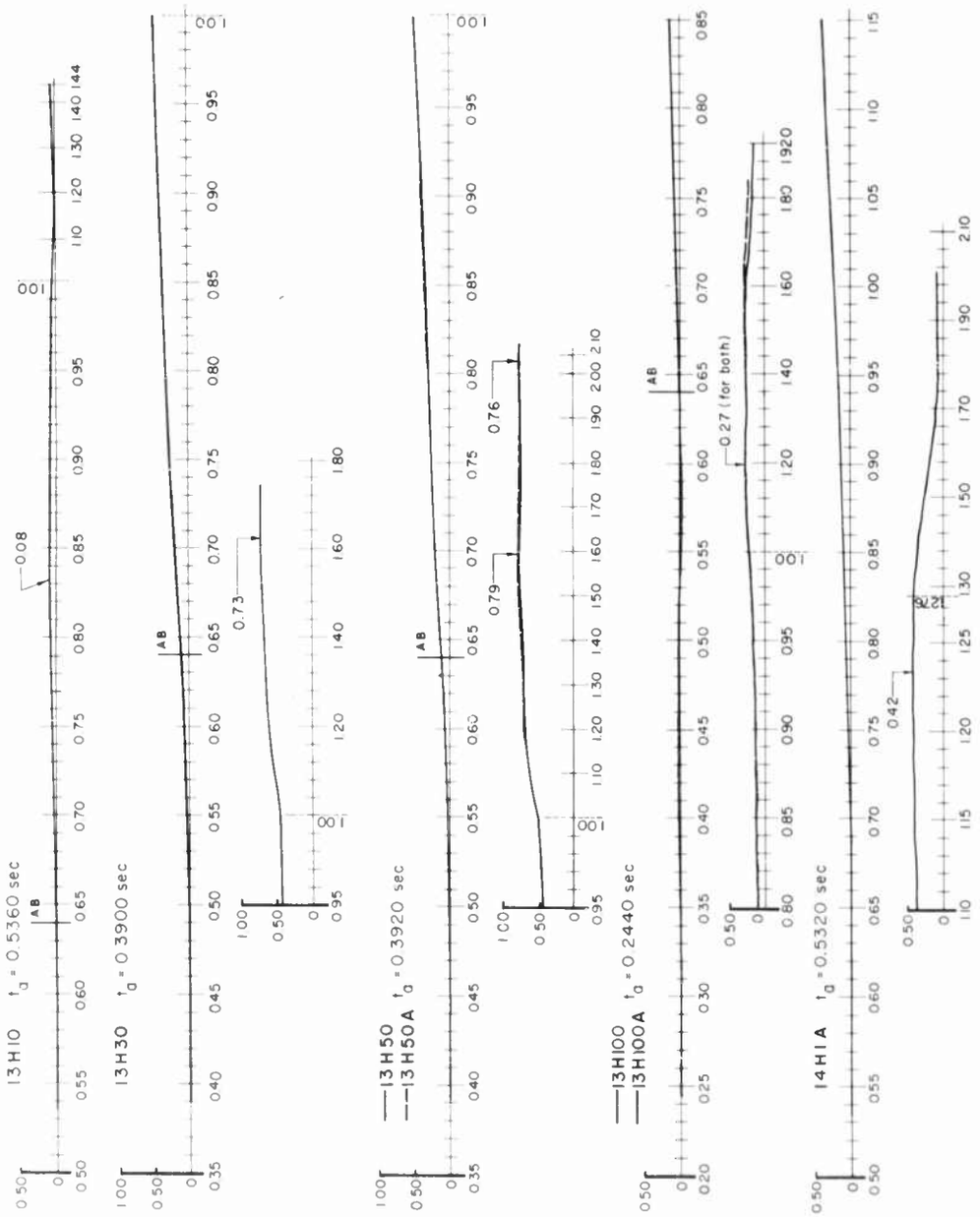

Figure 4.36 Horizontal displacement versus time, Stations 13 and 14, Shot Koa.

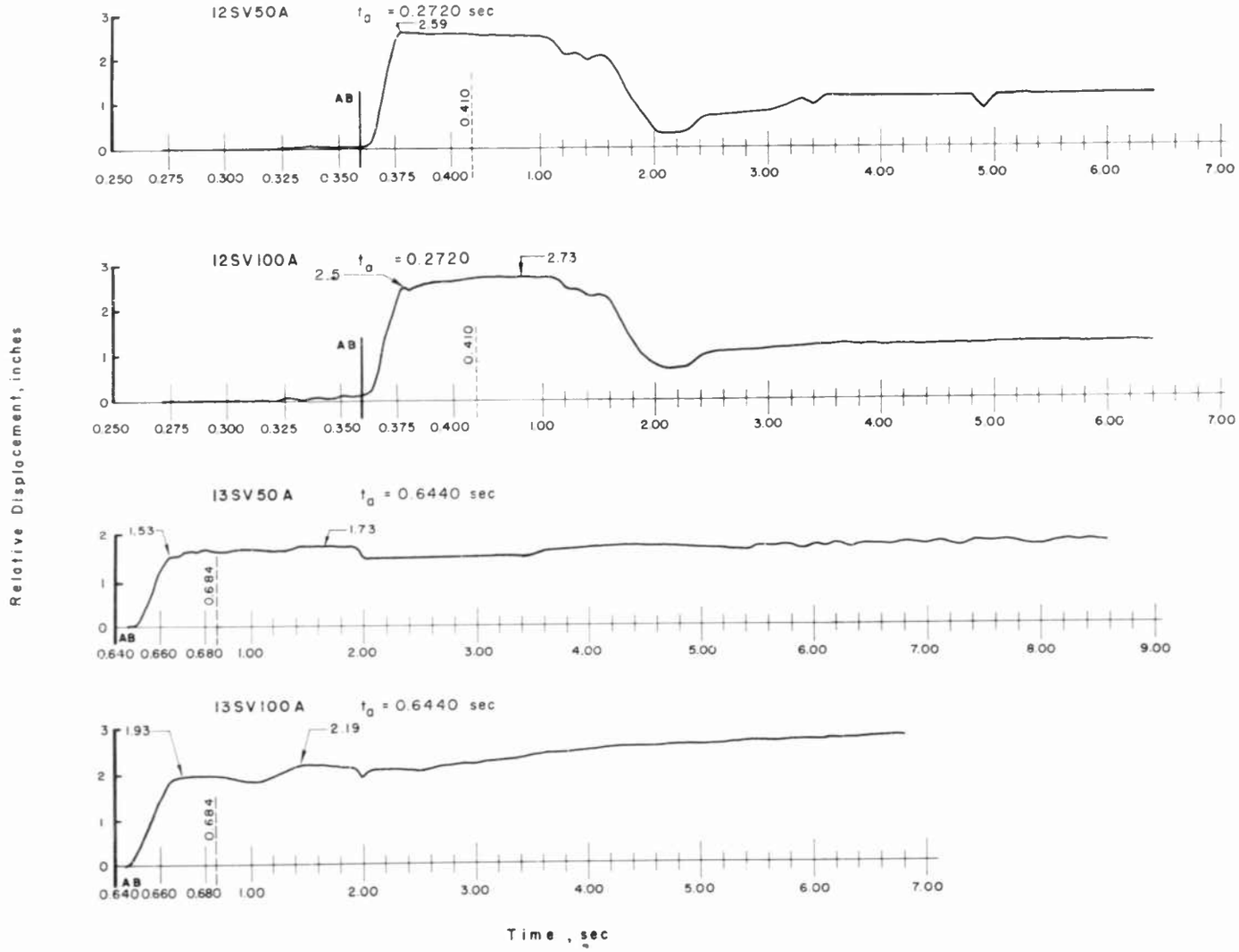

Figure 4.37 Relative displacement versus time, Stations 12 and 13, Shot Koa.

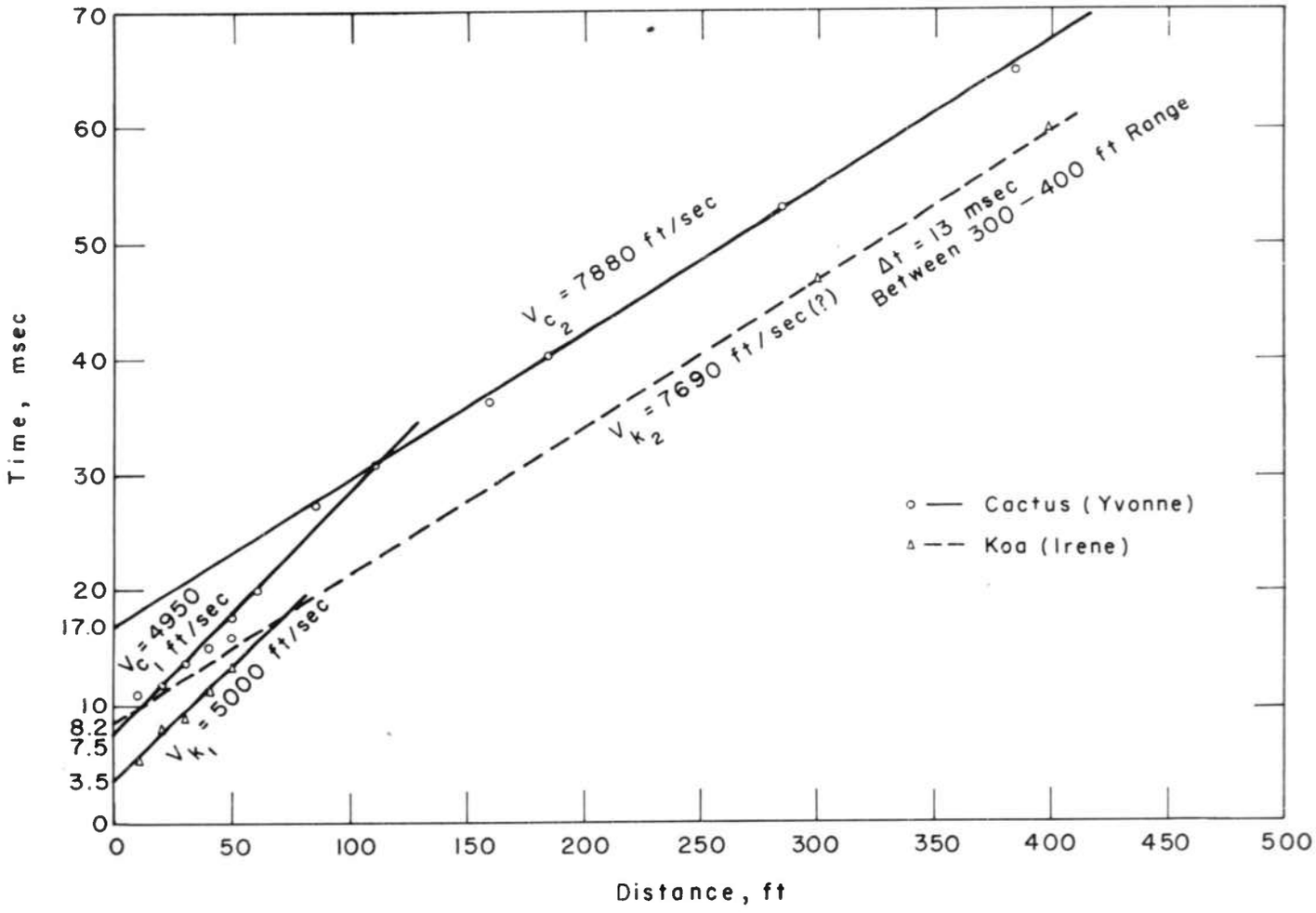

Figure 4.38 Seismic refraction time-distance curves (Yvonne and Irene).

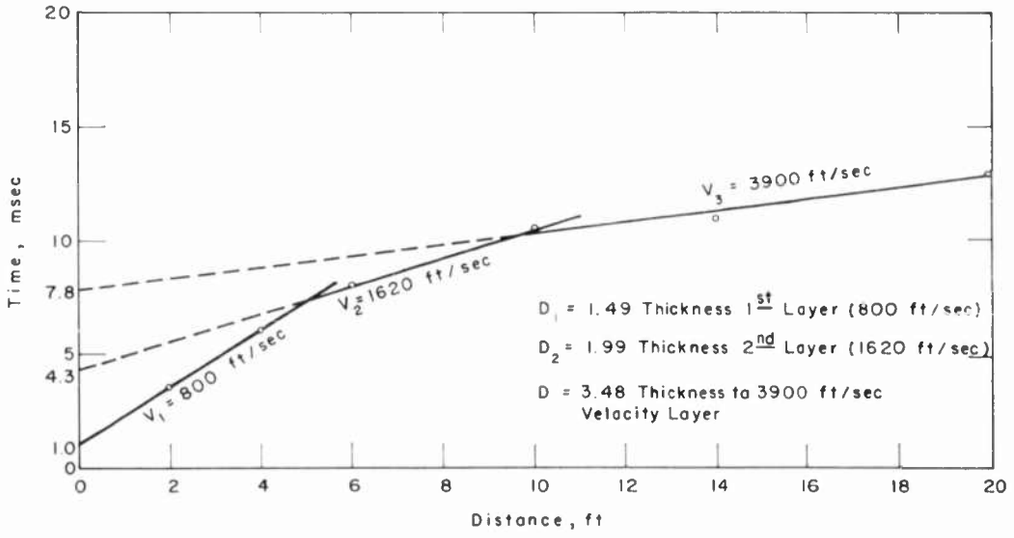

Figure 4.39 Short-range seismic refraction time-distance curve (Irene).

Chapter 5

DISCUSSION

5.1 AIRBLAST

Before the discussion of ground motion per se, some comments are in order on the airblast from Shots Cactus and Koa, since the airblast largely determines the characteristics of the ground motion, and since theoretically the motion cannot be scaled if the airblast is not scalable. Scaling factors (for scaling to 1 kt at sea level) for Cactus (18 ± 1.8 kt) and Koa (1.31 ± 0.08 Mt) are as follows:

Quantity	Cactus	Koa
S_p	1.0027	1.0027
S_d	0.3812	0.0932
S_t	0.3889	0.0952

How important, practically speaking, nonideal blast waves are in the scalability of ground motion is unknown.

Although the scaled ground ranges at which measurements were made are similar on Cactus and Koa and both were surface shots, the airblast waves are markedly different. Both shots show earlier arrivals and peak pressures differing from those that would be predicted over an ideal surface, with Cactus showing earlier arrivals and lower pressures than Koa. In fact, the pressure time waveform at the station nearest ground zero on Cactus (Station 1) can be classified as a type associated with precursor formation (Reference 24). Koa pressure-time waveforms on the other hand are essentially classical (Figure 4.18) with some features of anomalous disturbance. Perhaps the explanation for the dissimilar blast waves lies in the difference of surface over which the two shots were fired. Cactus was fired essentially over land, but the Koa environment contained a large expanse of water surface in a very critical place, i.e., between ground zero and the closest measurement station. There is some precedence at EPG for the nonideal behavior on Cactus in that two other nuclear surface bursts, Shots Lacrosse (~ 39.5 kt) and Zuni (~ 3.4 Mt) during Operation Redwing, both fired over mixed land and water surfaces, produced precursors (References 25 and 26).

5.1.1 Arrival Times and Shock Velocities. Figure 5.1 compares the scaled arrival times at each of the three stations of Cactus and of Koa with a curve of ideal arrival times based on the assumption of 1.6-kt effective yield of a 1-kt surface shot. (The free-air curve used in Figure 5.1 is the "U.S. 1959 Empirical Free-Air Pressure-Distance Curve of 1 Kt at Sea Level." It differs only negligibly from the revised DASA curve at overpressures above 10 psi.) While it would be possible to pass a single line within 1 msec (A-scaled) of both the Koa and Cactus points in this figure, the difference in their deviation from the ideal curve is probably meaningful, and the trend of Cactus arrivals toward precursorlike earliness is clear. Scaled Lacrosse arrivals (Reference 25) in this region are similar to those of Koa, but the Lacrosse precursor, evidenced by distortion in the

waveform, appeared only at scaled ground ranges between 300 and 450 feet, whereas that of Cactus was only at shorter ranges.

Even on Koa, the scaled arrival times at the first two stations were about 1 and 2 msec earlier than would be expected from 1.6W theory, although from Reference 27 the opposite is to be expected, since overpressures and consequent velocities at close-in ground ranges from surface bursts are given as generally somewhat less than those predicted by 1.6W theory. Apparently the early arrivals on Cactus were due to a thermal disturbance, whereas those on Koa were more nearly due to the unexpectedly high peak overpressures at short ranges, as described in Section 5.1.2.

Figure 5.1 shows that the arrivals at the most remote stations tend to return to the ideal curve. This tendency is almost universally observed, at least where the early perturbations are caused by surface effects. The early arrivals at the first stations, particularly on Cactus, indicate a higher-than-normal propagation velocity in the early blast wave history. The return to normal arrival times necessitates a correspondingly lower-than-normal velocity at later times, even though the peak overpressures may not be abnormally low. In fully formed precursor conditions, this slowing down is recognized as part of the cleanup phase; in any case, it may be recognized as an adjustment of surface pressure and velocity to those existing in the free air at height.

5.1.2 Peak Overpressure. Figures 5.2 and 5.3 summarize the scaled maximum overpressure-distance variations on Cactus and Koa. (In the figures, SRI is the abbreviation for Stanford Research Institute.) The composite surface burst curve from Reference 26, the 2-kt free-air curve, and BRL data have been included in the figures (information contained in a letter from Ballistic Research Laboratories (BRL) to Field Command, Defense Atomic Support Agency, dated 8 September 1959; the judgment of the relative validity of the points, which is indicated in the figures, is that of BRL).

Except for that at Station 1, Cactus peak overpressures are not unusual. At Station 1 (158 ft/kt$^{1/3}$), the overpressure is considerably lower than the composite surface burst curve (Figure 5.2), but the BRL-measured pressures near 200 ft/kt$^{1/3}$ ground range do not seem so. Zuni and Lacrosse measurements also show no comparable pressure depression, but neither they nor the BRL measurements extend as close as Station 1.

Since the validity of the close-in BRL measurements is in most cases questionable, these measurements require a good deal of interpretation as to the true peak values. Taking this into consideration along with the higher-than-expected average blast wave speed between Stations 1 and 2 and the early arrival and precursor-type overpressure waveform at Station 1 points to the existence of a precursor of limited extent in the neighborhood of 150 ft/kt$^{1/3}$. The precursor appeared to clean up quickly so that it was not particularly evident (except in the waveform) at Station 2. This behavior is consistent with other observations on precursor formation during surface detonations (References 25 and 26).

Close-in Koa peak pressures (Figure 5.3) are remarkable also but for another reason: they appear to be inexplicably high. In fact, the blast effectiveness for ground ranges less than about 280 ft/kt$^{1/3}$ appears to be well above 2 kt. The two SRI measurements made at Station 11 agree to within 2 percent and at Station 12, to within 5 percent. Further, the BRL measurements are clearly of similar magnitude. The existence of unusually high pressures on Koa seems then to be well documented. It is paradoxical that these pressures are above 2W theory, since the usual procedure for yield determination for high-yield surface bursts relies on hydrodynamic theory, which implicitly requires the 2W yield assumption.

The slightly high early velocities mentioned in the preceding section are more than justified by these high pressures; in fact, the puzzle now becomes one of explaining how

the overpressure can be so great without producing much earlier arrivals. It seems clear that sufficiently low temperatures cannot have existed locally to reduce the velocities. This situation, combined with that of Cactus, simply emphasizes the hazard of deducing the peak overpressure from the propagation velocity, especially near the surface.

5.1.3 Pressure-Time Waveforms. None of the pressure histories from Cactus is strictly classical (Figure 4.1), although Station 3 produced a near-classical waveform. The record from Station 1 (1B) has been and continues to be controversial. Its low peak value has already been discussed. The overpressure waveform belongs in the precursor series (Reference 24), even if some of the noise is discounted as spurious. Cactus Station 2 history has three nonclassical features: the interrupted initial rise, the rounded peak, and the nonmonotonic pressure decay after front passage; but it seems qualitatively less disturbed than that from Station 1; and although it may be classed as a precursor type 2 overpressure waveform, its arrival time is not correspondingly early and its peak overpressure is not correspondingly low.

Koa waveforms show none of the effects of gross thermal disturbance (Figure 4.16), and since air shock pressure histories are important in determining ground motion, the Koa results have been compared in some detail with the theoretical pressure-time variations found in References 28 and 29.

Several alternative methods of computing the comparison theoretical curves are shown in Figure 5.4. The first method uses the overpressure waveform characteristic of the peak overpressure and scales time according to 2W theory, since overpressure duration appears to scale more nearly as 2W than as 1.6W as does peak overpressure. The remainder of the methods employ various combinations of 1.6W and 2W scaling. The hybrid scaling of 1.6 W for range, i.e., for peak overpressure, and of 2W for time, i.e., for duration, results in the best fit to the observed pressure after 30 msec. The decay pressure behind the shock front is much more rapid than that predicted by theory, which gives rise to the postulate that the high peak pressure is the result of a superimposed spike. In any event, the overpressure pulse at Station 11 is not characteristic of a 1,000-psi shock overpressure.

The overpressure pulses at Stations 12 and 13 (Figures 5.5 and 5.6) exhibit the initial rapid decay similar to that observed on Station 11. Also, both of these pulses are accompanied by a secondary rounded peak, which is certainly not characteristic of even the most advanced theory (Reference 28). These secondary pressure pulses however decay fairly rapidly so that the pressure returns to that predicted by the hybrid scaling system.

The origins of these perturbations are uncertain. They are not characteristic of thermal disturbances. A possible explanation of the high shock pressures lies in the fact that the Koa device was detonated in a large water tank. The vastly increased opacity of the surface surroundings may have affected the early hydrodynamic history of the explosion, to cause the close-in pressures to be high and of short duration. As previously mentioned, such an effect should have evidenced itself in the device yield. The secondary disturbances may be due to meteorological refractions—an equally uncertain postulate.

On the basis of these measurements, there appears to be no reason to change the composite surface burst curve (Reference 27).

The effect of these nonstandard waveforms on ground motion is uncertain; however, it is believed that it will be less than the higher-than-normal overpressures would indicate.

5.1.4 Pressure Impulse. The Cactus overpressure baseline evidenced considerable noise, possibly due to failure of the induction signal protection equipment, which prohibited accurate determination of the positive phase duration for this shot. This difficulty also

applies, although to a lesser extent, to the determination of overpressure impulse from the gage records. The values used here were obtained by integrating the Koa records out to the approximate crossover, and then determining the duration of integration of the Cactus records by scaling times for corresponding stations. These results are shown in Table 4.2.

In Figure 5.7, A-scaled impulse is plotted as a function of A-scaled ground range. For comparison, curves derived from the ideal free-air curve and data from Shot Lacrosse are included (Reference 25). The Hardtack results at EPG are generally consistent with those from Lacrosse and differ somewhat from the ideal curve, particularly in the steepness of the slope of the curve. The major exception is Station 1 of Cactus where the impulse is nearly 2:1 lower than the projected trend. This, of course, is the gage record that shows the most severe waveform distortion and the greatest depression of peak overpressure.

In Figure 5.8, scaled overpressure impulse is shown as a function of peak overpressure and compared with data from Lacrosse and from a number of Plumbbob shots (Reference 20). (In Figure 5.8, SC is the abbreviation for Sandia Corporation.) Koa measurements are consistently lower than those from Cactus and Plumbbob because of the previously mentioned higher-than-average overpressures. This again points to abnormal pressure-time histories on Koa.

5.1.5 Summary. Airblast phenomena measured on this project showed a number of departures from the values predicted. On Cactus, what appears to be a more or less normal precursor formed quite early and cleaned up before the pressure dropped to 100 psi, in contrast to Lacrosse where it was observed at lower overpressures and to other EPG surface shots where no precursor was observed. (In many cases, a precursor similar to that of Cactus may have existed but was not documented.) The resultant distortion of waveform and suppressed peak pressure may have affected the shallow ground motion at Station 1. There is no choice but to accept the measurement at 1B as valid, in view of the early arrival time. The erratic nature of the precursor and its early cleanup may be considered characteristic of a surface shot.

On Koa, the unusual characteristics are the high peak pressures and the unusually rapid initial decay at short ground ranges. Again, these characteristics probably affected only the shallow earth motion at these stations, since it will be seen later that the indirectly arriving energy predominated at moderate depths, even very close-in.

It should be mentioned that neither of these shots was a controlled experiment, as far as blast effects were concerned. Both were surrounded by considerable extra mass — on Cactus it was proportionately greater but farther away, while on Koa the additional mass was very closely associated with the device. Either of these conditions can change the initial conditions sufficiently to affect the effective yield and/or change the conditions of symmetry in the vertical plane. Unfortunately, these are the circumstances with which the blast effects experimenter must expect to contend.

5.2 EARTH MOTION

Since the primary objective of this project was to study earth motion, it is desirable to derive all the information possible from these results, but this information should be that which is generally applicable and not that which is peculiar to a specific island or even to EPG. Thus, some of the phenomena are examined only to the extent necessary to identify them as being local peculiarities; others are investigated more fully to derive general guidance from them.

5.2.1 Acceleration. Preshot predictions of Hardtack acceleration, used for range setting, were based on classic-waveform air-pressure inputs and the observed attenuation of acceleration with depth determined from several nuclear airbursts at NTS. The primary predictions were confined to the vertical component of acceleration, and it was assumed that the horizontal component would not exceed about a third or a half the vertical magnitudes. No consideration was given to accelerations produced otherwise than by local airblast slap.

Under these circumstances, the degree to which the results resembled the predictions was surprisingly good, in view of the complex nature of the waveforms (Figures 4.2 through 4.15, 4.17 through 4.22). A casual examination of these records shows that, except for the near-surface, close-in stations, the peak accelerations are not directly related to the local airblast, in contrast to the experience at NTS.

Figure 5.9 shows measured peak accelerations as a function of depth for Cactus, and Figure 5.10 shows similar data for Koa. There is a general tendency, not well established, for the vertical peak values to decrease more rapidly with depth than was predicted on the basis of NTS results. On Cactus, the upward peaks were sometimes greater than the downward. Sometimes, too, the horizontal peak acceleration was greater than the vertical, showing the importance of the horizontally traveling waves from distant sources and indicating that local airblast slap is not the dominant factor.

The evidence of Figures 5.9 and 5.10 and a superficial study of the gage records are sufficient to show that there is no value to be had from an attempt to identify the various wave components or to trace energy paths to their origins. There are too many interacting arrivals of energy at each gage to permit other than very general conclusions to be drawn from the acceleration records. A qualitative examination of the records, however, explains this confusion and gives some clues to the source of some of the disturbing arrivals. On Cactus, as has been pointed out, the sharp downward acceleration due to local airblast, which is common in most areas, is almost entirely missing. At Station 1, it appears to begin at the expected time only to be overcome by upward peaks at 1-, 10-, and 30-foot depths, but at 50 feet the appearance is more normal. At Stations 2 and 3, there is an even more striking lack of these downward peaks. The same is true on Koa, particularly at Stations 12 and 13.

In contrast, at Station 1, the horizontal accelerometers show the abrupt outward arrivals that appear to conform to the general experience, with the angle of arrival of the slap such as to produce generally an outward radial component. However, two features cause question of whether this is the true airblast slap. First, at 1H10, this arrival time is after that of the downward signal on 1V10 and is almost precisely that of the sharp upward acceleration here and at 1V1. At 1H30 and 1H50, this arrival is at the time of the downward pulse on the corresponding vertical gages. Second, at Station 2 similar arrivals are noted on the horizontal gages, but here they are all at essentially the same time and are simultaneous with airblast arrival, whereas at Station 3 they arrive before the airblast. From the arrival times of these waves, using the 30-foot depth, these waves are traveling about 7,100 ft/sec, which is only slightly slower than the measured seismic P wave velocity of 7,880 ft/sec. This is consistent with experience with moderate to strong waves.

Entirely similar events are noted at Stations 11 and 12 on Koa, but here they outrun the blast wave before the second station, and a new set is generated before arrival of the blast wave at Station 13. Thus on both Cactus and Koa the outrunning ground motion is of the type associated with a transseismic airblast, in contrast to the refractive type of outrunning observed at low overpressures at NTS. During refractive outrunning, the trace velocity of the ground motion arrivals corresponds to the P wave velocity of the refracting layer rather than to that of the surface layer as is the case at EPG. These waves can be observed at about 0.640 second after the explosion at Station 13, the time of airblast

arrival, the original wave front observed at Station 12 arriving at Station 13 at 0.390 second. Note that the wave front beneath the surface is essentially vertical, as indicated by arrival times, which is another characteristic of transseismic outrunning. These signals cannot be considered to be coming from the local airblast nor can they be considered to be originating at ground zero; they are a cumulative effect of the blast wave interaction with the surface at intermediate ranges. Their magnitude is, hence, only indirectly related to the magnitude of the local blast wave.

Returning to the examination of the vertical acceleration records, there is seen in general on both shots a pronounced tendency for all marked vertical arrivals to be coincident with these remotely derived horizontal arrivals. Sometimes an outward horizontal peak produces an upward peak, sometimes a downward one. This is probably dependent primarily on the position of the gage in one of the several layers observed in each hole; horizontal compressional stress may produce either an upward or downward motion, depending upon the proximity of a free surface or an interface between two velocity regimes. Thus, even this behavior is a function of the fine-grain local detail of the medium and not a function of its general character.

At Station 13 on Koa, and on Station 2 on Cactus, some very sharp second arrivals are seen, with peak accelerations generally higher than the primary peaks. Similar but less pronounced events are visible at Stations 11 and 12 on Koa and at Station 1 on Cactus. These events appear to be related but have some inconsistencies. If they are treated as continuously transmitted waves originating near ground zero, a propagation velocity of about 4,300 ft/sec is found—a velocity that is faster than the average blast wave velocity, which is probably consistent with the shear or surface wave velocity. Also, particularly at Koa Station 13, this signal arrives earliest at the deepest gage, which is characteristic of a signal arriving from a distance. However, this event is very sharp and strong at Station 13 and less so at Stations 11 and 12. Furthermore, it does not show up at all at the shelter (Station 14), although this station is only 750 feet from Station 13.

If these secondary events have any meaning at all with respect to a continuously propagated wave, it must be that they are local disturbances generated by formation failure caused by the passage of some sort of long-duration, surface or near-surface wave.

From the preceding discussion, it would appear that under outrunning ground motion conditions, correlations of maximum acceleration versus ground range and weapon yield or a combination of both would inherently contain a high degree of scatter. This is indeed the situation on Cactus and Koa and appears to be characteristic of all previous EPG data and of United Kingdom (UK) experiments as well.

Maximum vertical accelerations, irrespective of sign, for all EPG experiments, the UK Buffalo and Antler trials, and Jangle S (Yucca test area, NTS) are plotted in Figure 5.11 versus A-scaled ground range. Presentation of data in this manner rather than as scaled maximum acceleration, i.e., $a_m W^{1/3}$, versus scaled ground range as would be expected from the results of high explosive (HE) and underground nuclear detonations is based on the larger scatter of the latter presentation (Figure 5.12). The choice of the correlation of Figure 5.11 is significant in that the accelerations at the same scaled ground range do not decrease as device yield increases.

Although the scatter of data in Figure 5.11 is sixfold, note that, with the exception of Lacrosse, results from individual experiments are neither systematically high nor low with respect to the average curve and that in some cases acceleration measurements at the same ground range but 180° apart differ by as much as 300 percent. Some variation is also to be expected because of the variation in depth of measurement (surface to 17 feet). Within the sixfold scatter of data, the test site does not appear to be a dominant factor. The data of Jangle S (~ 1 kt at NTS) and the data of Buffalo Round 2 (1 kt at Maralinga, Australia) are in good agreement and are in juxtaposition to the EPG data to approximately

the same extent that the Buffalo and Antler data agree within themselves. The best evidence in favor of the correlation of Figure 5.11 is the correlation of the Mike data with the Blackfoot data (a ratio of 11:1 in $W^{1/3}$) and with the Jangle S and Buffalo Round 2 data (a ratio of 22:1 in $W^{1/3}$).

By themselves, the Hardtack results do not serve to strengthen the correlation of Figure 5.11, nor do they detract from it. Whereas the agreement of the Koa data with the average curve can be considered excellent, the Cactus results deviate to the extremes of the correlation at the smallest and largest ground ranges. Unfortunately, additional Hardtack measurements were not made at greater ranges, with the purpose of tying firmly to previous data.

Maximum horizontal accelerations on Hardtack when compared with previous outrunning ground motion data (Figure 5.13) lead to a correlation similar to that for the vertical accelerations. Although the scatter of data is somewhat great, being 8:1 compared with 6:1 for the vertical accelerations, Figure 5.13 tends to support the proposed scaling procedure. Since the trend of the horizontal acceleration is much the same as that for the vertical accelerations, an average curve similar to that of Figure 5.11 has been drawn in Figure 5.13 with the average of the horizontal accelerations being half the average of the vertical accelerations.

The nonuniform slope of the curves of Figures 5.11 and 5.13 warrants comment. At the larger ground ranges, the slope is minus 2 which agrees with HE data in this region (Reference 30).

At intermediate ground ranges, the slope is approximately minus 3, the conclusion reached in (Reference 31).

However, at smaller ground ranges, the data support a slope of minus 3.5.

Of the data displayed in Figures 5.11 and 5.13, only Cactus, Koa, and Jangle S accelerations were measured at a number of depths. These measurements (Figures 5.14 and 5.15) were normalized by dividing by the mean acceleration as determined by the curve of Figures 5.11 or 5.13, since this presented a more systematic variations of acceleration with depth than dividing the acceleration by the acceleration at some standard depth, e.g., the maximum acceleration at 10 feet, as is usually done when the airblast is superseismic.

5.2.2 Particle Velocity. Maximum vertical velocity, irrespective of sign, is plotted versus scaled ground range in Figure 5.16 for EPG experiments for which these measurements are available and for the UK Buffalo and Antler experiments. Device yields range from 1 kt (Buffalo Round 2) to 10.4 Mt (Mike) and scaled heights of burst from surface to 100 feet (Blackfoot). The correlation of Figure 5.16 is surprisingly good considering the differences in seismic characteristics between test areas and suggests that these differences are not significant. Depth of measurement also varies; however, on a scaled basis this difference is not significant.

For fully developed outrunning ground motion, the particle velocity u_m correlation of Figure 5.16 is given by

$$u_m = 5 \times 10^5 \, (R/W^{1/3})^{-2}. \; {}^{+60}_{-40} \text{ percent}$$

where u_m is in ft/sec, R in feet, and W in kilotons. The minus 2 slope is in substantial agreement with the minus 1.8 slope deduced for HE results in Reference 30.

Ground motion measurements at EPG where the blast wave was definitely superseismic are limited to the high-pressure regions of Koa and Cactus, and Lacrosse. These results are listed in Table 5.1 with the exception of those for Cactus where the blast wave was nonideal, and the accelerogram was too confused to determine the velocity jump. In addition, the estimated densities and measured seismic velocities are shown, and the theoretical

velocity-overpressure ratio has been calculated in the right-hand column. The general agreement between the measured and calculated ratios tends to confirm the postualte that the superseismic particle velocity (and hence displacement) decreases linearly with increasing seismic velocity.

Maximum horizontal particle velocities for EPG and Maralinga experiments (Figure 5.17) show a larger dispersion than do the vertical velocities. It is in fact difficult to ascribe a mean line for the data. It appears that the decay of horizontal velocity with ground range lies somewhere between a minus 2 and minus 1.5 slope, the minus 1.5 slope being more applicable for scaled ground ranges greater than 700 feet (overpressures less than approximately 20 psi). At smaller ground ranges (overpressure greater than 20 psi), the maximum horizontal velocity appears to be a fourth to a half of the vertical velocity.

Vertical velocities (Figure 5.18) were normalized by dividing by the mean velocity as determined by the curve of Figure 5.16. The scatter of the correlation is only somewhat greater than the scatter of Figure 5.16, and hence it must be concluded that outrunning vertical velocities attenuate with depth more or less independently of device yield. Note that the two superseismic data points for Koa do not vary significantly with depth; however, the measurements are too scant to be considered factual.

Horizontal velocities (Figure 5.19) were treated in the same manner except that the correlation of horizontal velocity with scaled ground range (Figure 5.17) is not well defined. Consequently, both curves of Figure 5.17 were used for normalization purposes. The vertical lines of Figure 5.19 represent the limits of these two calculations. Horizontal velocity does not appear to have any significant attenuation depth down to a depth of 100 feet, similar to the situation observed at NTS for the superseismic blast wave (Reference 5).

In summary, the accelerations produced on both Cactus and Koa are much more complex and erratic than those observed at NTS. This is the combined result of (1) a surface shot compared with an airburst, (2) a high near-surface seismic velocity, and (3) high attenuation in the near-surface layers of vertically traveling signals. The second is probably the most powerful influence and will produce complex waveforms whenever the blast wave is transseismic. This behavior is consistent with the (extrapolated) results of previous experiments where the ground motion was outrunning and leads to a correlation differing from that proposed for the superseismic blast-wave region (References 5 and 32). The attenuation of acceleration with depth is, however, essentially the same for both the outrunning ground motion and superseismic blast wave regions insofar as EPG and NTS are concerned.

5.2.3 Particle Displacement. The most definitive measurements of surface displacement on Koa are believed to be the relative displacement gages anchored at 50- and 100-foot depths at Stations 12 and 13 (Figure 4.37). Since positive relative displacement represents a decrease in span of the gage, the surface moves downward as expected. The rise time of displacement at Station 12 is approximately 12 msec, after which follows an almost constant downward displacement for a period of about 1 second, after which the surface moves up. This behavior would be considered unusual except for the fact that both gages at Station 12 and the Station 13 gages exhibit the same trend. The downward and upward movement of the surface is reminiscent of the long-span gage measurements on Priscilla (Reference 6); however, great weight should not be put on this similarity, because the airblast and geological conditions between the two shots are vastly different. Since the 12V30 and 12V100 displacements (Figure 4.33) are nearly the same for times less than 0.7 second, the missing 12V50 displacement is expected to be nearly that of the 12V100 displacement during this period, which does not exceed $\frac{1}{2}$ inch. Thus the relative displacement of 12SV50A and 12SV100A would be expected to be very nearly the same, which they are

(Figure 4.37). This and the identical long-time behavior of the two records almost precludes gage malfunction, and hence these records can be considered as surface displacement, within an error of $\frac{1}{2}$ inch at most.

The only available comparison between the relative displacement and integrated accelerometer displacements is at Station 12 (12V1 minus 12V100 versus 12SV100A); these are shown in Figure 5.20 where it is evident that there is considerable discrepancy after a time of 0.4 second. Beyond 0.4 second the particle acceleration is very small compared with the maximum value (Figure 4.26), and hence integration is subject to errors of unknown magnitude because of small reading errors. To illustrate this, a displacement corresponding to a 1-g acceleration error (0.2 percent of maximum acceleration) for 12V1A is also shown in Figure 5.20. It is readily apparent that an error of this magnitude (corresponding to about 0.005 inch on the camera record) may account for the major portion of the discrepancy noted.

Another independent check on the surface displacement, as measured by relative displacement, is the reed gage data (Reference 33), although this check is not absolute, because the reed gages did not go to the very low frequencies necessary to record particle displacement. A 2- to 2.5-inch vertical surface displacement at Koa Station 12 is entirely consistent with the data of Figure 25 of Reference 33. However, it should be noted that a particle displacement of between 2 and 6 inches might be considered consistent. A 2-inch vertical surface displacement at Koa Station 13 is consistent with the low-frequency gage data of Figure 27 of Reference 33 but is larger than would be predicted from the extrapolation of the high-frequency gage data (Figure 28, Reference 33).

On Cactus, the maximum relative displacement at Station 3, 3SV50A (Figure 4.15) is only half that predicted by the extrapolation of the high-frequency reed gage data (Figures 18 and 19, Reference 32). However, if this record is corrected using the integrated 3V50 displacement, a maximum surface displacement of 1.7 inches is obtained at 0.44 second (the limit of the 3V50 integration), which agrees very well with the reed gage data.

The above discussion also suggests that although it was possible to match very closely the velocity-time curves of the 12V1 and 12V1A records with smaller baseline shifts than 1 g, the agreement for times beyond 0.4 second is indeed fortuitous. Another example is the apparently excellent agreement of two corrected velocity records at 12V30 and 12V30A (Figure 4.26). The two velocity records are in good agreement, especially since such different baseline corrections were made. However, the maximum displacements on integration are 0.12 foot positive for 12V30, and 0.12 foot negative for 12V30A. Yet the 12V10 velocity records appear to agree to no less an extent—they agree in sign and magnitude within 25 percent. Thus the old questions of how to correct velocity records and for what length of time displacements found from integration of corrected velocity may be considered valid appear to remain unanswered.

The large upward displacements at late times at Station 11 and the large horizontal displacement recorded by 11H10 and 11H10A require comment. Although it cannot be certified that these are indeed true records, they can be explained as the result of crater lip formation. It is known that the crater edge extends to a range just short of Station 11. Postshot photometric surveys do not show a crater lip; however, a lip 2.5 feet high formed 1 second after detonation would probably be eroded away by subsequent wave action. A horizontal displacement of 15 feet should remain more or less permanently; however, this cannot be checked because of the lack of postshot surveys at this ground range.

The large horizontal displacements deduced for Koa Station 12 (15.6 to 24 inches) do not appear to agree with the surface reed gage data (Figure 26, Reference 33) which, if extrapolated to zero frequency, would show a maximum displacement of the order of 1 inch. The displacements found by integration results from a low-frequency ($\sim$1 cps) velocity which,

if true, would cause the 1-cps reed gage displacement to be larger than the 250-cps reed gage displacement (the lowest frequency reed gage record). However, comparing these with other records it is hard to imagine that the 1- and 25-cps displacements would differ by any order of magnitude. Thus, the Station 12 horizontal displacements must be viewed with suspicion.

The maximum horizontal displacements at 10-foot depth at Cactus Station 3 and Koa Station 13 agree with the surface reed gage data, but this agreement may be fortuitous, since the maximum displacements at greater depths for both stations are larger and of longer duration, and the argument of the previous paragraph must be applied here as well.

To summarize: on Koa, the maximum downward surface displacement appears to be approximately 2.5 inches at Station 11, 2 to 2.5 inches at Station 12, and 2 inches at Station 13, with a possible upward displacement at Station 11 of 2.5 feet due to crater lip formation. The values for 10-, 30-, 50-, and 100-foot depths are very uncertain and may be as large as 1 inch at 100-foot depth. The horizontal displacement measurements are equally if not more uncertain and can only be interpreted as giving an order of magnitude for the maximum displacement of approximately 2 to 6 inches, excepting the possible very large (15-foot) displacement at 10-foot depth at Station 12 due to crater lip formation.

At Cactus Station 3, the maximum surface displacement is 1 to 1.5 inches downward, and the remaining vertical and horizontal displacements are of the order of 2 to 6 inches.

From these results it would appear that the maximum horizontal and vertical displacements on Koa and Cactus were quantitatively similar despite the 4.5:1 difference in $W^{1/3}$ between the two detonations. To generalize this observation would be hazardous in the light of the specialized geology and the lack of theoretical information on outrunning ground motion.

TABLE 5.1 SUMMARY OF SUPERSEISMIC DATA, EPG

Shot	Δp_s	Waveform *	Depth	$\frac{u_j}{\Delta p_s}$	$\frac{a_{vm}}{\Delta p_s}$	Specific Gravity	Seismic Velocity ‡	$\frac{1}{C_L}$
	psi		ft	ft/sec/psi	g/psi		ft/sec	ft/sec/psi
Koa	990	8	1	0.046	1.13	1.4 to 1.7	800	0.055 to 0.066
	990	8	10	0.0056	0.067	2.1	5,000	0.0071
	990	8	50	0.0061	0.048	2.1	8,000	0.0044
	245	8	1	0.089	1.6	1.4 to 1.7	800	0.055 to 0.066
Lacrosse	425	0	2.5	–	0.51	1.4 to 1.7	800	0.055 to 0.066
	200 †	0	2.5	0.034	0.40	1.4 to 1.7	800	0.055 to 0.066
	154	0	2.5	0.018	0.44	1.4 to 1.7	800	0.055 to 0.066
	23 §	1	2.5	0.11	0.74	1.4 to 1.7	800	0.055 to 0.066
	55			0.057	0.29			

* See Reference 5. † Interpolated. ‡ Estimated from Reference 21. § Precursor.

Δp_s = overpressure

$\frac{u_j}{\Delta p_s} = \frac{\text{velocity jump}}{\text{overpressure}}$

$\frac{a_{vm}}{\Delta p_s} = \frac{\text{maximum vertical acceleration}}{\text{overpressure}}$

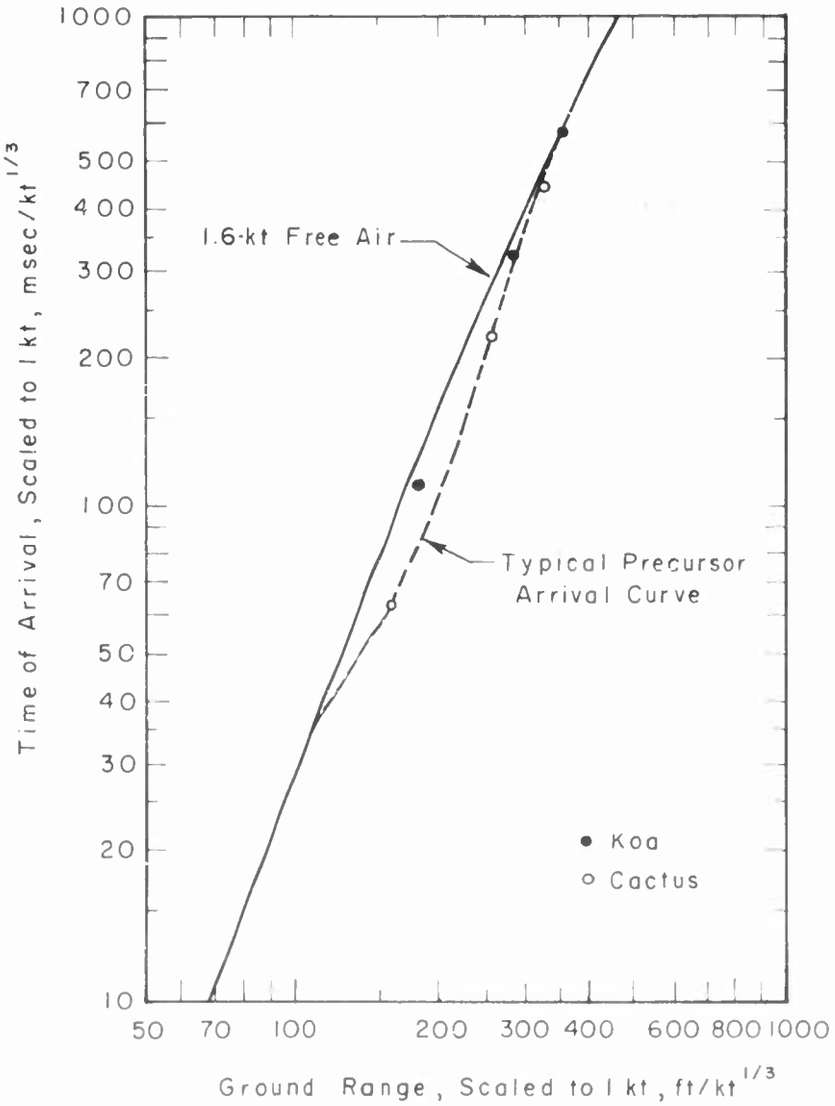

Figure 5.1 Scaled airblast arrival time versus scaled ground range, Shots Cactus and Koa.

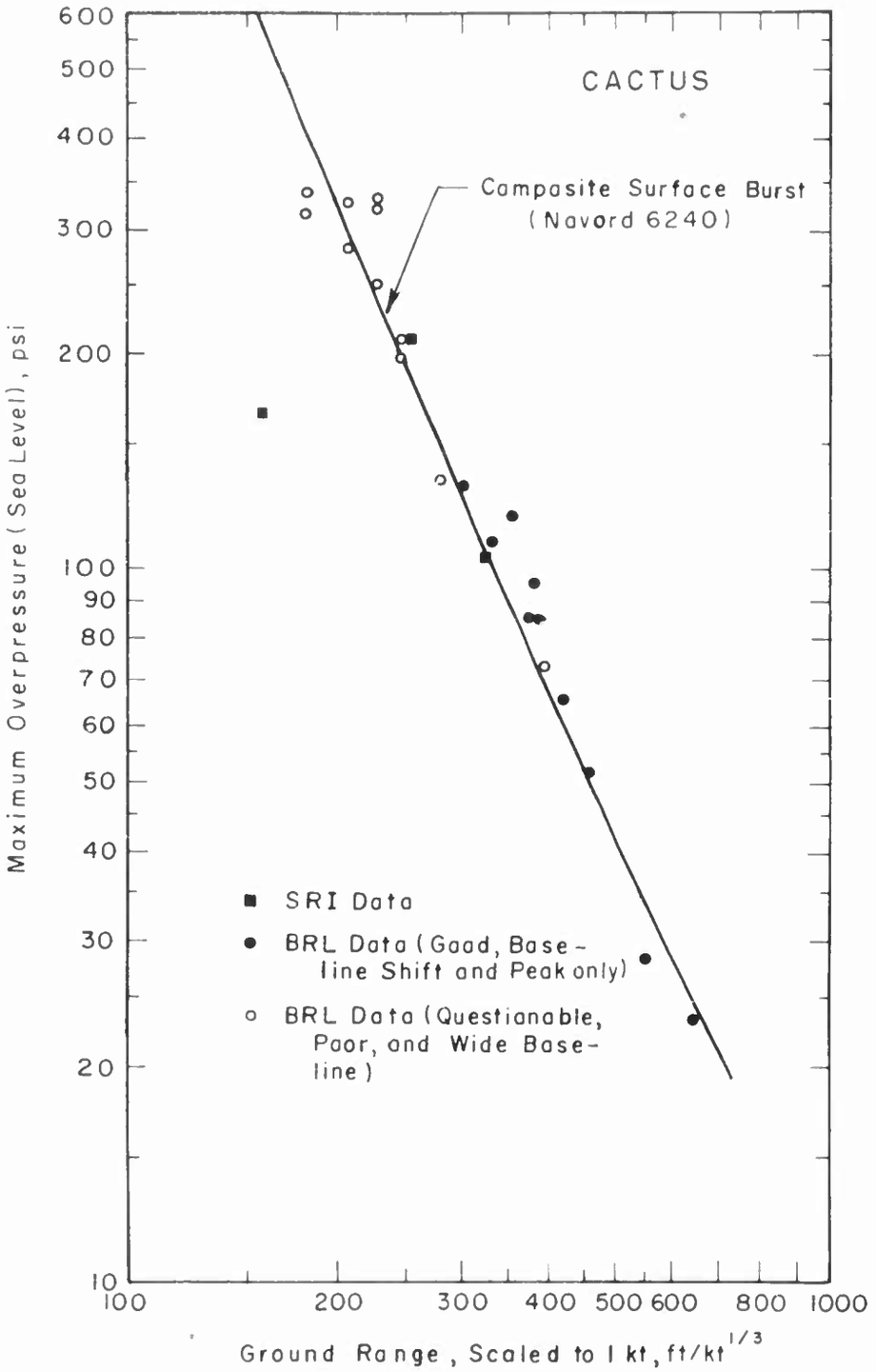

Figure 5.2 Maximum overpressure versus scaled ground range, Shot Cactus.

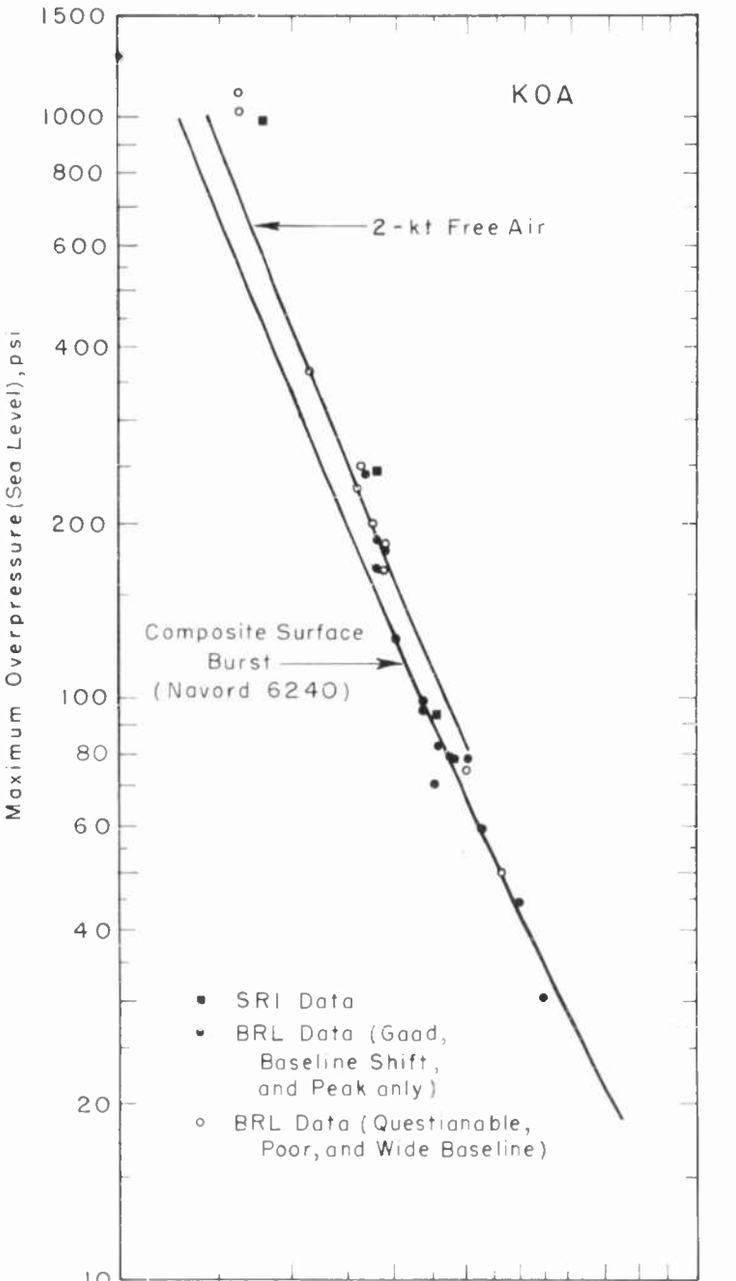

Figure 5.3 Maximum overpressure versus scaled ground range, Shot Koa.

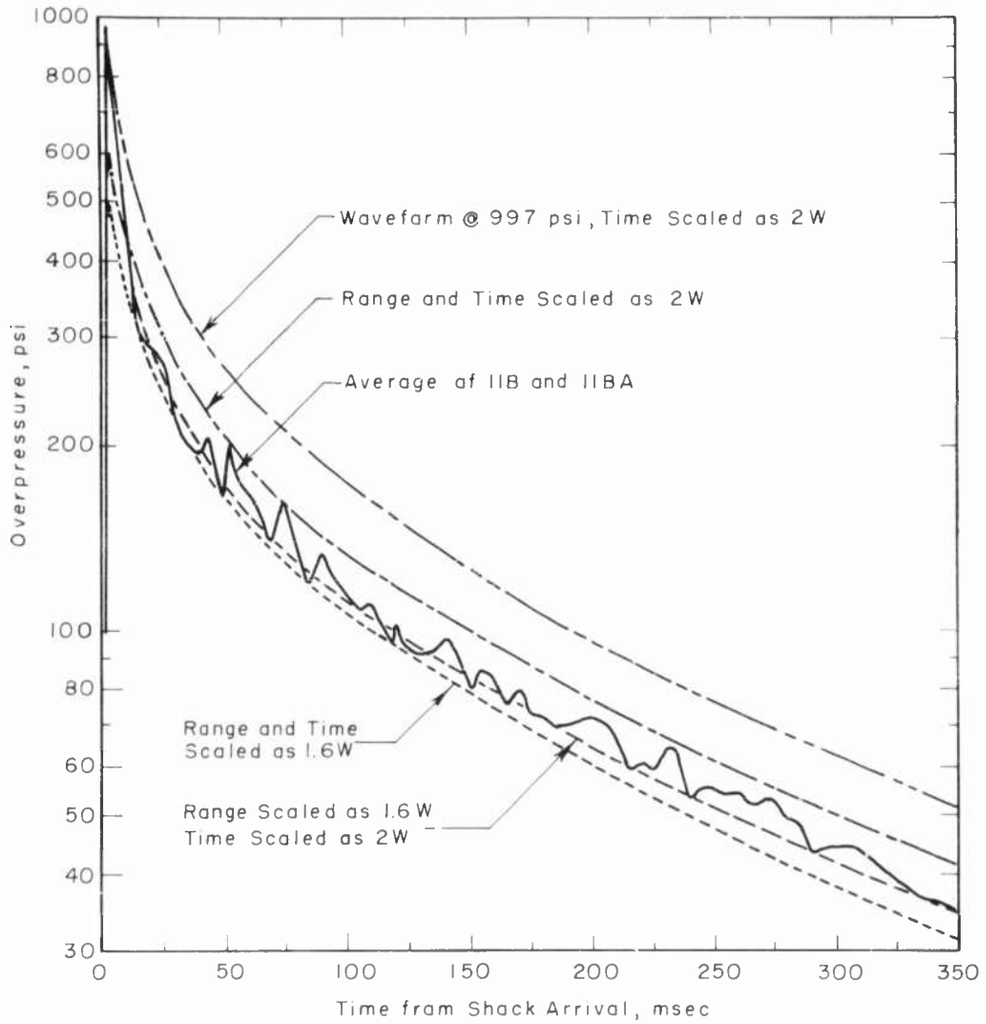

Figure 5.4 Comparison of measured and theoretical overpressure waveforms, Station 11, Shot Koa.

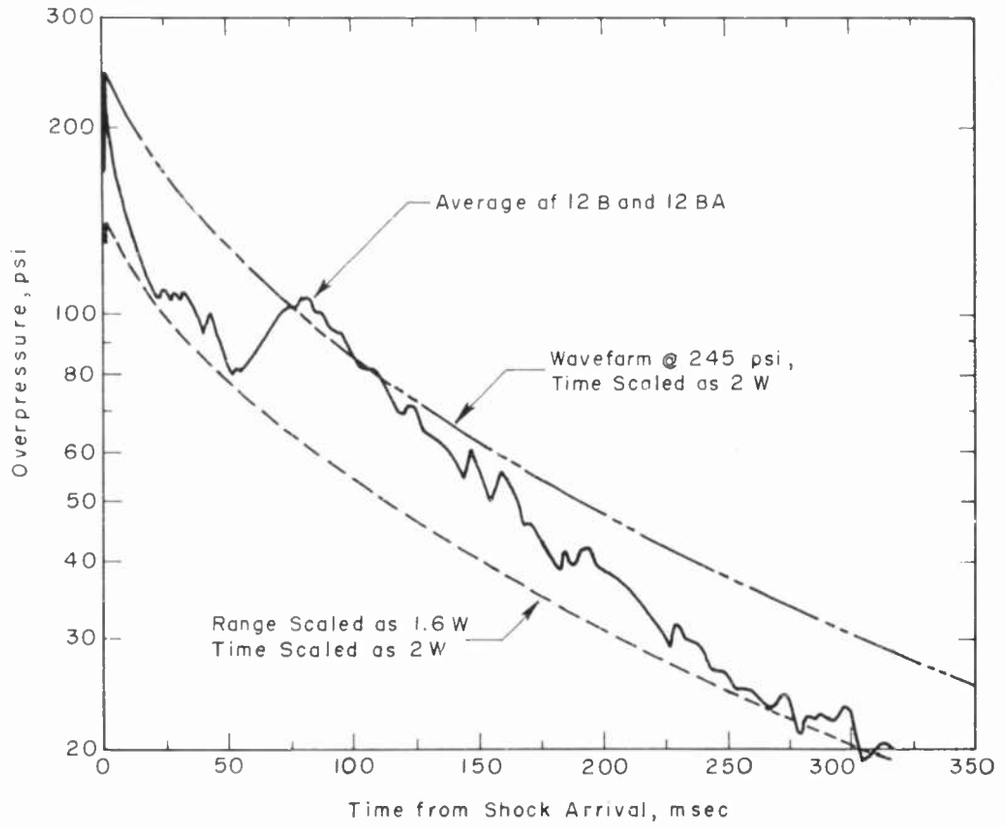

Figure 5.5 Comparison of measured and theoretical overpressure waveforms, Station 12, Shot Koa.

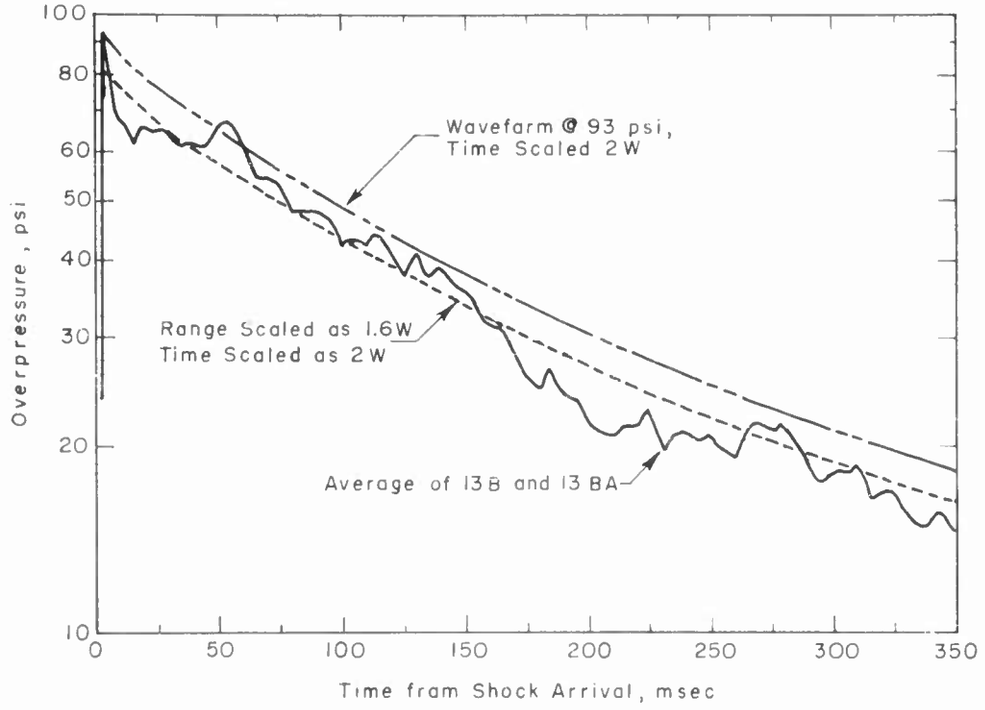

Figure 5.6 Comparison of measured and theoretical overpressure waveforms, Station 13, Shot Koa.

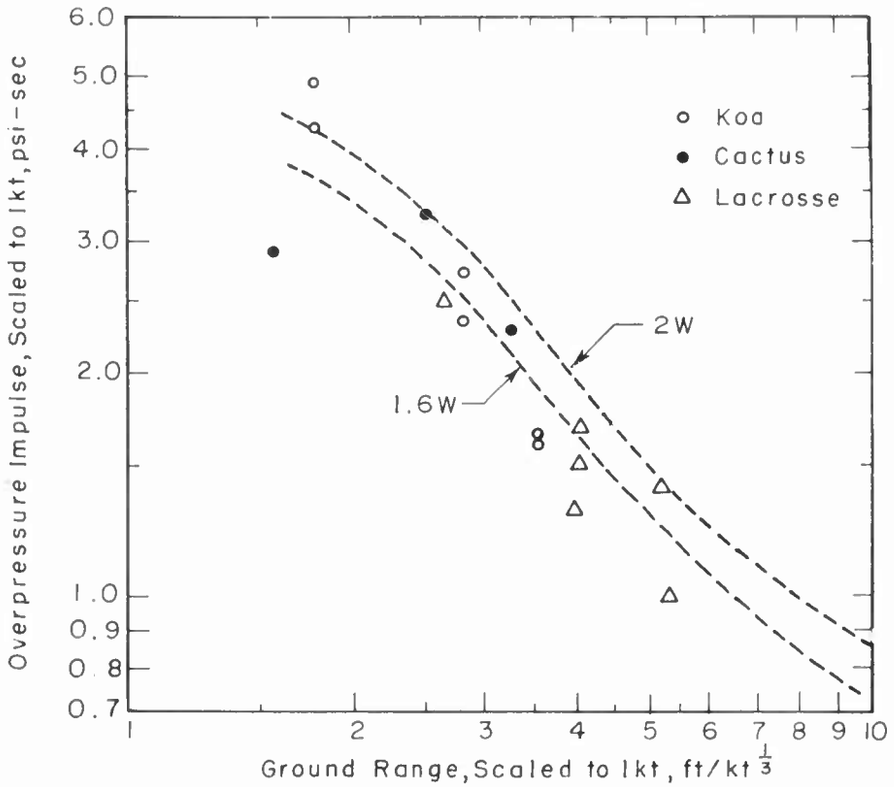

Figure 5.7 Scaled impulse versus scaled ground range, Shots Cactus, Koa, and Lacrosse.

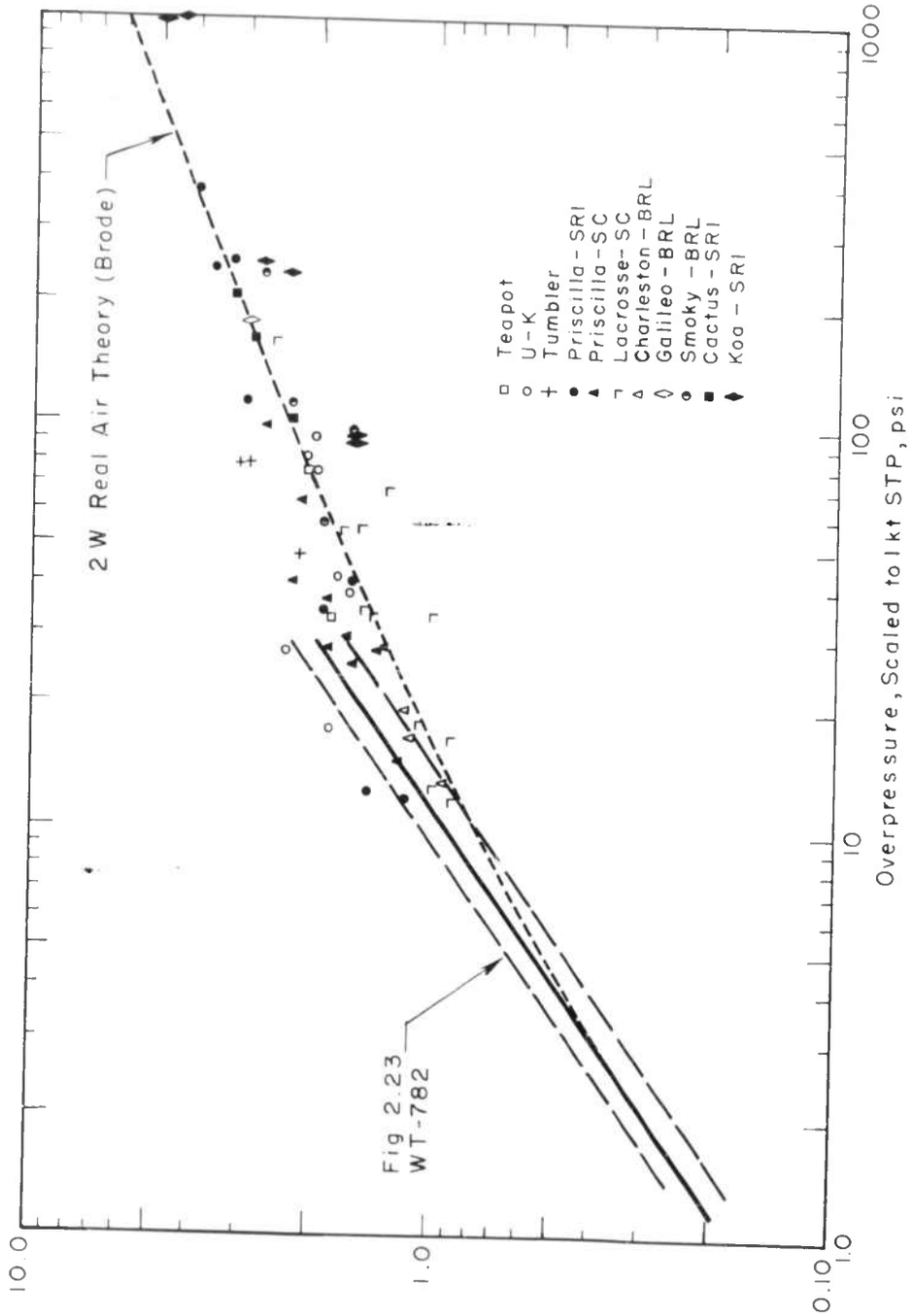

Figure 5.8 Cactus and Koa scaled impulse versus scaled overpressure compared with data from previous shots and 2W theory. Measurements are corrected to standard temperature and pressure (STP).

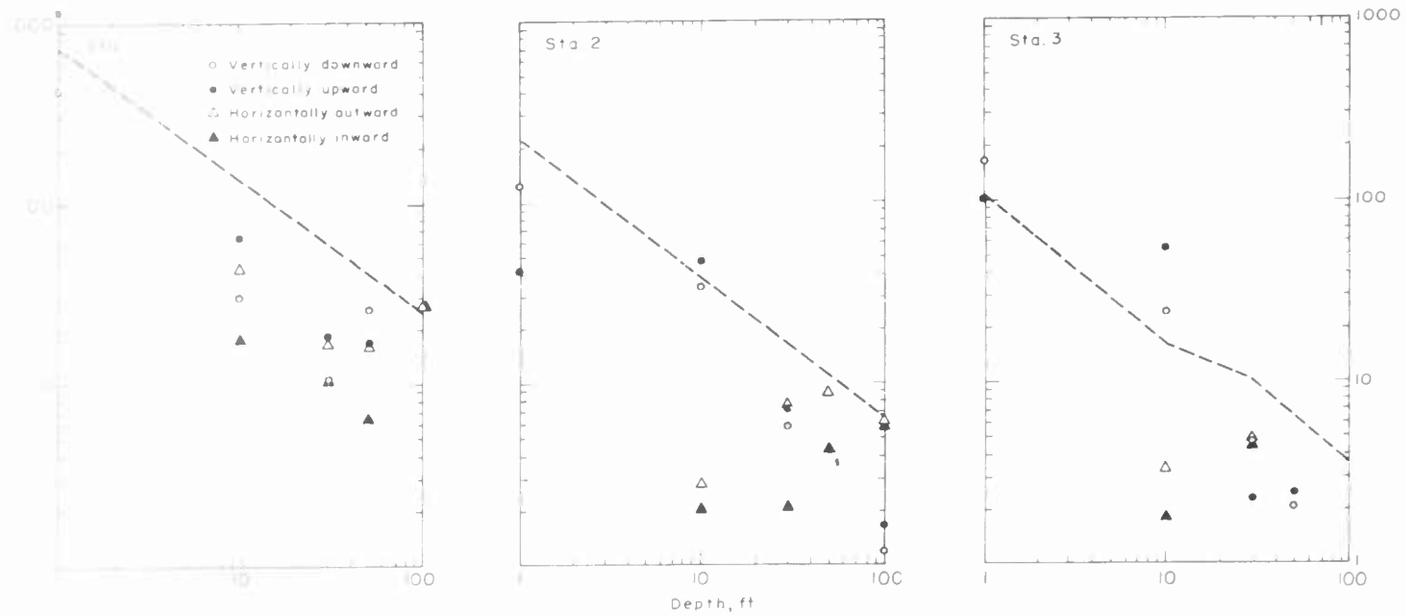

Figure 5.9 Maximum acceleration versus depth, Shot Cactus.

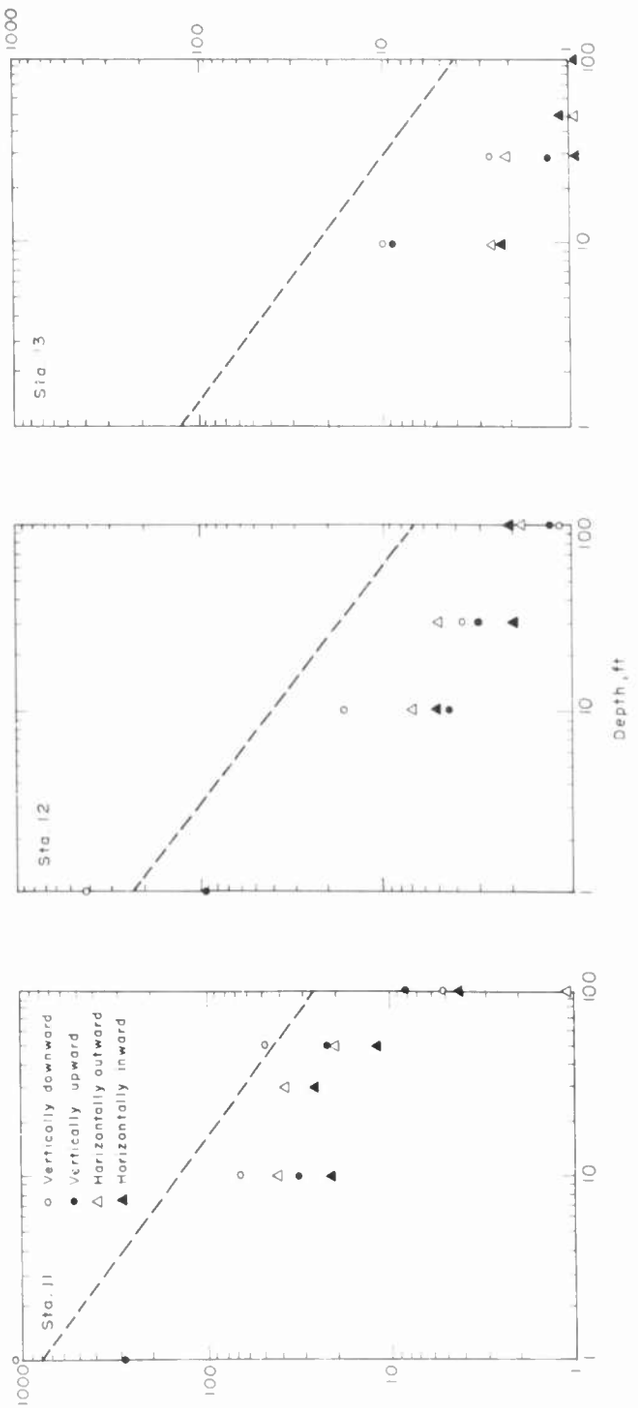

Figure 5.10 Maximum acceleration versus depth, Shot Koa.

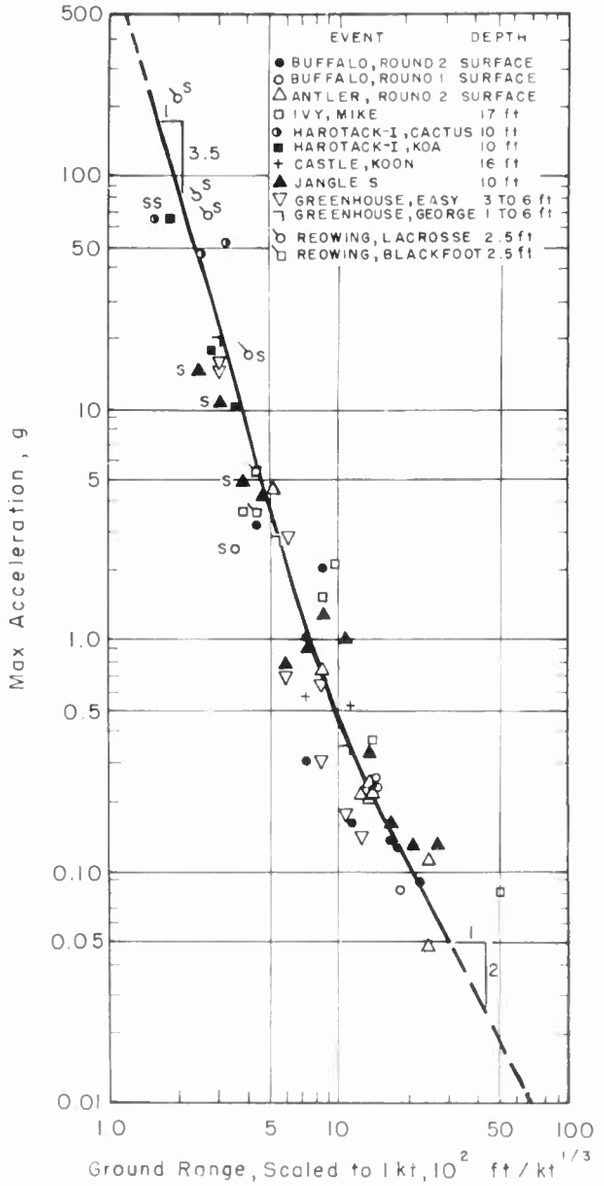

Figure 5.11 Maximum vertical acceleration versus ground range for outrunning ground motion, EPG. (The letter "S" indicates superseismic blast wave.)

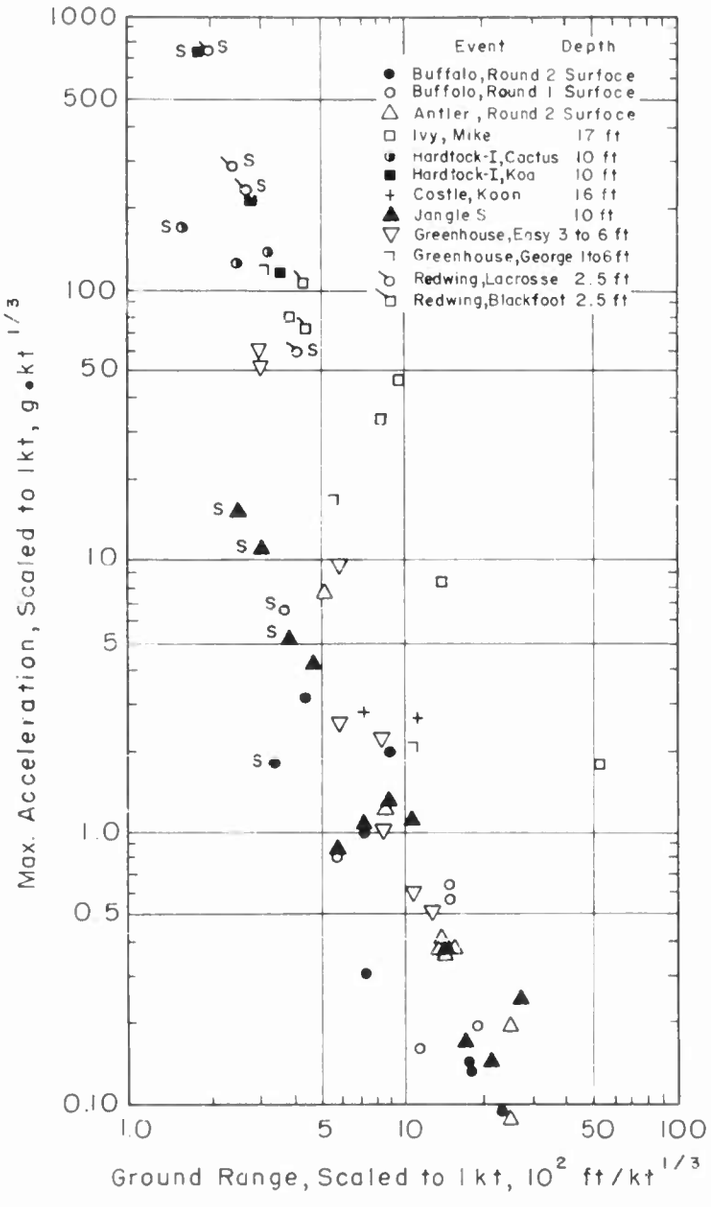

Figure 5.12 Maximum scaled vertical acceleration versus scaled ground range, for outrunning ground motion, EPG. (The letter "S" indicates superseismic blast wave.)

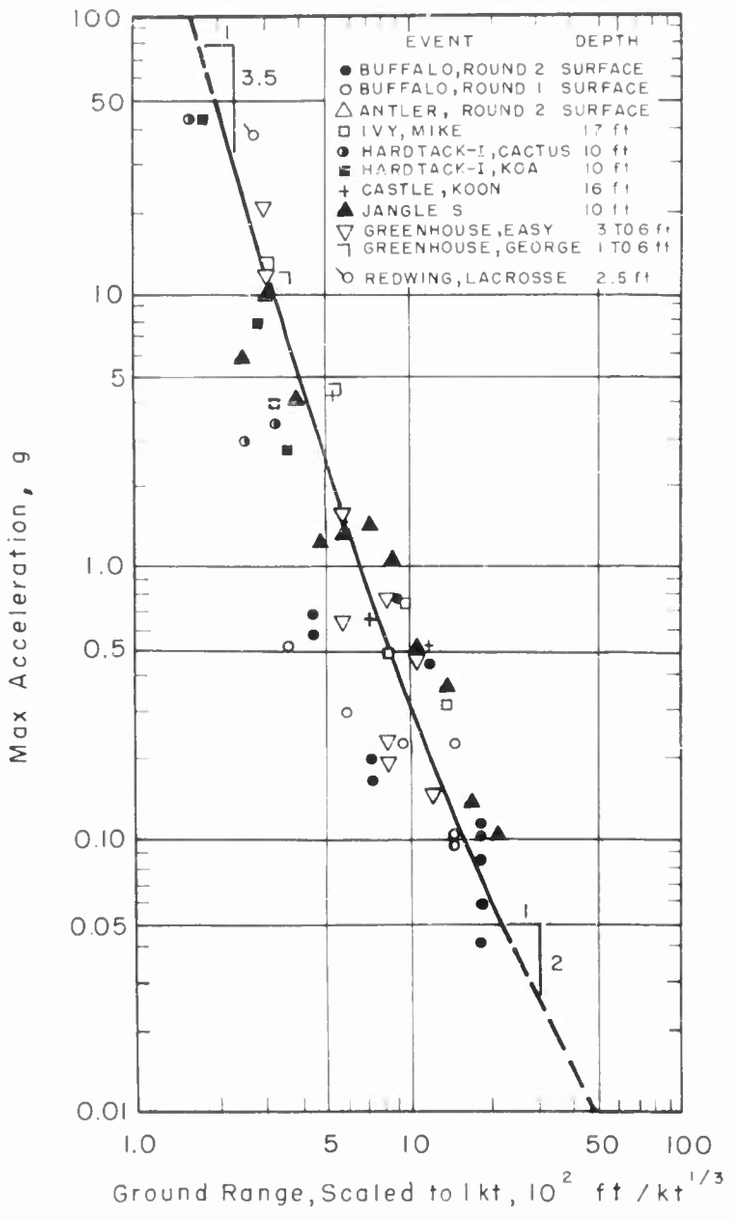

Figure 5.13 Maximum horizontal acceleration versus ground range for outrunning ground motion, EPG.

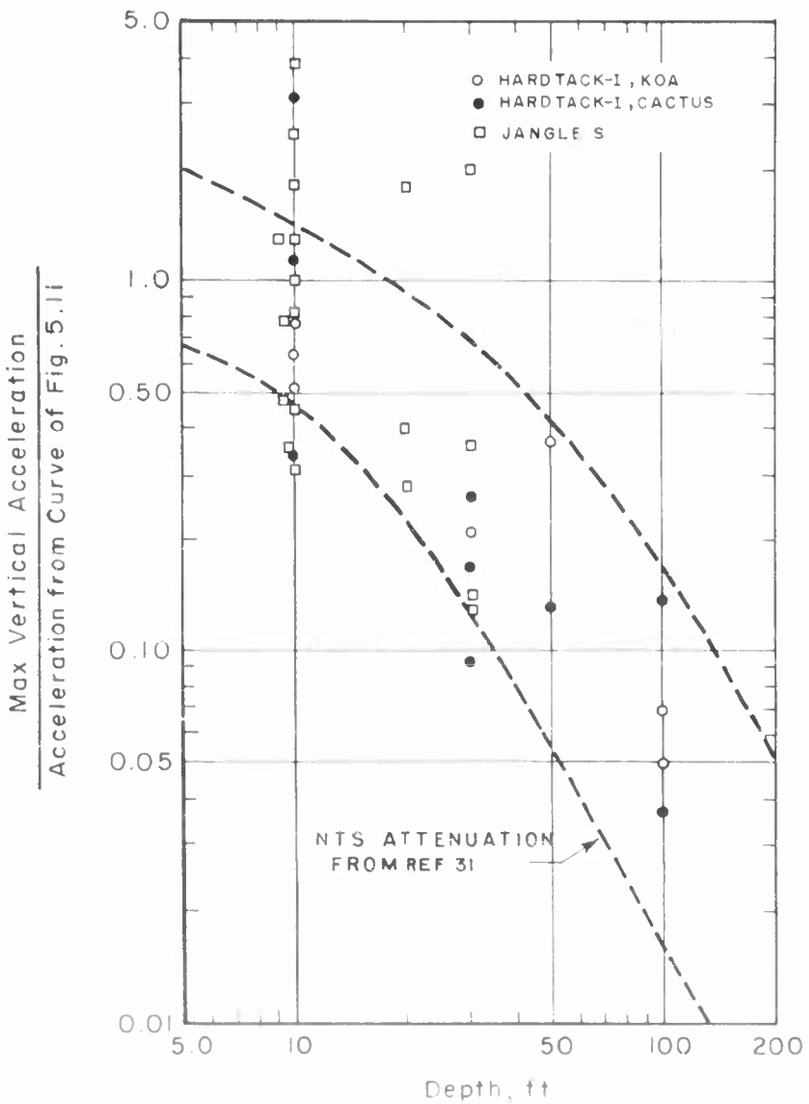
5.0
1.0
0.50
0.10
0.05
0.01
5.0
10
50
100
200
Depth, ft
Max Vertical Acceleration
Acceleration from Curve of Fig. 5.11
HARDTACK-I, KOA
HARDTACK-I, CACTUS
JANGLE S
NTS ATTENUATION
FROM REF 31

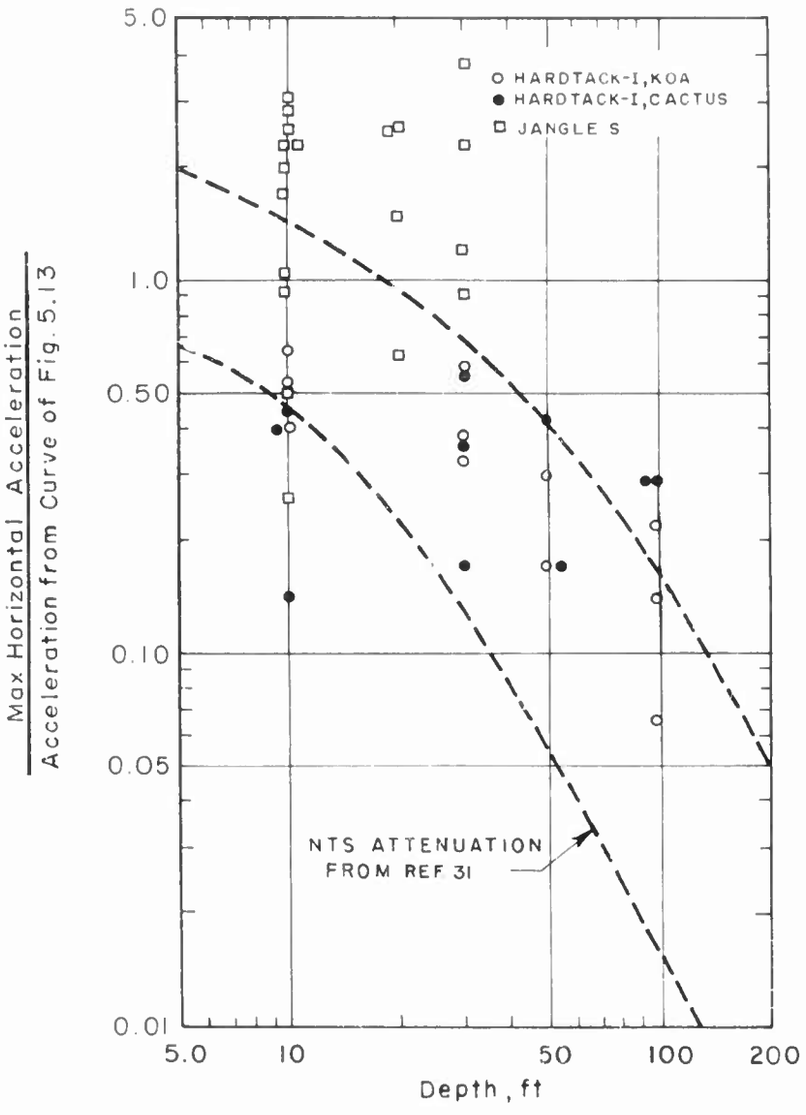

Figure 5.15 Horizontal acceleration versus depth for outrunning ground motion, EPG.

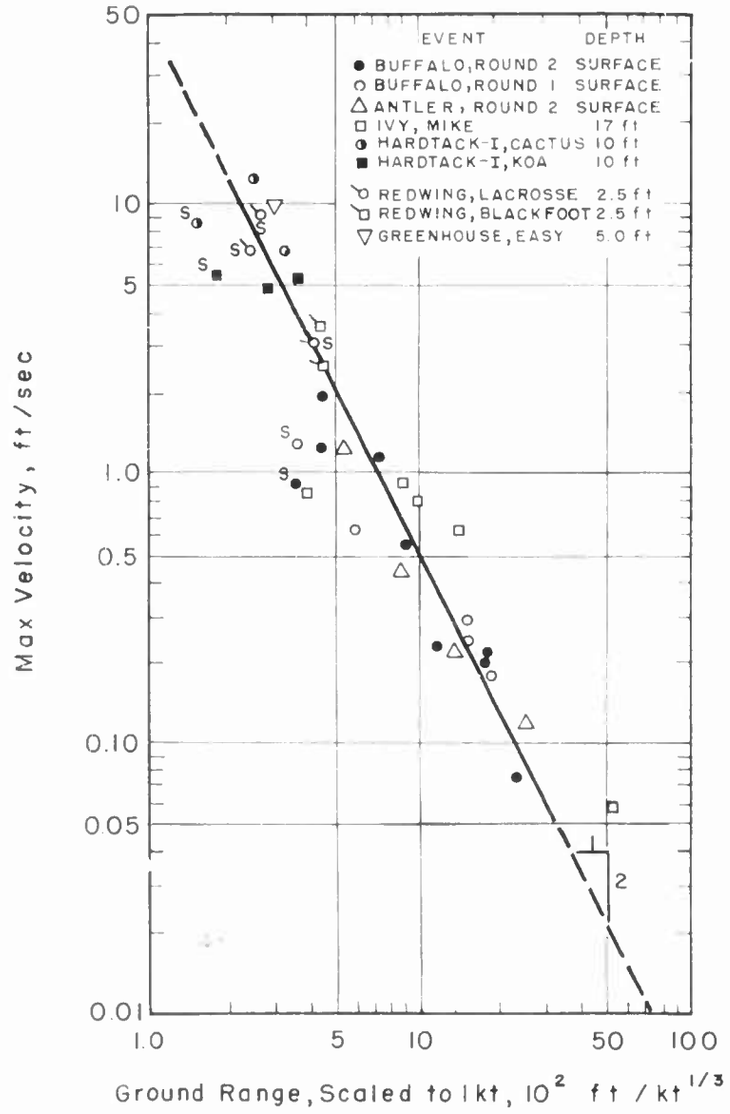

Figure 5.16 Maximum vertical velocity versus ground range for outrunning ground motion, EPG. (The letter "S" indicates superseismic blast wave.)

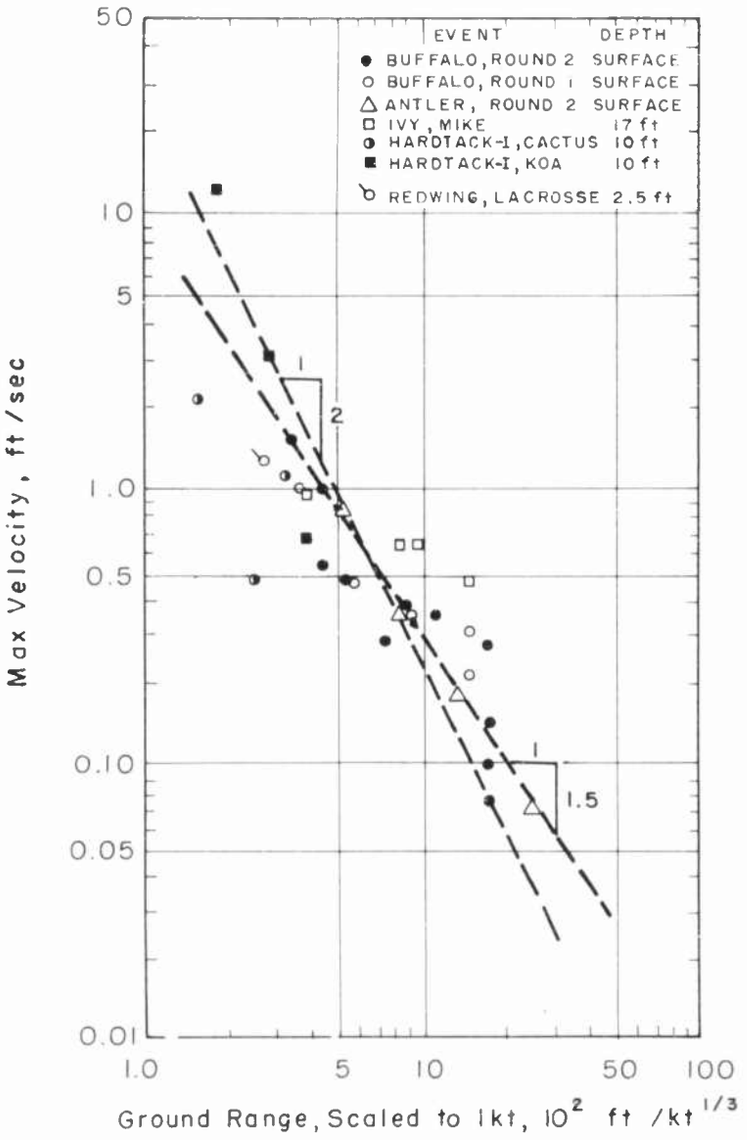

Figure 5.17 Maximum horizontal velocity versus ground range for outrunning ground motion, EPG.

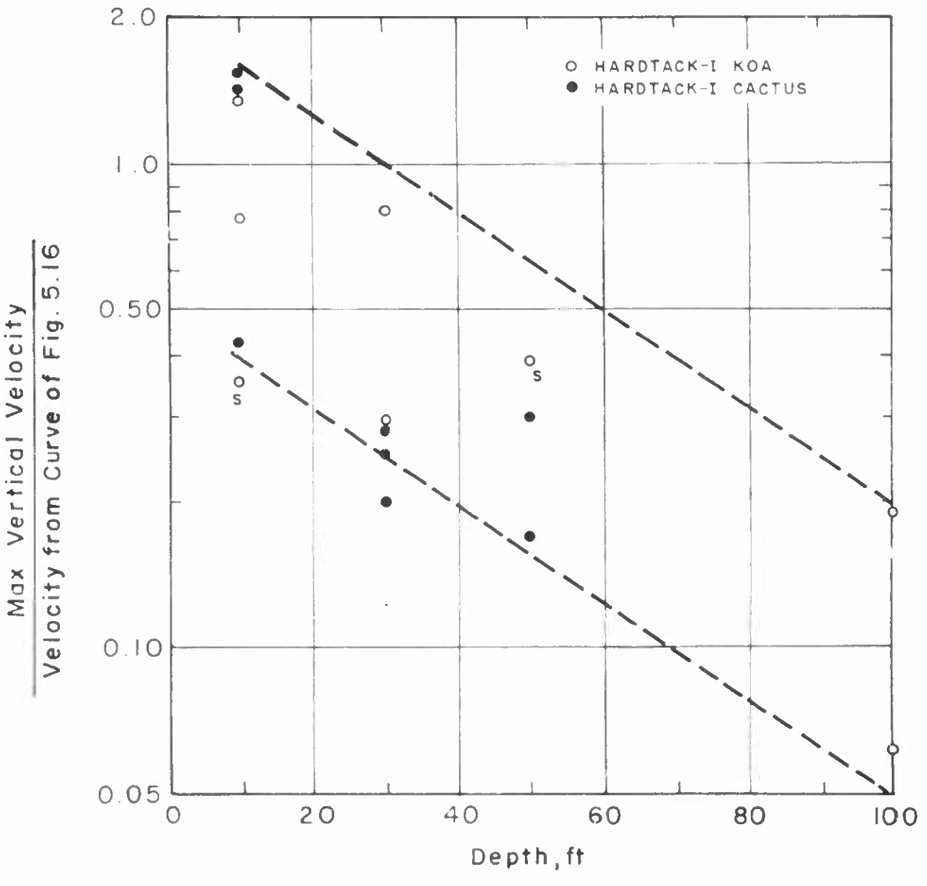

Figure 5.18 Vertical particle velocity versus depth for outrunning ground motion, EPG. (The letter "S" indicates superseismic blast wave.)

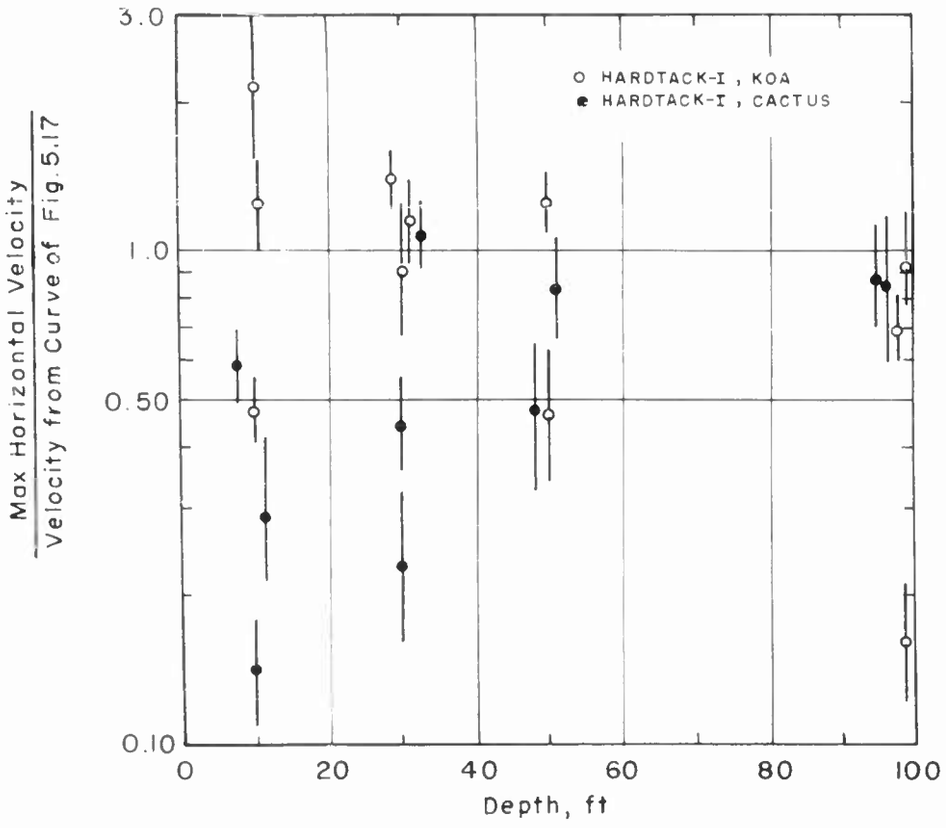

Figure 5.19 Horizontal particle velocity versus depth for outrunning ground motion, EPG. (Vertical lines indicate extent of uncertainty in correlation of Figure 5.17.)

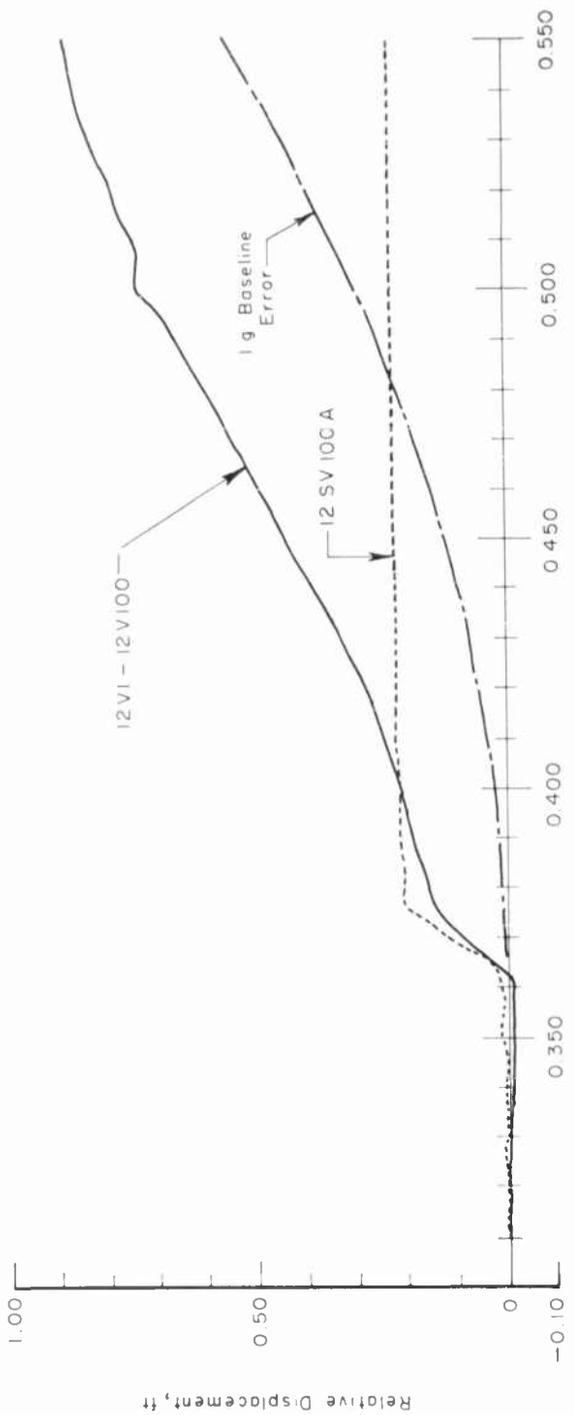

Figure 5.20 Comparison of relative displacement between 1 and 100 feet as measured by relative displacement gages and by double integration of acceleration records, Station 12, Shot Koa.

Chapter 6

CONCLUSIONS AND RECOMMENDATIONS

6.1 CONCLUSIONS

1. The low maximum overpressure measured on Cactus at a scaled ground range of 158 ft/kt$^{1/3}$ is the result of precursor formation. This precursor was short-lived and apparently cleaned up prior to or shortly after reaching the first BRL blast station (GR = 179 ft/kt$^{1/3}$).

2. The higher-than-normal overpressures measured on Koa at scaled ground ranges of 180 ft/kt$^{1/3}$ and 283 ft/kt$^{1/3}$ appear to be the result of a spike superimposed on a normal surface burst overpressure waveform. The reason for the appearance of this spike is not known; however it is speculated that it is the result of unusual occurrences in the early fireball hydrodynamics associated with the unusual geometry of the device. Hence, it is not recommended that the Naval Ordnance Laboratory 1959 surface burst overpressure-distance curve (Reference 27) be modified by these data.

3. Except for the first station on Koa, the ground motion on both Cactus and Koa outruns the airblast because of the high seismic velocity of the shallow substratum. The effect of the low-velocity overburden appears to be negligible as far as the ground motion in the high-velocity substratum is concerned, and outrunning occurs because of a transseismic blastwave as opposed to the refractive outrunning that is observed to occur at low overpressures at NTS.

4. Because of the differing ground motion phenomenology between the two sites (NTS and EPG) a direct comparison between all Hardtack results at EPG and results from NTS experiments is not possible. In this respect, one of the primary project objectives of extending NTS ground motion data to large (Megaton) yields was not fulfilled and, in light of the present degree of hindsight, was ill-conceived.

5. The few particle velocity data in the superseismic airblast region on Koa ($\Delta p_s \sim 1{,}000$ psi) tend to confirm the relationship that the maximum particle velocity equals the overpressure divided by the impedance (ρC) of the medium. Furthermore, the observed attenuation with depth of these data can be accounted for by changes in the compressional wave velocity between that at the surface and that at depth, which supports (but does not prove) the postulate, advanced on the basis of analysis of NTS data, that soils at moderately high overpressure (500 to 1,000 psi) can be considered, from an engineering viewpoint, to be nearly elastic. It follows from the last statement that the attenuation of maximum velocity is a function of the A-scaled depth; hence, for megaton yields very small rates of attenuation would be observed in the superseismic blastwave region.

6. The maximum vertical and horizontal accelerations at 10-foot depth on both Cactus and Koa are compatible, on a scaled basis of comparison, with the results of all previous EPG experiments and with the results of the UK experiments in Australia. Maximum acceleration is shown to be independent of yield at the same A-scaled ground range (within a scatter of data of 6:1 for vertical accelerations and 8:1 for horizontal accelerations) as opposed to the data from HE where the acceleration, at the same scaled ground range, varies inversely as the one-third power of the device yield. On the average, the horizontal

acceleration is half the vertical acceleration.

7. The attenuation of maximum vertical and horizontal acceleration with depth on Hardtack at EPG is comparable with that observed at NTS and within a wide scatter of data appears independent of yield and overpressure.

8. Maximum vertical particle velocities at 10-foot depth agree with the results of all previous EPG experiments and the results of the UK experiments in Australia and are a function only of A-scaled ground range.

9. The maximum horizontal particle velocities at 10-foot depth are comparable with previous data; however, the scatter is greater than for vertical particle velocity, and considerable judgment must be used in establishing the average curve of particle velocity as a function of A-scaled ground range.

10. The experiment failed to obtain conclusive results on maximum transient displacements. Quantitatively, the maximum vertical surface displacements on Koa were from 2.5 to 2 inches downward at Stations 11, 12, and 13, in that order, with a possible 2.5-foot upward and 15-foot outward displacement at Station 11 ($\Delta p_s \sim 1{,}000$ psi) due to crater lip formation. At Station 3 on Cactus ($\Delta p_s \sim 100$ psi), the maximum downward surface displacement was approximately 1 to 1.5 inches. These results are in quantitative agreement with the Space Technology Laboratories reed gage data (Reference 13). For all other vertical and horizontal displacements, the measurements are uncertain and can only be assigned the qualitative value of 2 to 6 inches; hence, it is impossible to specify the attenuation of displacement with depth. However, at 100-foot depth, the vertical displacement may be as large as 1 inch.

11. From the results of 10 above, it would appear that maximum transient displacements during Hardtack at EPG are a weak function of ground range (or pressure level) under conditions of outrunning ground motion and are also essentially independent of yield. To generalize this observation would be hazardous in the light of the meager data and lack of basic information on the mechanisms involved.

6.2 RECOMMENDATIONS

1. This project is a graphic example of the difficulty of attempting to extend nuclear effects from one milieu to another. The singularity of the environments of NTS and of EPG and the dissimilarity of the test devices preclude the use of data from one situation to predict the effects for the other. It is therefore recommended that in future full-scale operations, the experiment plan include measurements not only at the ranges of primary military interest but also measurements at sufficient ranges to give a sequential picture of the characteristics of the wave propagation throughout its entire history. This is necessary to provide a firm tie-in to previous ground motion data.

2. This project also points out the difficulties in the empirical correlation of ground motion data without adequate theory. This is especially true when data from one area is compared with data from another that is geologically dissimilar. It is recommended that increased emphasis be placed on obtaining theoretical guides that will provide greater confidence in the techniques that must be used in these correlations.

3. It is further recommended that the double integration of acceleration records to obtain particle velocity and displacement be abandoned in data reduction procedures. The errors in the measurement of acceleration are grossly magnified in this integration process; they are cumulative; and the corrections are based upon arbitrary assumptions of the magnitude of the terminal velocity or displacement so that it is impossible to assign validity to the resulting values. As an alternative, continued emphasis should be placed on the development of direct-measuring velocity and displacement gages.

Appendix

DESIGN AND PERFORMANCE OF A MINIATURIZED RECORDING SYSTEM

A.1 INTRODUCTION

In the early planning for Operation Hardtack at EPG, it was considered highly possible that no shot of the general yield range of Koa would be provided on an island complex that would permit the use of a central recording station. At that time it was intended that Project 1.8 instrument two stations only on each of two shots, with the stations located at pressure levels of 200 and 100 psi.

Under these conditions, an operating plan was set up using conventional recording gear on a shot of the general yield of Cactus but using special miniaturized recording gear on the larger shot, with the expectation that the two stations might be on islands separate from each other and from the shot. These stations were to have consisted of miniaturized magnetic tape recorders and variable frequency oscillators of the general type used in radiotelemetry. Four separate units were designed and constructed with the intent of using two units at each of two stations.

The magnetic recorder chosen for this operation was the Northam MR(A1), which was at that time being produced for use on missiles, rocket sled tracks, etc. This recorder was completely self-contained and was operated from small Yardney Silvereel storage batteries included in its case. It was primarily designed for direct recording or for a type of analog recording known as the carrier erase system, but test runs in the laboratory of FM systems led to the belief that the proposed use was practicable. The FM oscillators used with this system were Teledynamics Inc. (TDI) 874 variable reactance subcarrier oscillators. All oscillators were designed for a center frequency of 2.3 kc but were, in general, operated at a slightly lower frequency.

The transducers used were conventional Wiancko movements but with specially wound tapped coils designed for operation with this type of subcarrier oscillator. The use of a relatively low carrier frequency permitted cable lengths of up to 300 feet, without having the capacitance of the cable exceed the total capacitance necessary to reach resonance at the operating frequency.

A transistorized timing oscillator was included in the recorder, operating at a frequency of 2,000 cps. The signal from this oscillator was applied to one of the recording heads on each stack to serve both as a time reference and as a measure of tape transport wow and flutter as described below.

The Northam recorder and the TDI oscillators were rated to operate through shocks of 50 g, but it was considered highly probable that higher accelerations than this would be experienced by a recording unit buried near the surface at the planned pressure levels. As a consequence, it was necessary to incorporate the complete oscillator-recorder unit in a shock-mounted structure, which also served to protect it from damage due to blast and weather. The operating components, including batteries for operation of the oscillators and relays to perform the necessary timing functions, were mounted in a space frame shown in Figure A.1. This frame was mounted in an outer heavy-wall canister (Figure A.2) with spacers of polyurethane foam serving as shock mounts. The thickness and shape of these foam sections were determined by experiment with the objective of limiting the acceleration to 25 g when the case was subjected to a step function input of 20 ft/sec velocity.

After four of these units were essentially complete, an additional task was added to Project 1.8—that of instrumenting stations at still higher pressure levels than 600 psi. At this time it was also determined that there would be a large shot located on an island complex, and that cables would be run to the instrument stations from a central recording station. This instrument plan was adopted for Shot Koa, eliminating the need for the small independent recording units. However, it was decided to install two of these units on an experimental basis since they were already essentially complete.

A.2 EXPERIMENT PLAN

One of these miniaturized recording units was installed at Station 12 (Section 2.1), and the other was located at Station 13A at a ground range of about 4,200 feet, between Structures 320.02 and 320.03. Structure 320.02 was the large structure of Project 3.2 at ground range of about 3,950 feet. Structure 320.03, the smaller one, was at about 4,450 feet.

At Station 12 the following gage channels were installed:

M2BA, airblast pressure at Station 2
M2VD, vertieal acceleration at 2 feet outside canister
M2HD, horlzontal acceleration at 2 feet outside canister
M2VE, vertical accelcration inside canister
M2HE, horlzontal acceleration lnside canister

At Station 13A the following gage channels were installed:

M3VA, vertical acceleration of floor of Structure 320.02
M3VB, vertical acceleratlon of floor of Structure 320.03 (high sensitivity)
M3VC, vertical acceleration of floor of Structure 320.03 (low sensitivity)
M3VD, vertical acceleration at 2 feet outside canister
M3VE, vertieal acceleration inside cannister

All channels operated although the cables of M3VA, -VB, and -VC were broken sometlme after the airblast passage, and the baffle of gage M2BA was severely tilted as was the recording canister at Station 12. The recorded tapes were not played back in the tield but were carried to the laboratory for processing.

A.3 DATA REDUCTION AND DISCUSSION

Each channel was played back separately along with a reproduction of the output of the demodulator connected to the standard frequency signal. The noise output from this referenee signal represented the fluctuations occurring during recording and playback (principally of the former, since the playback was made on a high-quality transport), and the output of the signal channel represented the applied signal plus this noise. Subtracting the one from the other eliminated a large amount of the total noise. This effect is illustrated in the trace of M3VD in Figure A.3, where the three recorded channels are shown together. The upper trace is the output of the signal channel. The lower traee is the output of the reference channel, and the middle trace is the difference between the two. (The time marks shown were derived from the reference oscillator and represent actual time at the time of the recording with no reference to time during playback.) It can be seen that this noise reduction is very pronounced, but that the total noise is somewhat greater than was expected so that the residual noise was still higher than an acceptable level, particularly on channels other than M3VD, which was ehosen as an example. On the basis of these observations, the only reasonable conclusion concerning the design of the equipment is that further noise reduction during recording is necessary before the system is an entirely satisfactory field unit.

Figures A.3 and A.4 and Table A.1 show the waveform and the as-read peak values taken from the records played back by this method.

Record M2BA, shown in Figure A.4 was a measurement of airblast at Station 12, but it will be seen to differ rather markedly from the record from Gage 12B (Figure 4.16). It is not certain whether this difference is instrumental or whether it is due to damage to the gage baffle, which was found after the shot to have been severely tilted and somewhat displaced. Since the high-frequency noise observed on this signal appears to be more pronounced on the signal channel than on the reference channel, it is believed to be due to instrumental difficulties.

A comparison of M2VD with M2VE shows a considerable suppression of the high-frequency components of the acceleration signal on the latter record, although some of the noises observed on M2BA are also present on M2VE. The peak values of acceleration observed on these two records shown in Table A.1 show a very pronounced suppression of positive peak acceleration by a factor of approximately 8 to 1. The peak of 23.5 g to which the equipment was subjected indicates that the shock mounting procedure was satisfactory and that equipment of this type can be designed to operate through the blast wave at an overpressure of approximately 200 psi. This was the objeetive of this design. Comparison between M2HD and M2HE shows similar but somewhat less pronounced suppression of the peak horizontal acceleration.

Similar results were obtained from M3VD and M3VE which measured the vertical aeeelerations observed at Station 13A (Figure A.3). As might be expected, the ratio of suppression is not quite as great at this station, primarily because the duration of the peak is naturally somewhat longer. The other two records, M3VA and M3VB, show the measured values of peak acceleration observed at the two structures of Project 3.2. These values were somewhat lower than predicted values. M3VC, which was the same as M3VD except with lower sensitivity, showed practically no detectable deflection; consequently, the data was not reduced.

In conclusion, the results obtained from the test of this equipment show that it is mechanically feasible to protect the equipment under the conditions assumed in the original design but that improvements are required either in the tape speed stability of the Northam recorder or in the percentage frequency swing obtained from the Wiancko gages to reduce the noise to an acceptable level. Either or both of these modifications are probably practicable.

TABLE A.1 AS-READ PEAK VALUES, PRESSURE, AND ACCELERATIONS FROM MAGNETIC TAPE RECORDERS

Gage	Primary Peaks				Secondary Peaks				Tertiary Peaks	
	Positive Acceleration	Time	Negative Acceleration	Time	Positive Acceleration	Time	Negative Acceleration	Time	Positive Acceleration	Time
	g	sec	g	sec	g	sec	g	sec	g	sec
M2BA	165 *	0.005	–							
M2VD	200	0.010	−51	0.015						
M2VE	23.5	0.010	−4.2	0.020			−5	0.040	−8.2	0.069
M2HD	31	0.010	−29.5	0.015						
M2HE	6.3	0.025	−0.7	0.055			−2.4	0.100		
M3VA	7.8	0.035	−8.2	0.045	9.0	0.080	−7.7	0.190	−9.3	0.325
M3VB	1.6	0.175	−3.7	0.120	0.8	0.590	−0.6	0.135	−2.8	0.310
M3VD	59	0.005	−33	0.010	–	–	−15	0.060	−15	0.125
M3VE	13.8	0.010	−4.3	0.020	–		−6.4	0.130		

* This gage measured pressure in pounds/in^2.

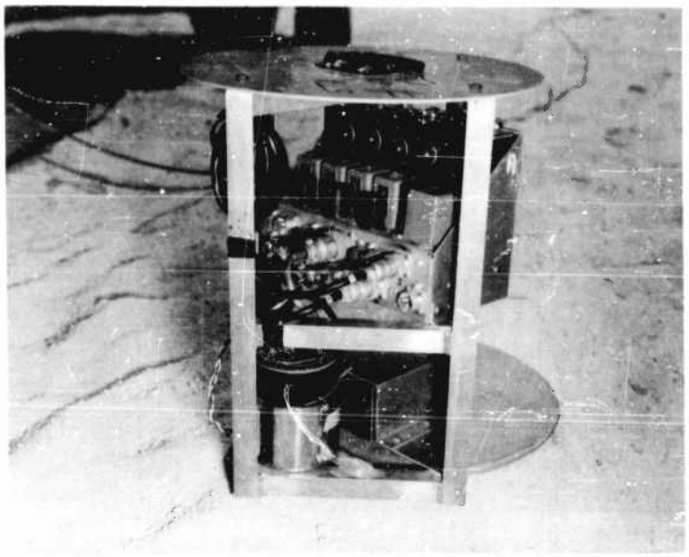

Figure A.1 Instruments mounted in space frame.

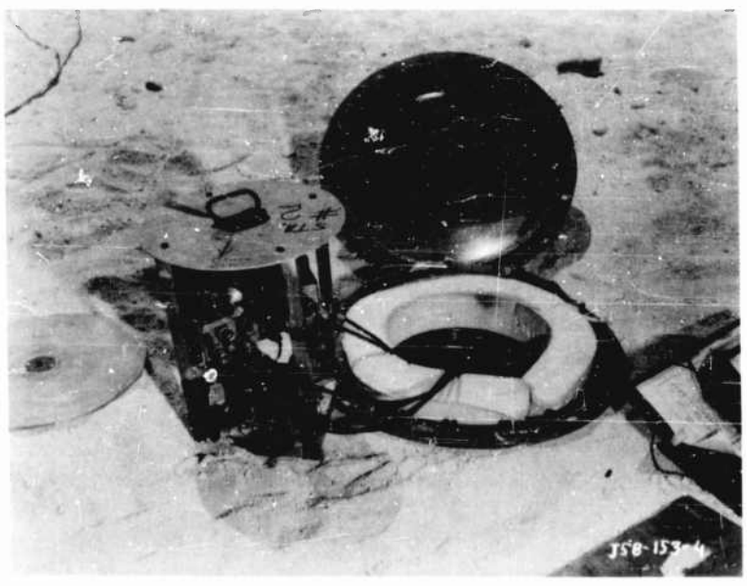

Figure A.2 Instruments and canister.

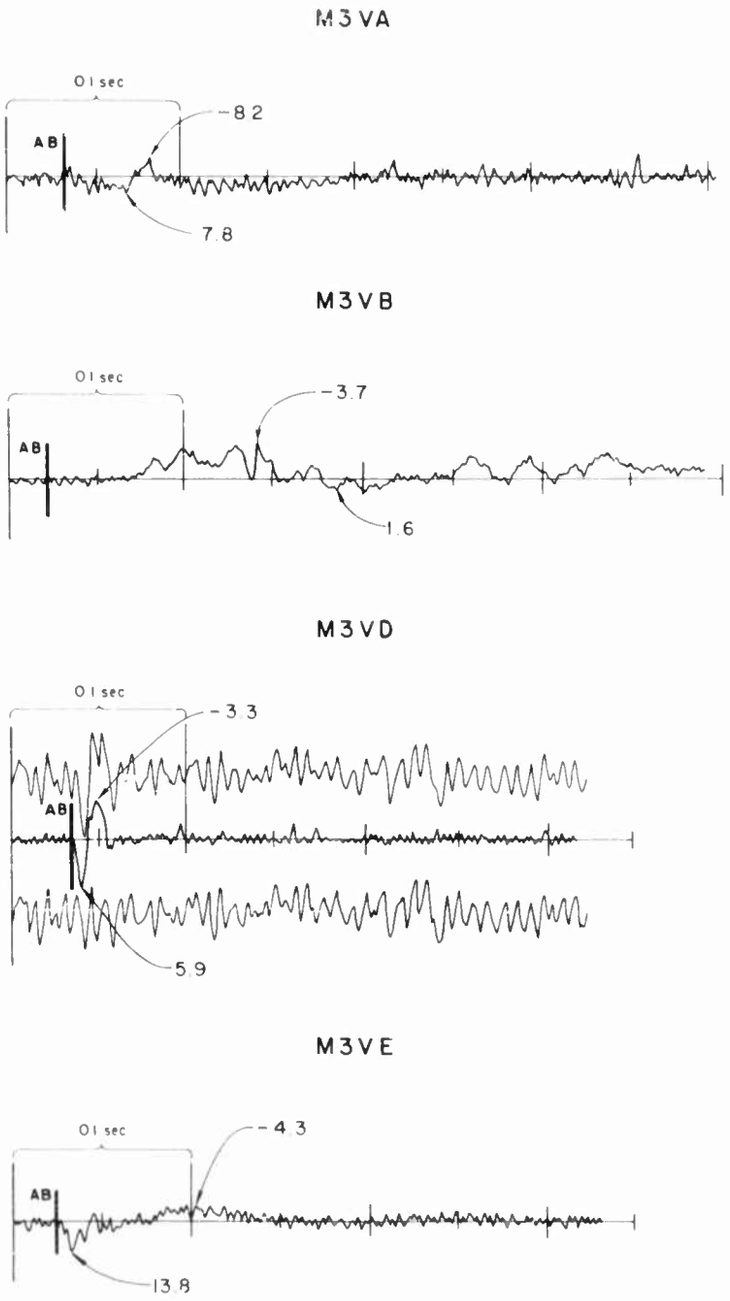

Figure A.3 Recordings at Station 13A.

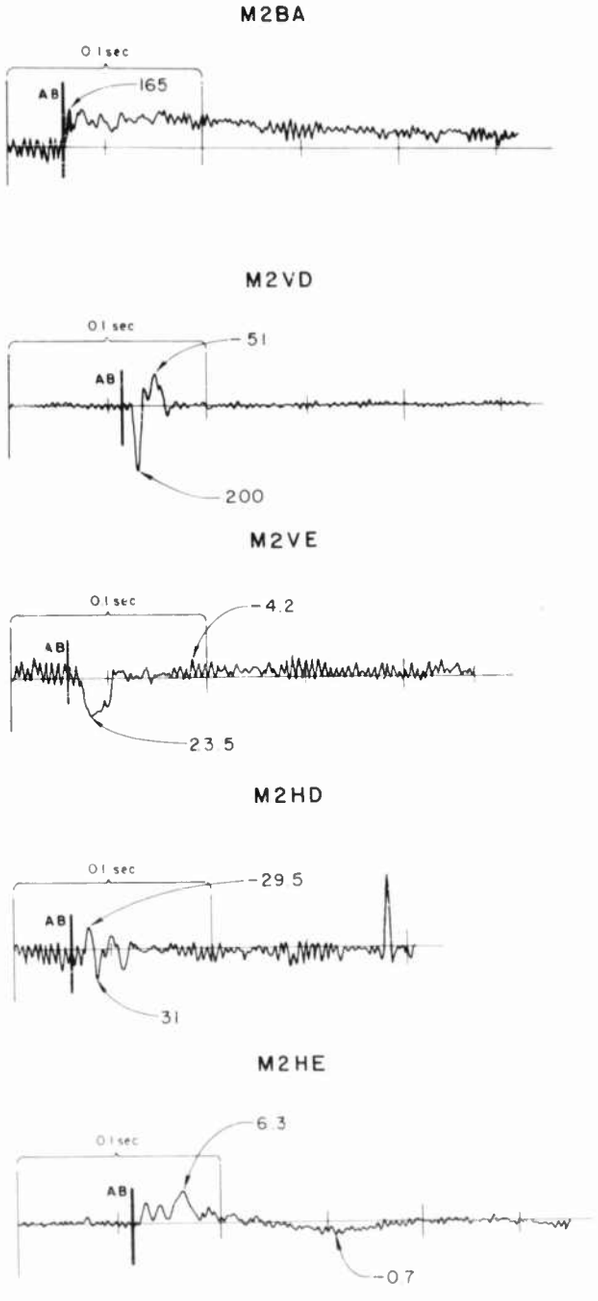

Figure A.4 Recordings at Station 12.

REFERENCES

1. D. C. Sachs and L. M. Swift; "Underground Explosion Effects"; Project 1.7, Operation Teapot, WT-1106, March 3, 1958; Stanford Research Institute, Menlo Park, California; Unclassified.

2. V. Salmon and S. R. Hornig; "Earth Acceleration Versus Time and Distance"; Project 1.7, Operation Tumbler/Snapper, WT-517, February 1953; Stanford Research Institute, Menlo Park, California; Unclassified.

3. L. M. Swift and D. C. Sachs; "Air Pressure and Ground Shock Measurements"; Project 1.1b, Operation Upshot-Knothole, WT-711, January 1955; Stanford Research Institute, Menlo Park, California; Confidential-Formerly Restricted Data.

4. W. R. Perret and V. L. Gentry; "Free-Field Measurements of Earth Stress, Strain, and Ground Motion"; Project 1.4, Operation Upshot-Knothole, WT-716, February 1955; Sandia Corporation, Albuquerque, New Mexico; Secret-Formerly Restricted Data.

5. L. M. Swift, et al; "Ground Acceleration, Stress, and Strain at High Incident Overpressures (U)"; Project 1.4, Operation Plumbbob, WT-1404, May 1960; Stanford Research Institute, Menlo Park, California; Secret-Formerly Restricted Data.

6. William R. Perret; "Ground Motion Studies at High Incident Overpressure"; Project 1.5, Operation Plumbbob, WT-1405, June 1960; Sandia Corporation, Albuquerque, New Mexico; Unclassified.

7. John W. Miles; "On the Response of an Elastic Half Space to a Moving Blast Wave"; EM-8-21, 24 November 1958; Space Technology Laboratories, Los Angeles, California.

8. I. N. Sneddon; "Fourier Transforms"; McGraw-Hill Book Company, New York, New York; Unclassified.

9. J. D. Cole and J. H. Huth; "Elastic Stresses Produced in a Half Plane by Steady Moving Loads"; Journal of Applied Mechanics No. 25, 433, December 1958; Unclassified.

10. P. Chadwick; "Estimates of the Incident Stress upon Buried Shelters from Megaton Bombs"; FWE 171, August 1958; United Kingdom Atomic Energy Authority, Atomic Weapons Research Establishment, Aldermaston, Berks., England, Confidential.

11. J. K. Wright; "A Theory of Movement in the Ground Caused by the Passage of Air Blast Over the Surface"; FWE-237, November 1959; United Kingdom Atomic Energy Authority, Atomic Weapons Research Establishment, Aldermaston, Berks, England; Confidential.

12. G. Cinelli and L. E. Fugelso; "Theoretical Study of Ground Motion Produced by Nuclear Bursts"; AFSWC-TR-60-9; Air Force Special Weapons Center, Kirtland AFB, New Mexico; Unclassified.

13. J. F. Halsey; "Ground-Shock Spectra from Surface Bursts"; GM 59-0000-07256 (draft of WT-1487), May 1959; Space Technology Laboratories, Los Angeles, California; Secret.

14. John W. Miles; "On the Response of a Layered Half-Space to a Moving Load"; EM 9-2, 29 January 1959; Space Technology Laboratories, Los Angeles, California; Unclassified.

15. C.R. Wylie, Jr.; "Advanced Engineering Mathematics," First Edition - p. 194; McGraw-Hill Book Company, New York, New York; 1951.

16. J.W. Craggs; "On the Propagation of Stress in a Half Space"; Technical Report 44, Division of Applied Mathematics, October 1958; Brown University, Providence, Rhode Island; Unclassified.

17. P. Weidlanger (Consultant); "Progress Report on Ground Shock at High Intensity Pressure Levels"; prepared by G.B. Panero Engineers, Survivability of Her Defense Systems, for the Mitre Corporation, Lexington, Massachusetts; 1 April 1960; Secret.

18. Hyman Serbin; "The Intense Stress Field Produced in the Elastic Earth by a Bomb Blast at the Surface"; Report No. P-1210, 23 August 1957; The RAND Corporation, Santa Monica, California; Unclassified.

19. G.H. Albright, et al; "Response of Earth-Confined Flexible-Arch-Shell Structures in High-Overpressure Region", Project 3.2, Operation Hardtack, ITR-1626-1, September 1958; U.S. Naval Civil Engineering Research and Evaluation Laboratory (NCEL), Port Hueneme, California; Secret-Restricted Data.

20. L.M. Swift, et al; "Air-Blast Phenomena in the High-Pressure Region (U)"; Project 1.3, Operation Plumbbob, WT-1403, December 1960; Stanford Research Institute, Menlo Park, California; Secret-Formerly Restricted Data.

21. M.B. Dobrin, et al; "Subsurface Constitution of Bikini Atoll as Indicated by a Seismic-Refraction Survey"; Bulletin of the Geological Society of America, 50, May 1949.

22. F.B. Porzel; "Soil Pressures and Energy Transfer on Mike Shot"; LA-1529, October 1952; Los Alamos Scientific Laboratory, Los Alamos, New Mexico.

23. W.R. Perret; "Ground-Motion Studies"; Project 30.2, Operation Redwing, WT-1264, June 1958; Sandia Corporation, Albuquerque, New Mexico; Confidential- Formerly Restricted Data.

24. J.R. Kelso; "Symposium on Air Blast Phenomena"; AFSWP-898, February 1957; Air Force Special Weapons Project, Washington 25, D.C.; Secret - Formerly Restricted Data.

25. C.D. Broyles; "Blast Measurements on a Medium-Yield Surface Burst (U)"; Project 1.2, Operation Redwing, WT-1302, January 1960; Sandia Corporation, Albuquerque, New Mexico; Secret - Formerly Restricted Data.

26. C.N. Kingery, et al; "Ground Surface Air-Blast Pressure Versus Distance (U)", Project 1.1, Operation Redwing, WT-1301, May 1960; Ballistic Research Laboratories, Aberdeen Proving Ground, Maryland; Secret - Restricted Data.

27. L.J. Belliveau, et al; "The Prediction of Shock Overpressures from Surface Burst Nuclear Weapons Along the Surface"; NAVORD-6240, 21 January 1959; Naval Ordnance Laboratory, White Oak, Silver Spring, Maryland; Secret - Formerly Restricted Data.

28. H.L. Brode; "Theoretical Description of the Blast and Fireball for a Sea Level Megaton Explosion"; RM-2248, 2 September 1959; The RAND Corporation, Santa Monica, California; Secret - Formerly Restricted Data.

29. H. L. Brode; "Point Source Explosion in Air"; RM-1824-AEC, 3 December 1956; The RAND Corporation, Santa Monica, California

30. J. K. Wright and J. O. Herbert; "Measurement of Ground Shock in Homogeneous Media: Surface Movement Due to a 2-oz. Charge Detonated on the Ground"; FWE-161, July 1958; United Kingdom Atomic Energy Authority, Atomic Weapons Research Establishment, Aldermaston, Berks., England; Confidential.

31. W. R. Perret; "Ground-Motion Studies on Operations Ivy and Castle"; WT-9002, February 1955; Sandia Corporation, Albuquerque, New Mexico; Secret Restricted Data.

32. Fred M. Sauer; "Ground Motion Produced by Aboveground Nuclear Explosions (U)"; AFSWC-TR-59-71, April 1959; Air Force Special Weapons Center, Kirtland AFB, New Mexico; Secret-Formerly Restricted Data.

33. J. F. Halsey, et al; "Ground Shock Spectra from Surface Bursts"; Project 1.12, Operation Hardtack, WT-1617, September 1960; Space Technology Laboratories, Inc., Los Angeles, California and Air Force Ballistic Missile Division, Air Research and Development Command, Inglewood, California; Secret--Formerly Restricted Data.

DISTRIBUTION

Military Distribution Categories 12 and 14

ARMY ACTIVITIES

1 Deputy Chief of Staff for Military Operations, D/A, Washington 25, D.C. ATTN: Dir. of SW&R
2 Chief of Research and Development, D/A, Washington 25, D.C. ATTN: Atomic Div.
3 Assistant Chief of Staff, Intelligence, D/A, Washington 25, D.C.
4 Chief of Engineers, D/A, Washington 25, D.C. ATTN: ENGNB
5 Chief of Engineers, D/A, Washington 25, D.C. ATTN: ENGEB
6 Chief of Engineers, D/A, Washington 25, D.C. ATTN: ENGTB
7- 8 Office, Chief of Ordnance, D/A, Washington 25, D.C. ATTN: ORDTN
9- 11 Commanding General, U.S. Continental Army Command, Ft. Monroe, Va.
12 Director of Special Weapons Development Office, Headquarters CONARC, Ft. Sliss, Tex. ATTN: Capt. Chester I. Peterson
13 President, U.S. Army Artillery Board, Ft. Sill, Okla.
14 President, U.S. Army Air Defense Board, Ft. Sliss, Tex.
15 Commandant, U.S. Army Command & General Staff College, Ft. Leavenworth, Kansas. ATTN: ARCHIVES
16 Commandant, U.S. Army Air Defense School, Ft. Slise, Tex. ATTN: Command & Staff Dept.
17 Commandant, U.S. Army Armored School, Ft. Knox, Ky.
18 Commandant, U.S. Army Artillery and Missile School, Ft. Sill, Okla. ATTN: Combat Development Department
19 Commandant, U.S. Army Aviation School, Ft. Rucker, Ala.
20 Commandant, U.S. Army Infantry School, Ft. Benning, Ga. ATTN: C.D.S.
21 Commandant, U.S. Army Ordnance and Guided Missile School, Redstone Arsenal, Ala.
22 Commanding General, Chemical Corps Training Comd., Ft. McClellan, Ala.
23 Commanding General, The Engineer Center, Ft. Belvoir, Va. ATTN: Asst. Cmdt, Engr. School
24 Director, Armed Forces Institute of Pethology, Walter Reed Army Med. Center, 625 16th St., NW, Washington 25, D.C.
25 Commanding Officer, U.S. Army Research Lab., Ft. Knox, Ky.
26 Commandant, Walter Reed Army Inst. of Res., Walter Reed Army Medical Center, Washington 25, D.C.
27 Commanding General, Qm R&D Comd., QM R&D Cntr., Natick, Mass. ATTN: CBR Liaison Officer
28- 29 Commanding Officer, Chemical Warfare Lab., Army Chemical Center, Md. ATTN: Tech. Library
30 Commanding General, Engineer Research and Dev. Lab., Ft. Belvoir, Va. ATTN: Chief, Tech. Support Branch
31 Director, Waterways Experiment Station, P.O. Box 631, Vicksburg, Miss. ATTN: Library
32 Commanding Officer, Picatinny Arsenal, Dover, N.J. ATTN: ORDBB-TK
33 Commanding Officer, Diamond Ord. Fuze Labs., Washington 25, D.C. ATTN: Chief, Nuclear Vulnerability Br. (230)
34- 35 Commanding General, Aberdeen Proving Grounds, Md. ATTN: Director, Ballistics Research Laboratory
36 Commanding General, Frankford Arsenal, Bridge and Tacony St., Philadelphia, Pa.
37 Commanding Officer, Watervliet Arsenal, Watervliet, New York. ATTN: ORDBF-RR
38 Commander, Army Rocket and Guided Missile Agency, Redstone Arsenal, Ala. ATTN: Tech Library
39 Commanding General, White Sands Missile Range, N. Mex. ATTN: ORDBS-OM-TL
40 Commander, Army Ballistic Missile Agency, Redstone Arsenal, Ala. ATTN: ORDAB-HT
41 Commanding General, Ordnance Tank Automotive Command, Detroit Arsenal, Centerline, Mich. ATTN: ORDMC-RO
42 Commanding General, Ordnance Weapons Command, Rock Island, Ill.
43 Commanding General, U.S. Army Electronic Proving Ground, Ft. Huachuca, Ariz. ATTN: Tech. Library
44 Commanding General, USA Combat Surveillance Agency, 1124 N. Highland St., Arlington, Va.
45 President, Beach Erosion Board, Corps of Engineers, U.S. Army, 5201 Little Falls Rd., N.W., Washington 16, D.C.
46 Commanding General, U. S. ORD Special Weapons-Ammunition Command, Dover, N.J.
47 Commanding General, Southern European Task Force, APO 168, New York, N.Y. ATTN: ACofS G-3

NAVY ACTIVITIES

48- 49 Chief of Naval Operations, D/N, Washington 25, D.C. ATTN: OP-03EG
50 Chief of Naval Operations, D/N, Washington 25, D.C. ATTN: OP-75
51- 52 Chief of Naval Research, D/N, Washington 25, D.C. ATTN: Code 811
53- 55 Chief, Bureau of Naval Weapons, D/N, Washington 25, D.C. ATTN: DLI-3
56- 60 Chief, Bureau of Naval Weapons, D/N, Washington 25, D.C. ATTN: RAAD-25
61 Chief, Bureau of Ordnance, D/N, Washington 25, D.C.
62 Chief, Bureau of Ships, D/N, Washington 25, D.C. ATTN: Code 423
63 Chief, Bureau of Yards and Docks, D/N, Washington 25, D.C. ATTN: D-440
64 Director, U.S. Naval Research Laboratory, Washington 25, D.C. ATTN: Mrs. Katherine H. Cass
65- 66 Commander, U.S. Naval Ordnance Laboratory, White Oak, Silver Spring 19, Md.
67 Director, Material Lab. (Code 900), New York Naval Shipyard, Brooklyn 1, N.Y.
68 Commanding Officer and Director, Navy Electronics Laboratory, San Diego 52, Calif.
69 Commanding Officer, U.S. Naval Mine Defense Lab., Panama City, Fla.
70- 71 Commanding Officer, U.S. Naval Radiological Defense Laboratory, San Francisco, Calif. ATTN: Tech. Info. Div.
72- 73 Commanding Officer and Director, U.S. Naval Civil Engineering Laboratory, Port Hueneme, Calif. ATTN: Code L31
74 Commanding Officer, U.S. Naval Schools Command, U.S. Naval Station, Treasure Island, San Francisco, Calif.
75 Superintendent, U.S. Naval Postgraduate School, Monterey, Calif.
76 Commanding Officer, U.S. Fleet Sonar School, U.S. Naval Base, Key West, Fla.
77 Commanding Officer, U.S. Fleet Sonar School, San Diego 47, Calif.
78 Officer-in-Charge, U.S. Naval School, CEC Officers, U.S. Naval Construction Bn. Center, Port Hueneme, Calif.
79 Commanding Officer, Nuclear Weapons Training Center, Atlantic, U.S. Naval Base, Norfolk 11, Va. ATTN: Nuclear Warfare Dept.
80 Commanding Officer, Nuclear Weapons Training Center, Pacific, Naval Station, San Diego, Calif.
81 Commanding Officer, U.S. Naval Damage Control Tng. Center, Naval Base, Philadelphia 12, Pa. ATTN: ABC Defense Course

82 Commanding Officer, Air Development Squadron 5, VX-5, China Lake, Calif.
83 Commanding Officer, Naval Air Material Center, Philadelphia 12, Pa. ATTN: Technical Data Br.
84 Commanding Officer U.S. Naval Air Development Center.
85 Commanding Officer, U.S. Naval Medical Research Institute, National Naval Medical Center, Bethesda, Md.
86- 87 Commander, U.S. Naval Ordnance Test Station, China Lake, Calif.
88 Commanding Officer and Director, David W. Taylor Model Basin, Washington 7, D.C. ATTN: Library
89 Commander, Norfolk Naval Shipyard, Portsmouth, Va. ATTN: Underwater Explosions Research Division
90 Commandant, U.S. Marine Corps, Washington 25, D.C. ATTN: Code A03H
91 Director, Marine Corps Landing Force, Development Center, MCS, Quantico, Va.
92 Commanding Officer, U.S. Naval CIC School, U.S. Naval Air Station, Glynco, Brunswick, Ga.
93-100 Chief, Bureau of Naval Weapons, Navy Department, Washington 25, D.C. ATTN: RR12

AIR FORCE ACTIVITIES

101 Air Force Technical Application Center, HQ. USAF, Washington 25, D. C.
102 Hq. USAF, ATTN: Operations Analysis Office, Office, Vice Chief of Staff, Washington 25, D. C.
103 Director of Civil Engineering, HQ. USAF, Washington 25, D.C. ATTN: AFOCE-ES
104-108 HQ. USAF, Washington 25, D.C. ATTN: AFCIN-3D1
109 Director of Research and Development, DCS/D, HQ. USAF, Washington 25, D.C. ATTN: Guidance and Weapons Div.
110 The Surgeon General, HQ. USAF, Washington 25, D.C. ATTN: Bio.-Def. Pre. Med. Division
111 Commander, Tactical Air Command, Langley AFB, Va. ATTN: Doc. Security Branch
112 Commander, Air Defense Command, Ent AFB, Colorado. ATTN: Operations Analysis Section, ADCOA
113 Commander, Hq. Air Research and Development Command, Andrews AFB, Washington 25, D.C. ATTN: RDRWA
114 Commander, Air Force Ballistic Missile Div. HQ. ARDC, Air Force Unit Post Office, Los Angeles 45, Calif. ATTN: WDSOT
115 Commander, Second Air Force, Barksdale AFB, La. ATTN: Operations Analysis Office
116-117 Commander, AF Cambridge Research Center, L. G. Hanscom Field, Bedford, Mass. ATTN: CRQST-2
118-122 Commander, Air Force Special Weapons Center, Kirtland AFB, Albuquerque, N. Mex. ATTN: Tech. Info. & Intel. Div.
123-124 Director, Air University Library, Maxwell AFB, Ala.
125 Commander, Lowry Technical Training Center (TW), Lowry AFB, Denver, Colorado.
126 Commandant, School of Aviation Medicine, USAF Aerospace Medical Center (ATC), Brooks AFB, Tex ATTN: Col. G. L. Hekhuis
127-129 Commander, Wright Air Development Center, Wright-Patterson AFB, Dayton, Ohio. ATTN: WCA T (For WCOSI)
130-131 Director, USAF Project RAND, V A: USAF Liaison Office, The RAND Corp., 1700 Main St., Santa Monica, Calif.
132 Commander, Rome Air Development Center, ARDC, Griffiss AFB, N.Y. ATTN: Document Library, RCSSL-1
133 Commander, Air Technical Intelligence Center, USAF, Wright-Patterson AFB, Ohio. ATTN: AFCIN-4Bla, Library
134 Headquarters, 1st Missile Div. USAF, Vandenberg AFB, Calif. ATTN: Operations Analysis Office
135 Assistant Chief of Staff, Intelligence, HQ. USAFE, APO 633, New York, N.Y. ATTN: Directorate of Air Targets
136 Commander-in-Chief, Pacific Air Forces, APO 953, San Francisco, Calif. ATTN: PFCIE-MB, Base Recovery

OTHER DEPARTMENT OF DEFENSE ACTIVITIES

137 Director of Defense Research and Engineering, Washington 25, D.C. ATTN: Tech. Library
138 Chairman, Armed Services Explosives Safety Board, DOD, Building T-7, Gravelly Point Washington 25, D.C.
139 Director, Weapons Systems Evaluation Group, Room 1E-880, The Pentagon, Washington 25, D.C.
140-143 Chief, Defense Atomic Support Agency, Washington 25, D.C. ATTN: Document Library
144 Commander, Field Command, DASA, Sandia Base, Albuquerque, N. Mex.
145 Commander, Field Command, DASA, Sandia Base, Albuquerque, N. Mex. ATTN: FCTG
146-147 Commander, Field Command, DASA, Sandia Base, Albuquerque, N. Mex. ATTN: FCWT
148 Administrator, National Aeronautics and Space Administration, 1520 "H" St., N.W., Washington 25, D.C. ATTN: Mr. R. V. Rhode
149 Commander-in-Chief, Strategic Air Command, Offutt AFB, Neb. ATTN: OAWB
150 U.S. Documents Officer Office of the United States National Military Representative - SHAPE, APO 55, New York, N.Y.

ATOMIC ENERGY COMMISSION ACTIVITIES

151-153 U.S. Atomic Energy Commission, Technical Library, Washington 25, D.C. ATTN: For DMA
154-158 Los Alamos Scientific Laboratory, Report Library, P.O. Box 1663, Los Alamos, N. Mex. ATTN: Helen Redman
159-161 Sandia Corporation, Classified Document Division, Sandia Base, Albuquerque, N. Mex. ATTN: H. J. Smyth, Jr.
162-164 University of California Lawrence Radiation Laboratory, P.O. Box 808, Livermore, Calif. ATTN: Clovis G. Craig
165 Division of Technical Information Extension, Oak Ridge, Tenn. (Master)
166-195 Division of Technical Information Extension, Oak Ridge, Tenn. (Surplus)

SUPPLEMENTARY

INFORMATION

DATE: Oct 25 1995 18:13:51
EAB51ZR
CLASSIFICATION: UNCLASSIFIED

TRIS INPUT REPORT
CYCLE ID: FM

4 \01 AD-338641
\02 191100,081100
\03 U
\05 stanford research inst menlo park calif
4 \06 OPERATION =HARDPROJECT= <1>.<8>. GROUND MOTION PRODUCED BY NUCLEAR DETONATIONS
\08 U
4 \10 Swift,L.M.
Sauer,F.M.
Wells,W.M.
\11 19620503
\12 126
\14 WT1613
\20 U
\23 (*NUCLEAR EXPLOSIONS, BLAST), (*SOILS, MOTION), SHOCK WAVES, PRESSURE, STRUCTURES, UNDERGROUND STRUCTURES, MOTION.
\24 U
\25 hardtack operation
\26 U
\27 The objective was to measure ground motion pro duced by nuclear explosions at Eniwetok Proving Ground (EPG) as it varied with input pressure level, depth, and yield, and to correlate the measurements with similar data obtained at Nevada Test Site (NTS). No conclusive results were ob tained on transient displacements. Maximum vertical surface displacements on Koa were 2.5 to 2 inches downward at 2,000-, 3,144-, and 3,950-foot ground ranges, in that order, with a possible 2.5-foot upward and 15-foot outward displacement at 2,000 feet due to crater lip formation. At 840-foot ground range on Cactus, maximum downward surface displacement was approxi mately 1 to 1.5 inches. Without suggesting that it be taken as a generalization, it appears that transient displacements on Cactus and Koa are a weak function of ground range (or pressure level), under conditions of outrunning ground motion and are independent of yield. (Author)
\28 U
\29 1
\30 Ground motion produced by nuclear detonations.
\32
\33 1
\35 332500
\36 1
\40 0611
\41 w
\49 951025 - d'clas s-frd to u/dna-sstl ltr dtd 18 sep 95); P'blc R'lse via same ltr, signed by J.B. Wood, Chief, Tech Support.
TITLE PUNCTUATION IMPROPER

Defense Nuclear Agency
6801 Telegraph Road
Alexandria, Virginia 22310-3398

SSTL

ERRATA -AD 338641

18 September 1995

MEMORANDUM FOR DEFENSE TECHNICAL INFORMATION CENTER (DTIC)
ATTENTION: OCD/Mr. Bill Bush

SUBJECT: Declassification of AD-338641

The Defense Nuclear Agency Security Office (ISTS) has declassified the subject report (AD-338641, WT-1613)

Distribution statement "A" applies.

FOR THE DIRECTOR:

JOSEPHINE WOOD
Chief, Technical Support

ERRATA

Defense Special Weapons Agency
6801 Telegraph Road
Alexandria, Virginia 22310-3398

MAY 8 1998

OPSSI

MEMORANDUM FOR DISTRIBUTION

SUBJECT: Declassification Review of Operation HARDTACK Test Reports

The following 28 reports concerning the atmospheric nuclear tests conducted during Operation HARDTACK in 1958 have been declassified and cleared for open publication/public release:

WT-1606 thru WT-1611, WT-1613 thru WT-1617, WT-1620, WT-1626, WT-1630, WT-1633, WT-1634, WT-1647, WT-1649, ITR-1653, ITR-1655, ITR-1656, WT-1661, WT-1662, WT-1676, WT-1685 thru WT-1687, and WT-1689.

An additional 29 WTs from HARDTACK have been re-issued with deletions and are identified with an "EX" after the WT number. These reissued versions are unclassified and approved for open publication. They are:

WT-1602, WT-1618, WT-1619, WT-1621 thru WT-1623, WT-1625, WT-1627, WT-1629, WT-1636 thru WT-1641, WT-1648, WT-1650, WT-1651-1, WT-1657, WT-1663, WT-1664, WT-1675, WT-1677, WT-1679 thru WT-1682, WT-1688 and WT-1690.

This memorandum supersedes the Defense Special Weapons Agency, OPSSI memorandum same subject dated June 13, 1997 and may be cited as the authority to declassify copies of any of the reports listed in the first paragraph above.

R'Metro

RITA M. METRO
Chief, Information Security

DISTRIBUTION:
See Attached